Applied Energy 305 (2022) 117849

Contents lists available at ScienceDirect

Applied Energy

journal homepage: www.elsevier.com/locate/apenergy

A review of nickel-rich layered oxide cathodes: synthetic strategies, structural characteristics, failure mechanism, improvement approaches and prospects

Yao Lv[a], Shifei Huang[a,*], Yufeng Zhao[a,*], Swagata Roy[a], Xionggang Lu[a], Yanglong Hou[b], Jiujun Zhang[a,*]

[a] College of Sciences and Institute for Sustainable Energy, Shanghai University, Shanghai 200444, China
[b] Department of Materials Science and Engineering, College of Engineering, Peking University, Beijing 100871, China

HIGHLIGHTS

- The capacity failure mechanisms are emphatically summarized and discussed.
- The improvement measures of nickel-rich cathodes in recent years are summarized.
- The prospects of nickel-rich materials are summarized.

GRAPHICAL ABSTRACT

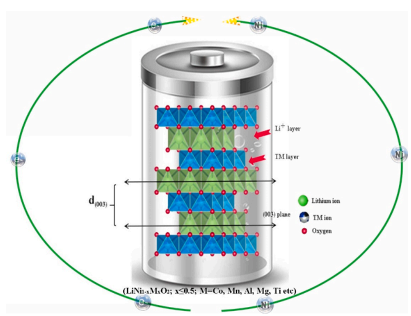

ARTICLE INFO

Keywords:
Lithium-ion batteries
Nickel-rich layered oxide cathode materials
Capacity failure mechanism
Strategies
Perspectives

ABSTRACT

Nickel-rich layered oxide cathode materials have high specific capacity and are environmentally-benign, hence they are considered as the most relevant next-generation positive-electrode materials for lithium-ion batteries, particularly for powering plug-in hybrid electric vehicles and battery electric vehicles. The rich nickel content in layered oxides is highly beneficial in improving the energy density, but the cycle ability, rate capability and thermal stability inevitably decrease with the increase of nickel percentage, leading to the gradual failure of lithium-ion batteries. Therefore, it is an essential requisite to give a thorough review of previous research, thereby providing a clear understanding of the relationships between the material structure and their electrochemical activities, and improving the electrochemical performances of nickel-rich layered oxide cathode materials through reasonable modifications. In this article, the structural characteristics and synthetic methods are systematically reviewed. Particularly, the capacity failure mechanism and the corresponding improvement strategies of nickel-rich layered oxides are emphasized and discussed from atomic scale to macro-scale along with the latest literature review. A brief analysis of the perspectives is also presented with several possible research directions for technical and commercial success of nickel-rich layered oxide cathodes.

* Corresponding authors.
E-mail addresses: huangsf2020@sz.tsinghua.edu.cn (S. Huang), yufengzhao@shu.edu.cn (Y. Zhao), jiujun.zhang@i.shu.edu.cn (J. Zhang).

https://doi.org/10.1016/j.apenergy.2021.117849
Received 23 June 2021; Received in revised form 25 August 2021; Accepted 7 September 2021
Available online 14 September 2021

1. Introduction

Over the past century, the wide application of fossil energy, such as oil, natural gas, coal and nuclear energy, has provided a strong driving force for the development of human society and the world economy.[1-9] Despite producing more and more energy from renewables each year, the global energy mix is still dominated by coal, oil, and gas. Not only does most of our energy ~ 84% of it come from fossil fuels, we continue to burn more each year: total production has increased from 116,214 to 136,761 TWh in the last 10 years (Fig. 1**a-b**). However, the earth's resources are limited. With the continuous consumption of resources, these resources will gradually dry up in the next 50–150 years (Fig. 1**c**). With the global energy crisis and environmental pollution becoming increasingly prominent, the development of energy-saving and environmental protection related industries has been highly valued, and the development of new energy vehicles has formed a consensus all over the world. In 2020, the global sales volume of new energy vehicles increased from 140,000 in 2012 to 3.07 million, with an annual compound growth rate of 47%; Permeability increased from 0.2% to 4%. In the short and medium term, the global energy conservation and emission reduction policies will drive the rapid increase of the penetration rate of new energy vehicles. In the long run, intelligent upgrading will bring a subversive revolution to the automobile industry and bring greater growth space to the new energy automobile industry. In this context, the global sales volume of new energy vehicles is expected to reach 10 million in 2025 and ~ 25 million in 2030, and the future market capacity growth is expected to exceed ten times **(**Fig. 1**d**). Due to the requirement of high energy density, the batteries used in electric vehicles are basically lithium-ion batteries. Battery system is the component with the highest cost in new energy vehicles, and its cost accounts for nearly 40%. With the popularity of new energy vehicles, the scale of power battery industry is expected to grow rapidly. In 2020, the global lithium battery output will be 747 GWh. Lithium ion battery super factory predicts that the global lithium battery output will reach 2492 GWh in 2025, and the compound growth rate from 2020 to 2025 will exceed 27% (Fig. 1**e**).

Further enhancement of the energy and power density of LIBs are being highly focused in order to inflate their application in the EV market, as well as in the renewable energy involving wind and solar energy grid storage applications [10]. Electrode materials (cathodes and anodes) have a significant influence on the electrochemical performance of LIBs such as volumetric/gravimetric energy density, cycle performance, output potential and safety [11-21]. However, when compared with the industrialized anode materials having high specific capacity, such as graphite (372 mAh g^{-1}), especially silicon carbon anode (greater than600 mAh g^{-1}), it has been observed that the cathode materials chiefly restrict the energy density and power density of LIBs. Over the past two decades, conventional cathode materials such as $LiCoO_2$ [22] with hexagonal layered structure and $LiFePO_4$ [23] with polyanionic olivine structure, as well as $LiMn_2O_4$ [24] with spinel structure have been extensively studied. Among them, $LiCoO_2$ (140 mA h g^{-1}) [25] is widely used in traditional 3C field, but its application in large-scale energy storage system is limited due to the lack of cobalt resources, radioactivity, high price, poor overcharge resistance and cycle performance of lithium cobalt oxide batteries [26]. The lithium ions in olivine $LiFePO_4$ (140 mAh g^{-1}) [27,28] form a continuous linear chain with two dimensional mobility, stable oxidation state, good safety, high temperature performance and long cycle life, but their electronic as well as ionic conductivities are low. Therefore, their rate performance needs to be improved. $LiMn_2O_4$ (120 mAh g^{-1}) is a low cost material, having stable structure, excellent electronic and ionic conductivity as well as safety but it suffers from capacity decay due to the structural distortion upon charge/discharge cycles [29]. Till date, traditional cathode materials are mostly used in PHEVs and EVs, but cathode materials can only deliver around 120–160 mAh g^{-1}, which have significantly hindered the far-ranging application of LIBs due to the limited specific energy. Consequently, it will be difficult to satisfy the demand for passenger cars in the future. Clearly, the pursuit for high specific energy is a key research and development direction of LIBs in PHEVs and EVs. Recently, the new generation of layered oxide cathodes, particularly the Ni-rich oxides ($LiNi_{1-x-y}M_xN_yO_2$; $x + y \leq 0.5$; M、N = Co, Mn, Al, Mg, Ti etc.) have attracted intensive attention due to their higher reversible capacity (greater than200 mAh g^{-1}) and specific energy (~800 Wh kg^{-1}) as compared to $LiCoO_2$ (140 mA h g^{-1} and 570 Wh kg^{-1}) and $LiMn_2O_4$ (120 mAh g^{-1} and 440 Wh kg^{-1}), and are entrusted with heavy task to achieve the target of 350 Wh kg^{-1} cell-level specific energy and long endurance mileage by 2025 or sooner. Notably, Ni-rich oxide cathodes like $LiNi_xCo_yMn_zO_2$ and $LiNi_xCo_yAl_zO_2$ have solidified their status in EVs. The 18650-type LIBs which utilized $LiNi_{0.8}Co_{0.15}Al_{0.05}O_2$ (NCA) as

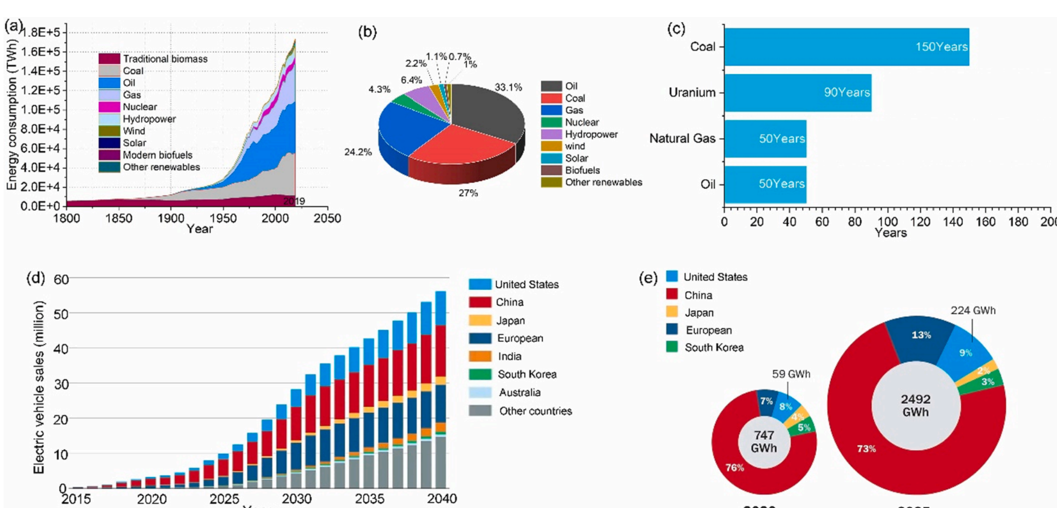

Fig. 1. (a) Global primary energy consumption by source (Primary energy is calculated based on the 'substitution method' which takes account of the inefficiencies infossil fuel production by converting non-fossil energy into the energy inputs required if they had the same conversion losses as fossil fuels.) (Source: Vaclav Smil (2017) &BP Statistical Review of World Energy). (b) Global primary energy consumption by source for 2019 (Our World in Data based on BP Statistical Review of World Energy (2020)). (c) Industry estimates of economically viable fossil fuel reserves (Source:World Coal Association, World Nuclear Association, International Gas Union Global Gas Report 2020, British Petroleum Statistical Review of world Energy 2020). (d) Annual sales of passenger pure electric vehicle (EV) and plug-in hybrid electric vehicle (PHEV) (Source: Bloomberg, electric vehicle outlook 2019). (e) Battery manufacturing capacity (Source: "lithium ion battery super factory evaluation", benchmark mineral intelligence, March 2021).

cathode materials have already been successfully used in Tesla Model 3 for EV application, with an advantage of more than 200 miles of ranges per charge. The above two cathodes were derived from $LiNiO_2$, which have a high theoretical capacity of 278 mAh g^{-1}. Multiple phase transitions rapidly deteriorate the discharge capacity of $LiNiO_2$ during delithiation while the intrinsic structural instability seriously hinders its commercial application. In order to prevent multiple phase transitions, $Li[Ni_{0.8}Co_{0.15}Al_{0.05}]O_2$ cathode materials were prepared by introducing Co^{3+} and Al^{3+} into $LiNiO_2$ to stabilize the structure. In another example, Ni was partially replaced by Co and Mn to form $Li[Ni_{0.8}Co_{0.1}Mn_{0.1}]O_2$ with a good capacity retention.

Till date, many researchers have shown great interest in Ni-rich layered materials, and numerous types of Ni-rich materials have been studied. Sun et al. synthesized Ni-rich $LiNi_xCo_yB_zO_2$ (NCB) [30] and $LiNi_xCo_yW_zO_2$ (NCW) [31] cathode materials by replacing Mn with B and W. Again, cobalt is highly expensive ($9000/ton) and also it is scarcely available in the earth's crust. Thereby, reducing or eliminating Co in Ni-rich materials has gradually become a consensus in the industry. In recent years, a renewed interest in $LiNiO_2$ with substitutions of cations other than Co, viz., $LiNi_{0.9}Mn_{0.1}O_2$ [32], $LiNi_{0.95}Mg_{0.05}O_2$ [33], $LiNi_{0.94}Al_{0.05}Mg_{0.01}O_2$ [34], and $LiNi_{0.96}Mg_{0.02}Ti_{0.02}O_2$ [35] have also been reported. However, the electrochemical performance and the control of element composition in cobalt free materials are not satisfactory. There are only a few long-term test reports that meet commercial standards. Good electrochemical performance, cost efficacy and high voltage are the notable features which have impelled high nickel and ultra-high nickel rich cathodes to be the major research interests as the next-generation of high energy density cathodes in the medium and long tenure. At the same time, some new cobalt free (LNMO: $LiNi_{0.5}Mn_{1.5}O_4$、NMA: $LiNi_xMn_yAl_zO_2$) and lithium rich (LMR: $Li_{1+n}M_{1-n}O_2$) cathodes are still in their initial stage of investigation [36]. Compared with Ni-rich cathodes, Li-rich layered oxide cathodes (LMR) can be can be represented by $x Li_2MnO_3 \cdot (1-x) LiMO_2$ (M = Mn, Ni, Co, Fe, etc.), which are generally considered to be composed of $LiMO_2$ and Li_2MnO_3 component. $LiMO_2$ have a typical rhombohedral crystal structure with $R\bar{3}m$ space group, Li^+ occupies octahedral 3b sites and TMs (Ni, Co and Mn) occupy octahedral 3a sites. The structure of Li_2MnO_3 (space group C2/m) is similar to $LiMO_2$, but one-third of the TM sites are occupied by Li^+ ions [37]. The structural transformation caused by cation migration during charge and discharge, and the activation of low potential $Mn^{4+/3+}$ redox pairs caused by the redox process of irreversible oxygen (lattice oxygen release, $O^{2-} \rightarrow O_2$). Compared with Mn and Co ions, Ni ions have higher and more stable redox potential [38]. The increase of nickel doping can improve the structural stability and oxygen redox reversibility of the material, so it can improve the capacity retention rate, inhibit the voltage attenuation, and obtain high energy density and long cycle stability [39]. In the long run, it is expected to break the monopoly of NCM and NCA in the Ni-rich cathodes and high energy density LIBs (Fig. 2).

The higher Ni content can result in higher charge–discharge capacity, however at the same time it can also be accompanied with accelerated capacity fading and poorer thermal stability as well as safety properties. The main reasons that cause capacity decay for Ni-rich cathodes can generally be summarized as following:1) environmental factors; 2) intrinsic structural factors; and 3) electrochemical parameters. The increase of nickel content makes the cathode materials more sensitive to temperature, moisture and carbon dioxide in the air, which is detrimental to the intrinsic structure and the stability of the structure during repeated charge/discharge [40]. Owing to the influencing factors of its intrinsic structure, secondary spherical particles formed by the accumulation of primary spherical particles in Ni-rich layered oxide cathode materials may lead to Li^+/Ni^{2+} mixing, thereby formation of、

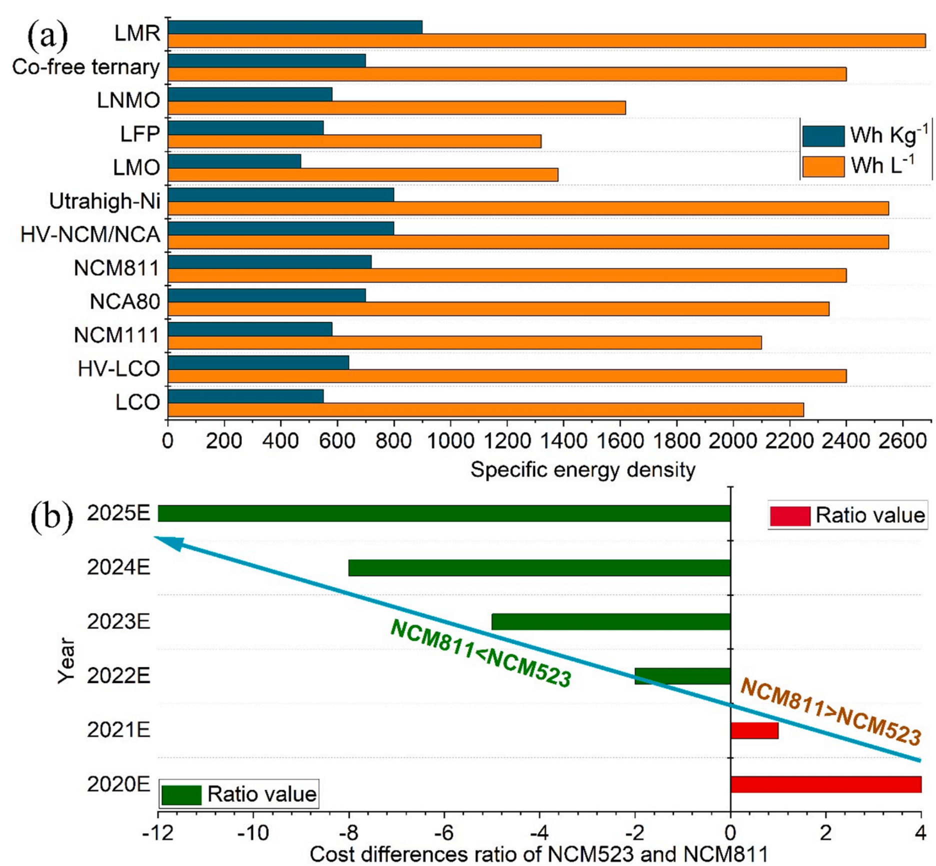

Fig. 2. (a) The mass and volume specific energy density for a series commercialized, next-generation and emerging cathodes for LIBs (LNMO: $LiNi_{0.5}Mn_{1.5}O_4$; LMR: $Li_{1+n}M_{1-n}O_2$; HV: high-voltage.). (b) The battery cell cost difference ratio of NCM523 and NCM811 in medium and long term development.

rock salt phase (NiO) and residual alkali (LiOH and Li_2CO_3) on the surface during the synthesis, diminishing the reversible capacity and stability.

In addition, the continuous Li^+ conduction channel formed by the radial distribution of grains can reduce the non-uniformity of charge distribution in the secondary particles and improve the stability of NCM during repeated charge/discharge, but it can have adverse effects on the structural integrity of the particles [41,42]. At the same time, a small number of vacancies, dislocations and lattice distortion are found as the intrinsic defects. Unstable structure of nickel-rich cathodes can be held responsible for several degradation phenomena induced by cycle and accompanied by the phase transition of defect chain reaction (DCR) [43]. The electrochemical parameters mainly include the structural degeneration of cathode material which is induced by both cycle process and the influence of discharge depth (DOD). During the cycling process, the phase transition of H2 → H3 occurs, which leads to oxygen release. The change of lattice constant/cell volume results in the occurrence of stress, which further leads to micro cracks and breakage of particles. The electrolyte immerses the particles, which further aggravates the side effects and affects the electrochemical performance. After a certain number of cycles, Ni/Co/Mn metal elements precipitate and dissolve, and the change of material structure leads to the loss of active material and decrease in capacity. Meanwhile, removal of lithium, especially in the deep charged state, involves multiple phase transitions instigating inherent instability of the materials, which hinders the further development of Ni-rich positive electrodes [44,45]. Transition metal ions and O^{2-} have energy band overlap (such as 3d orbit of Ni and 2p orbit of oxygen). Hence, with the increase of applied voltage, O^{2-} is oxidized and peroxy species or superoxide species are formed. While the electrode is deoxidized, the transition metal ions form unstable high oxidation by-products resulting in interface phase transition. Besides, the electrolyte oxidation reaction on the electrode surface can have a significant impact on the improvement of their activity (Fig. 3) [46].

The performance degradation of subsequent cycles can be attributed to several causes like complex chemical and mechanical interactions among lithium diffusion, anisotropic lattice strain, surface oxygen consumption and cathode particle deterioration. Among them, the transient performance of particle size of material remains the key factor of diffusion and deterioration process. Once the electrochemical process is interrupted for diffraction measurement, the charge rebalancing will occur, the movement of lithium ions will be along the radial direction of the particles and the anisotropy of the lattice parameters will be masked. Therefore, it is indispensable to use high-resolution experimental technology (such as submicron focused operando synchrotron radiation X-ray diffraction and in situ stacking tomography nano imaging) in time and space dimensions in order to explore the undisturbed charge discharge process for better understanding of the potential decomposition degradation mechanism [42] (Fig. 3). Researchers have carried out a series of improvement strategies such as lattice doping, surface coating, morphology design, regulating the crystal structure and electrolyte modification on the performance degradation mechanism of Ni-rich layered oxide cathode materials. In addition to the conventional doping, coating and electrolyte modification, the current research technologies for large-scale production include single crystal

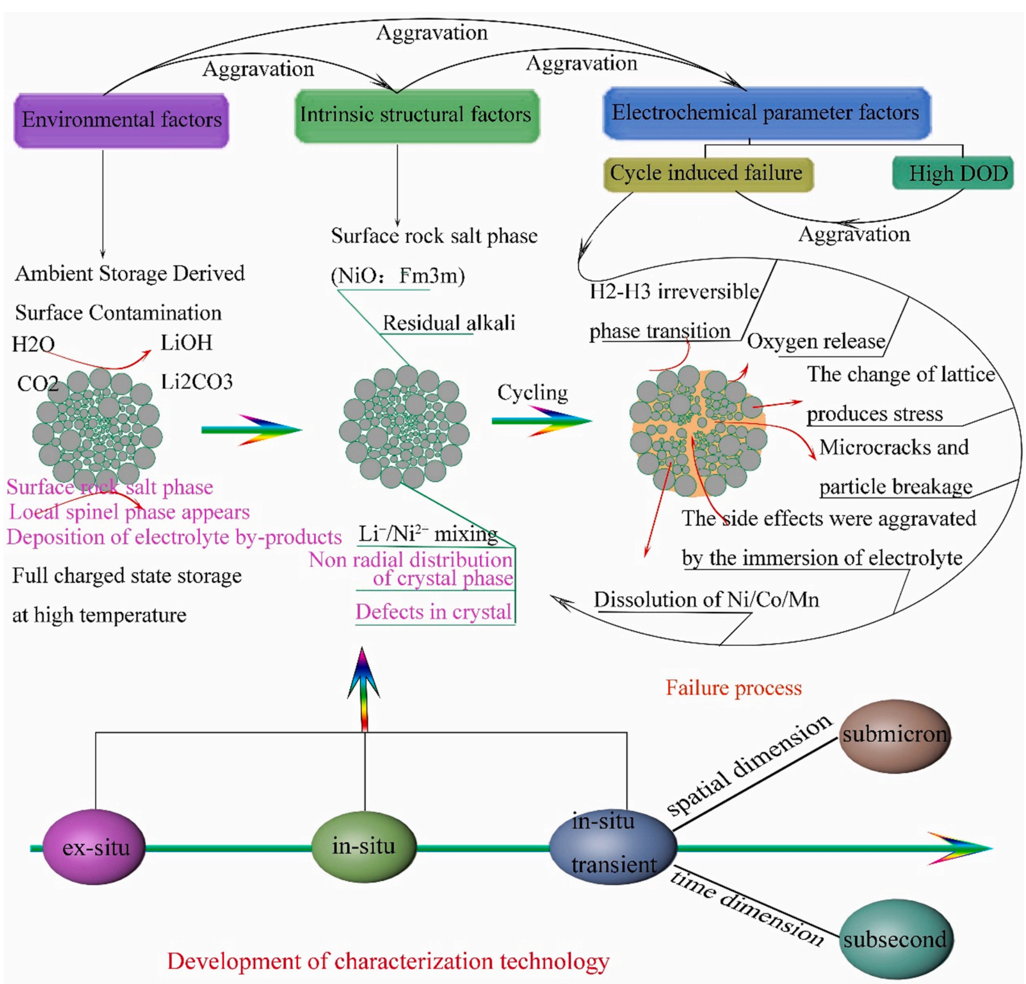

Fig. 3. Schematic diagram of failure factors, evolution process and characterization technology development of Ni-rich layered cathodes.

preparation [47] and regulating the morphology (core–shell, radial primary particles, etc.) [48,49].

In this paper, the synthesis, structure and redox mechanisms of Ni-rich cathode materials are briefly introduced. As a key point, we have mainly focused on the failure mechanism of Ni-rich cathode materials, through a large number of recent research progress analyses. For the first time, the three factors and their mutual influence on the failure of Ni-rich cathode materials have been summarized. Furthermore, combined with some advanced characterization techniques, the latest capacity failure mechanism (such as temperature effect at full charge; charge distribution guided by grain crystallographic orientations in poly-crystalline battery materials; structural evolution induced by crystal defects; influence of discharge depth et al.) of Ni-rich cathode materials and the modification approaches to solve these problems are analyzed (Fig. 4). Also, a detailed venation chart, depicting the remaining challenges and perspectives of Ni-rich oxide materials in recent years has been drawn. Finally, the new insights of Ni-rich cathode materials are discussed, which expand the research fields and promote their practical applications.

2. Preparation methods and electrochemical performances

The preparation methods have a significant influence on the micro-structure and electrochemical properties of Ni-rich layered materials. High temperature solid phase method, co-precipitation method, sol–gel method, spray drying method and combustion method are the few major synthesis techniques discussed here in detail.

2.1. High temperature solid phase method

In high temperature solid state method, the lithium source and the transition metal salt in accordance with the stoichiometric ratio are directly taken in the ball mill. The uniform mixture thus formed is pre-sintered at low temperature followed by sintering of the same at a higher temperature, to obtain the desired powder products. The non-uniformity of reaction during the synthesis has been considered as the major drawback of this method. The morphology and particle size distribution of the prepared materials are quite different. Consequently, only a few researchers use this method to synthesize Ni-rich cathode materials, and it is also not suitable for industrial production. Caballero et al. [50] developed a simple, rapid and direct method for synthesizing nano-crystalline oxides with either layered or spinel structures, including $LiMn_2O_4$, $LiCoO_2$, $LiNi_{0.5}Mn_{1.5}O_4$, and $LiCo_{0.5}Ni_{0.5}O_2$. The approach is based on the thermal decomposition by one step solid-state metathesis reactions of mixed nano-crystalline oxalates formed by grinding oxalic acid and hydrated salts. Saavedra-Arias et al. [51] synthesized $LiNi_{0.8}Co_{0.1}Mn_{0.1}O_2$ cathodes by solid-state reaction route using Li_2O, NiO, Co_3O_4 and MnO_2. The reagent mixtures were first ball-milled for 24 h in isopropanol and the resulting mixture was dried at 60 °C. Subsequently, the powder was calcined at 450 °C for 4 h and sintered at higher temperatures. X-ray diffraction (XRD) and Raman scattering (RS) spectra of various stages of lithiation-delithiation processes portrayed that the well layered structure is maintained throughout the electrochemical process along with the systematic change of lattice parameters in the range of 3.0–4.5 V. The initial discharge capacity obtained was 132 mAh g^{-1}

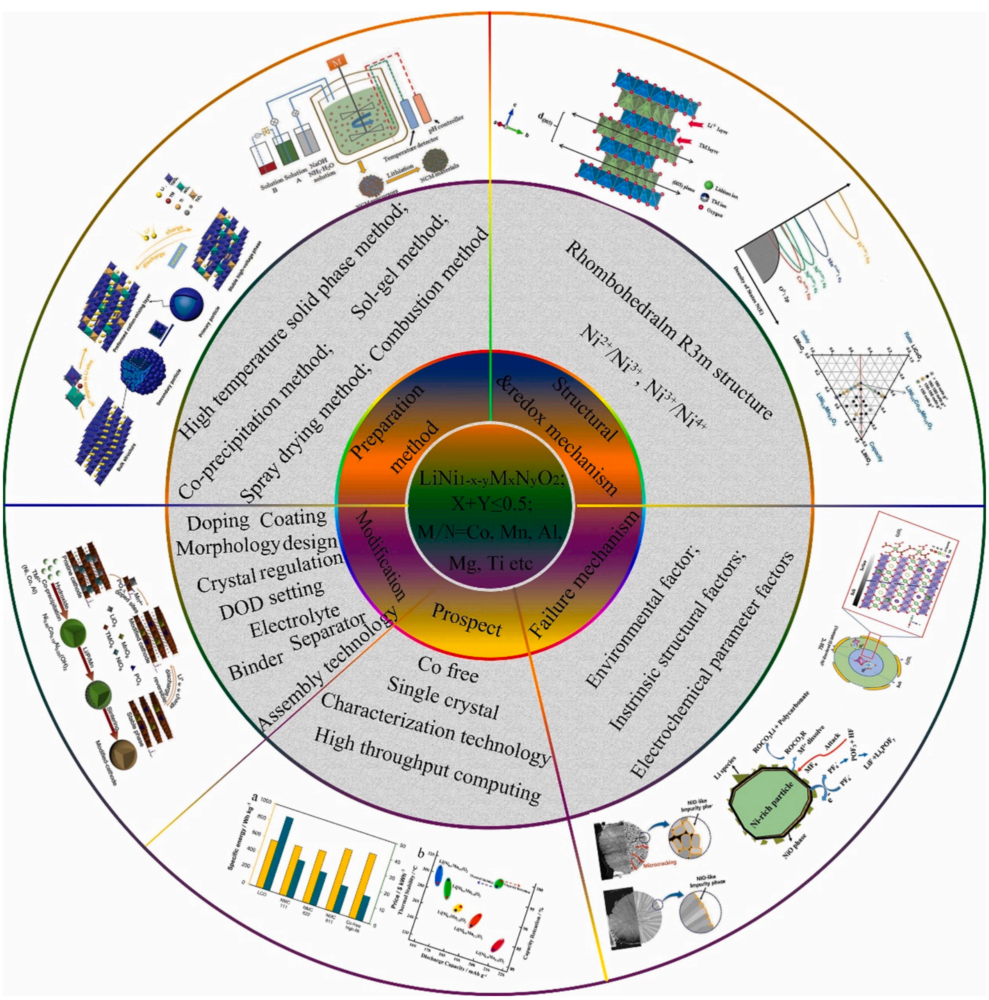

Fig. 4. Schematic diagram of structural characteristics, preparation method, failure mechanisms and modification of Ni-rich layered cathodes.

while the capacity retention rate was 86% after 20 cycles.

2.2. Co-precipitation method

Co-precipitation method can address the problems of inhomogeneous mixture and wide particle size distribution which were found in traditional solid-phase method. By controlling the concentration of raw materials, droplet acceleration, stirring speed, pH value and reaction temperature, core–shell structure, spherical, nano flower and other morphologies with uniform particle size distribution can be prepared. The development of Ni-rich materials cannot be separated from the promotion of precursors. At present, Ni-rich materials face problems of secondary spherical particles breaking and pulverizing, which not only prevents it from participating in the charging-discharging process, but also creates more side reactions in the new interface of cracks. The above problems deteriorate the comprehensive performance in LIBs. In order to obtain a stable granular crystal structure and excellent comprehensive performance, it is necessary to design the whole process from the precursors. The co-precipitation method is a feasible approach for industrialized preparation of Ni-rich materials precursors [52]. For better understanding of the growth mechanism of Ni-rich precursors, a brief description of their formation has been provided. The precursor is prepared by mixing Ni, Co and Mn salts together and forming a soluble mixed solution. Hereafter, NH_3 and NaOH are further added to the former solution to form Ni-rich materials precursors by controlled reaction conditions. The reaction equations are as follows.

$$M + NH_3 \rightarrow [M(NH_3)_n]^{2+} \quad (1)$$

$$[M(NH_3)_n]^{2+} + OH^- \rightarrow M(OH)_2 + 3NH_3 \quad (2)$$

From the above equation it can be seen that M salt first reacts with the $NH_3{\cdot}H_2O$ to form $[M(NH_3)_n]^{2+}$, and then OH^- replaces to form $M(OH)_2$. In order to show the reaction process more vividly, Yang et al. [53] used the stick model in the above equation. Reaction equations and the stick growth model can provide a clear picture of the growth process of primary particles. By controlling the reaction conditions viz. temperature, pH, stirring and flow rate, the primary particles were gradually agglomerated into spherical secondary particles. Islam et al. [54], through his experiments, offered a better understanding of the influence of reaction conditions on the co-precipitation process. $LiNi_{0.6}Mn_{0.2}Co_{0.2}O_2$ materials were synthesized by co-precipitation method and the effects of the synthesis parameters such as stirring speed, pH and sintering temperature on the structural characteristic, particle size, morphology and cyclic stability were discussed in detail. The results show that the pH is the most important factor for the synthesis of precursor, because it affects the tap density and the morphology. The pH value of 10.8 exhibits the highest tap density. Stirring speed has a great impact on the crystallization process. As the stirring speed increases, the particle morphology changes from irregular agglomeration to dense spherical particles. However, when the stirring speed reached 1200 rpm, the particle morphology was destroyed, which resulted in cracking. XRD peaks showed that with the upsurge of sintering temperature from 780 °C to 860 °C, the value of I(0 0 3)/I(1 0 4) increased signifying a better layered structure. However, due to Li/Ni mixing, when the temperature escalated to 900 °C, the value of I(0 0 3)/I(1 0 4) decreased. The samples, when sintered at 860 °C, exhibited best electrochemical properties (168 mAh g^{-1} at 0.5C). Park et al. [55] synthesized $LiNi_{0.90}Co_{0.05}Mn_{0.05}O_2$ cathode material by co-precipitation method. The synthesized cathode material was charged and discharged at a current density of 0.1C in the voltage window ranging from 2.7 to 4.3 V. The discharge specific capacity of the composite was found to be 230 mAh g^{-1}, and the capacity retention was 89% after 50 cycles. $LiNi_{0.95}Co_{0.05}O_2$ cathode material was synthesized by Wu et al. [56] via co-precipitation method and exceptional cycle ability with capacity retention of 69.68% after 100 cycles at 0.1C was demonstrated by the material.

2.3. Sol-gel method

Sol-gel method is a synthesis technique which involves compounds containing high chemically active components as precursors. These raw materials are mixed in the liquid phase and are hydrolyzed. Thereafter, chemical reactions condense and form a stable sol–gel system/phase. The gel with a three-dimensional spatial network structure is formed by aging and slow aggregation of colloidal particles. The stoichiometric ratio of this method is precisely controlled, and some trace elements can be doped uniformly and quantitatively at the molecular level. The reaction is easy to execute, the required temperature is low, with good morphology [57]. Chandrasekar et al. [58] prepared $Ni_{0.7}Co_{0.15}Mn_{0.15}(OH)_2$ precursor by a solvothermal method using Ni$(CH_3COO)_2$, Co$(CH_3COO)_2$ and Mn$(CH_3COO)_2$. Stoichiometric amount of metal acetate was first dissolved in 50 ml of anhydrous alcohol and deionized water having a volume ratio of 4:1 and thereby transferred to a teflon-lined stainless-steel autoclave followed by heating at 200 °C for 12 h. Finally, the obtained slurry was filtered and washed with anhydrous alcohol and then dried. Li_2CO_3 and the $Ni_{0.7}Co_{0.15}Mn_{0.15}(OH)_2$ precursor in accordance with the stoichiometric ratio of 1.05:1 were thoroughly blended and the mixture was sintered at 480 °C for 5 h and 800 °C for 12 h in an atmosphere of O_2. Lu et al. [59] also prepared NCM811 cathodes by sol–gel and co-precipitation methods. The XRD patterns depicted that NCM811 positive electrode synthesized by these two methods can form a good layered structure. Rietveld refinement revealed some disparity in the degree of cation disorder between the two materials, among which the samples prepared by sol–gel method showed lower Li/Ni cation disorder. SEM and BET measurements revealed that the sol–gel samples were composed of relatively small aggregate particles with larger BET surface area compared to the co-precipitation samples. The electrochemical test showed that the material prepared by sol–gel method delivered better initial discharge capacity of 200 mAh g^{-1} with capacity retention rate of 82.2% after 50 cycles at 0.5C.

2.4. Spray-drying method

Spray drying method uses atomizing equipment to atomize the reaction solution and leads it into the reactor, so that the solution gets rapidly evaporated and dried. The process is simple, can prepare a large number of precursors in a short time, and the raw materials can be uniformly mixed at atomic level, with extraordinary consistency of particle size and regular morphology making it an efficient synthesis method. Li et al. [60] prepared $LiNi_{1/3}Mn_{1/3}Co_{1/3}O_2$ cathodes by a spray dry process between $Ni(CH_3COO)_2{\cdot}4H_2O$, $Mn(CH_3COO)_2{\cdot}4H_2O$, $Co(CH_3COO)_2{\cdot}4H_2O$ and $LiNO_3$. The stoichiometric amount of metal acetates were first dissolved in deionized water to obtain the starting solution and then was pumped into a spray dry instrument followed by pre-heating at 400 °C and sintering for 15 h in air. Yue et al. [61] also prepared micron-sized $LiNi_{0.6}Co_{0.2}Mn_{0.2}O_2$ cathode material at various sintering temperatures by spray drying method with a molar ratio of Li/Me = 1.04, and studied the effect of sintering temperature on the crystal structure, morphology and electrochemical properties of the material. The results showed an enhancement in the volume of a and c with the rise of sintering temperature. The particle prepared at 850 °C was an irregular primary aggregation with a size of 1 μm as well as of low cationic mixing degree. It exhibited a discharge capacity of 173 mAh g^{-1} of 0.1C and capacity retention of 89% after 50 cycles, which proved to be better than materials prepared at other temperatures.

2.5. Combustion method

The combustion method involves mixing of the raw metal salt with the fuel to form a dry gel at low temperature. Next, the dry gel is heated to a high temperature to make the system undergo combustion and exothermic reaction occurs resulting in the formation of precursor powder comprising of extremely fine particles. The powder is then roasted at a high temperature to obtain the final product. Ahn et al. [62] prepared micron-sized $LiNi_{0.6}Co_{0.2}Mn_{0.2}O_2$ cathode material by this method. Scanning electron microscopy (SEM) showed that a large number of spherical particles with a diameter of 100 nm agglomerated into secondary particles. The ratio of $Ni^{3+}/(Ni^{2+}+Ni^{3+})$ prepared at 800 °C was found close to their theoretical value. It exhibited a discharge specific capacity of 170.1 mAh g^{-1} while the capacity retention rate was 98.2% after 30 cycles.

3. Structure and redox mechanisms

The general structure of nickel rich layered oxide cathode materials $LiNi_xCo_yMn_zO_2(x > 0.6)$ is in form of a rhombohedral$R\overline{3}m$ structure, which can be derived from the ordered rock-salt structure of α-$NaFeO_2$ (Fig. 5) [63,64]. Li occupies octahedral 3b sites and Ni, Co and Mn (TMs) occupy octahedral 3a sites disorderly [65,66]. The formation of the whole crystal is designed by alternate stacking of $[MO_6]$ octahedron layer and $[LiO_6]$ octahedron layer [67], which is appropriate for lithium ion intercalation and de-intercalation. However, the ionic radius of Ni^{2+} (0.069 nm) is approximately similar to that of Li^+ (0.076 nm). Hence, Ni^{2+} can easily occupy Li^+ slabs and vice versa, resulting in the cationic mixing, increase of cell parameter a, and the weakening of the intensity of the diffraction peak (0 0 3) [68,69]. Cation disordering between these two sites of Li^+ and Ni^{2+} can compromise the structural stability of nickel rich layered oxide cathode materials. This is because during sintering, Ni^{2+} is oxidized to Ni^{3+} at a high temperature and oxygen atmosphere. However, the energy barrier of Ni^{2+} to Ni^{3+} is elevated, making it difficult for Ni^{2+} to get completely oxidized even in pure oxygen atmosphere. The remaining Ni^{2+} will still occupy 3a sites, which will further reduce the cation mixing. In order to preserve the charge balance, part of Ni^{2+} will occupy 3b sites. In addition, while charging, the minimal valence nickel in the transition metal layer will migrate to the lithium layer, occupying the lithium vacancy, and form the cation mixing arrangement.

The redox reactions of $Ni^{2+}/Ni^{3+}/Ni^{4+}$, Co^{3+}/Co^{4+} electron pairs mainly take place during the charging and discharging process. Mn has no electrochemical activity and does not participate in the redox reaction, but has a role in stabilizing the materials. Nevertheless, the structure of nickel rich layered oxide cathode materials is very unstable due to the release of a large number of Li^+. Material cycle capacity decay and deterioration in its thermal stability can be considered as its two significant outcomes. The ionic radius of Ni^{2+} in Li layer is less than that of Li^+. This reduces the thickness of inter-wafer and oxidizes it into Ni^{3+} or Ni^{4+} during charging, resulting in the partial collapse of inter-wafer space. Also, during discharging, it makes the ion embedment of Li^+ more difficult, thus reducing the reversible capacity of materials. When Li^+ enters the transition metal layer, the thickness of the main wafer will get enlarged. Thereby, it will be tough to get detached which in turn will depreciate the electrochemical performance of the material. Therefore, the smaller the inter-wafer thickness, the more difficult it is for Li^+ to be re-embedded. [70-73] The degree of ion mixing can be characterized by c/a and I(0 0 3)/I(1 0 4) value. When c/a greater than 4.9 and I(0 0 3)/I (1 0 4) greater than 1.2, the degree of ion mixing is low. [74,75] In addition, (0 0 6)/(1 0 2) crystal plane and (1 0 8)/(1 1 0) crystal plane have two pairs of splitting degree of the diffraction peaks [75,76], which reflect the integrity of the layered structure and have a greater impact on the electrochemical properties of nickel rich layered oxide cathode materials. [77-81] The greater splitting degree of the two pairs of diffraction peaks is accountable for the complete layered structure of $NaFeO_2$, as well as for improved electrochemical properties. Therefore, during synthesis, it is necessary to maintain a suitable Li^+/Ni^{2+} ratio, low mixing degree and complete layered structure for improving the electrochemical performance of nickel rich layered oxide cathode materials. Increasing Ni content can intensify the material capacity but decrease the cycle performance and stability. Increase in Co content can inhibit phase transformation and improve the rate performance. [72,73,82,83] Increasing Mn content can improve the structural stability, but reduce the capacity. Enterprises can reduce the content of Ni and increase the proportion of Co and Mn in the production process in order to enhance the cycle performance and thereby attaining a prolonged product life. [84,85] Moreover, Ni gains and loses electrons in the oxidation–reduction process, while it is difficult for Co^{3+} to get oxidized in nickel rich layered oxide cathode materials. The 3 de_g energy levels of Ni^{2+}/Ni^{3+}, Ni^{3+}/Ni^{4+} are higher than those of Co^{3+}/Co^{4+} $3dt_{2g}$ (Fig. 6**a**). [86] Therefore, in the charging process, Ni^{2+}/Ni^{3+}, Ni^{3+}/Ni^{4+} oxidation process takes place preferentially, and the corresponding HOMO energy levels are higher than Co^{3+}/Co^{4+}. The charge–discharge voltage of nickel rich layered oxide cathode materials is less than $LiCoO_2$. At most 0.8 lithium can be separated from the layered structure under the same voltage [87,88], so high nickel containing materials can transfer more electrons than $LiCoO_2$, that is, their charge–discharge capacity is higher than $LiCoO_2$. [89,90] In addition, Co^{3+}/Co^{4+} t_{2g} overlaps with the top of O^{2-} 2p energy level, while Ni^{3+}/Ni^{4+} overlaps only by a small part, indicating that $LiNiO_2$ is more stable at higher voltage. During the charging and discharging process of nickel-rich layered oxide, the valence state of Mn^{4+} remains unchanged, which stabilizes the layered structure of the material, hence, the safety is improved. The capacity is mainly provided by Ni^{2+}/Ni^{3+}, Ni^{3+}/Ni^{4+} pairs. The addition of Co can improve the conductivity and rate performance from the synergistic effects of Ni, Co and Mn (Fig. 6**b**) [12].

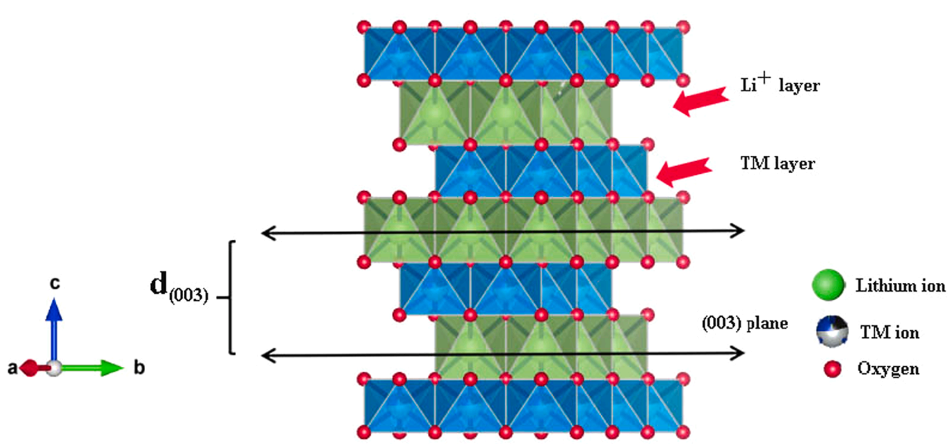

Fig. 5. Crystal structure of layered $LiNi_xCo_yMn_zO_2$ cathodes.

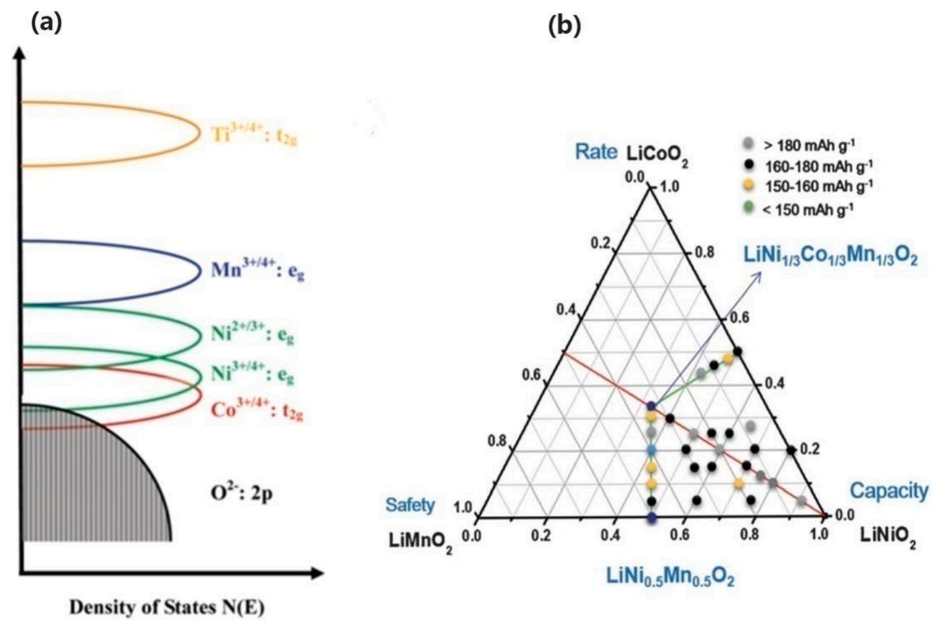

Fig. 6. (a) Schematic diagram of energy levels of layered electrons. Reproduced with permission. [86] Copyright 2011, American Chemical Society. (b) Compositional phase diagrams of lithium stoichiometric-layered transition-metal oxide: $LiCoO_2$-$LiNiO_2$-$LiMnO_2$. Reproduced with permission.[12] Copyright 2008, Royal Society of Chemistry.

4. Capacity failure mechanism and characterization technology

The failure of nickel rich layered oxide cathode materials are related not only to its surface rock salt phase (NiO), residual alkali and its internal structural (Li^+/Ni^{2+} mixing) characteristics, but also to a series of complex evolution processes during lithiation-delithiation as mentioned above. Further elucidating the failure mechanism has a great significance in the preparation and development of nickel rich cathode materials. With the development of characterization technology, especially in the application of in-situ electrochemical characterization and in-situ electrochemical transient characterization technology, these experimental techniques with high resolution in time and space dimension can demonstrate the potential degradation mechanism at a higher depth.

4.1. Li^+/Ni^{2+} cation mixing

During the preparation of Ni-rich oxide cathodes, a complete oxidation of Ni^{2+} to Ni^{3+} is extremely difficult. As a result, there remains a small amount of Ni^{2+} in Ni-rich oxide cathodes. Furthermore, the radius of Ni^{2+} (0.069 nm) is very close to that of Li^+ (0.076 nm), and Ni^{2+} can easily occupy the 3b sites of Li^+, resulting in the Li/Ni mixing. [63] Li/Ni mixing not only occurs in the synthesis of materials, but also during the charge–discharge process, which significantly affects the electrochemical properties including initial capacity, reversible capacity and cycle performance. During first charging, Li^+ in both the lithium layer and the transition metal layer can be deintercalated, but in the first discharge, part of Li^+ cannot return to the positive lattice due to the Li^+/Ni^{2+} mixing, which results in the lower efficiency (typically less than 90%) and increase in the irreversible capacity. When Ni^{2+} occupies the lithium layer, the thickness of the inter-granular layer will be reduced, and the redox reaction of Ni^{2+}/Ni^{3+}, Ni^{3+}/Ni^{4+} will occur during the charging process. The ionic radius will be further reduced, which will cause the partial structural collapse of the space of the inter-granular layer, hinder the migration of Li^+ during the charging and discharging process, increase the impedance, and lead to poor cycle stability. When Ni^{2+} occupies the Li^+ site completely, the space group structure of cathode materials changes from layered phase ($R\bar{3}m$) to the spinel-like phase ($Fd\bar{3}m$) and rock-salt phase ($Fm\bar{3}m$) during cycling at an elevated temperature, which in turn increases the diffusion of Li^+ and induces poor thermal stability [91]. Cation mixing occurs not only during the synthesis of nickel rich cathode materials but also during the electrochemical cycling process. The processes are represented by the reactions which are as follows [52,92,93]:

$$3Li_xNiO_2\ (R\bar{3}m) \rightarrow Li_xNi_2O_4\ (Fd\bar{3}m) + NiO\ (Fm\bar{3}m) + xLi_2O \quad (3)$$

$$Li_xNi_2O_4\ (R\bar{3}m) \rightarrow 2NiO\ (Fm\bar{3}m) + x/2\ Li_2O + (4\text{-}x)/2O_2 \quad (4)$$

$$3Li_xNiO_2\ (R\bar{3}m) \rightarrow 3NiO\ (Fm\bar{3}m) + 3x/2\ Li_2O + (6\text{-}3x)/4\ O_2 \quad (5)$$

New characterization techniques can help to further analyze the structural changes caused by cation mixing. For instance, Kim et al. [94] reported the structural degradation mechanism of $LiNi_{0.6}Co_{0.2}Mn_{0.2}O_2$ electrode by HAADF-STEM analysis. They realized that the surface crystal structures suffer from an irreversible transition from the pristine rhombohedral structure to a mixture of spinel as well as rock-salt phases as shown in (Fig. 7**a-b**). In addition, Han et al. [95] also exemplified that $LiNi_{0.8}Co_{0.8}Mn_{0.1}O_2$ material's surface has a thin cation disordered layer during the synthesis process. Both regions 1 and 2 exhibit an uneven NiO-type cation mixed layer with a thickness of 1–2 nm (Fig. 7**c-d**). Zou et al. [96] also observed the crystal structure rearrangement after lithium deintercalation by using transmission electron microscope (TEM). Some regions of the layered surface changed into layered/rock salt mixed structure. The structure gradually changed from the inside to the surface of the material particles, respectively: ordered layered structure (α-$NaFeO_2$), partially ordered structure and disordered rock salt phase structure (NiO). This transformation can be attributed to the mixture of transition metal ions and lithium ions along with the formation of rock salt phase as the precursor of particle crack (Fig. 7**e-g**). Zhao et al. [97] studied the phase transformation caused by mixed cation in the preparation of $LiNi_{0.8}Co_{0.2}O_2$, and optimized the sintering process (sintering temperature, sintering atmosphere and holding time), which greatly reduced the loss of Li and the formation of NiO rock salt phase on the surface of the structure. It also facilitated in obtaining a higher order $LiNi_{0.8}Co_{0.2}O_2$ layered structure and the mixed discharge rate of Ni^{2+}/Li^+ ions was found to be less than 2%. The specific capacity of the optimized high nickel layered anode material under wide working voltage (2.7–4.6 V) range reached more than 220 mAh g^{-1}, and the cycle stability was significantly improved (Fig. 7**h**). Duan et al. [98]

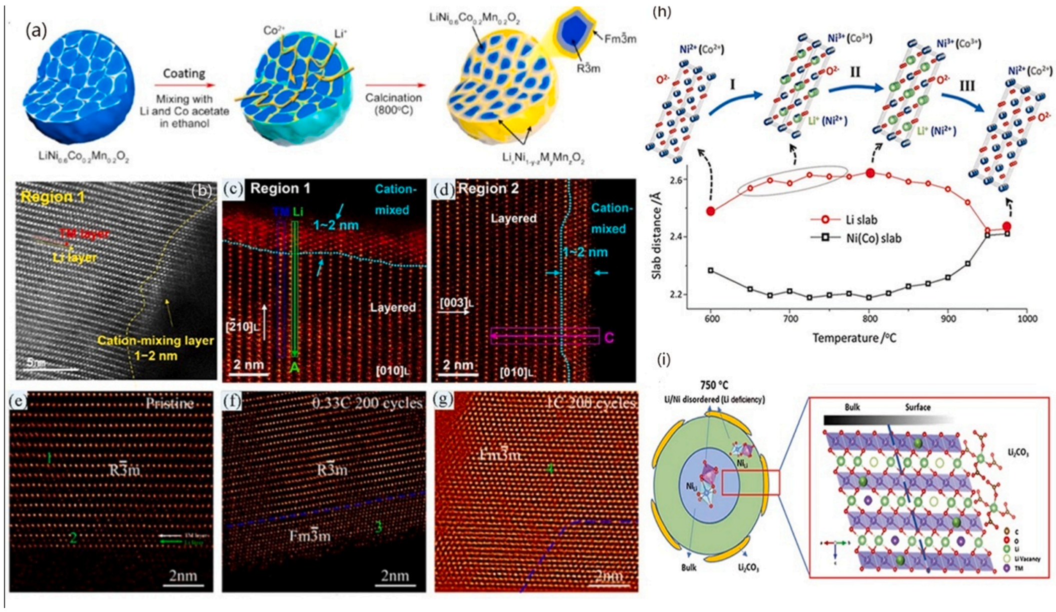

Fig. 7. Illustrations of the phase transformation from well-ordered layered structure (R-3 m) to the disordered spinel structure (Fd-3 m) and/or the rock-salt structure (Fm-3 m). (a) Schematic diagram of the surface treatment on the primary particles. (b) HAADF-STEM images of 622. Reproduced with permission.[94] Copyright 2015, American Chemical Society**.** (c-d) STEM images of pristine 811. Reproduced with permission.[95] Copyright 2018, American Chemical Society. (e) HAADF-STEM image of the pristine sample showing the majority of the bulk maintains R3¯m structure. The white and green arrows point to the TM layer and Li layer. (f and g) HAADF-STEM image of the 200-cycle $LiNi_{0.76}Co_{0.10}Mn_{0.14}O_2$ at 0.33C and 1C. The blue dashed lines outline the boundary of the converted phase, below and above which are the disordered rock salt and layered structure. Reproduced with permission.[96] Copyright 2018, American Chemical Society. (h) Schematic illustration of the phase evolution, cationic ordering of the intermediates. Reproduced with permission.[97] Copyright 2016, Wiley-VCH. (i) Schematic illustrations of how cationic ordering is coupled to surface reconstruction of NMC71515 under different sintering temperatures. Reproduced with permission.[98] Coyright 2019, The Royal Society of Chemistry. (For interpretation of the references to color in this figure legend, the reader is referred to the web version of this article.)

concluded that surface reactions have substantial impacts on the cationic ordering/disordering kinetics in the bulk. Insufficient sintering temperatures do not provide enough driving force for Li_2CO_3 decomposition as well as Li-ion diffusion during the ordering process, leading to the cation mixing Li^+ and Ni^{2+} (Fig. 7**i**). In order to gain a deeper understanding of the correlation between surface chemistry and performance decay, Zhang et al. [99] synthesized nickel rich single crystal cathode materials and used operando X-ray spectroscopy imaging and nano-tomography to monitor the compositional and structural evolution before and after 200 cycles. The redox reaction occurred along all directions and phase-transition fronts propagated drastically during the initial cycle, indicating a high electrochemical reversibility. Nevertheless, high reversibility failed to survive after 200 cycles. Operando X-ray spectroscopy imaging and nano-tomography chemical phase mapping unambiguously revealed the above outcomes. Four representative regions from the bulk to the surface were selected and the corresponding content of Ni oxidation states was illustrated. The 2D histogram highlights inhomogeneous Ni oxidation state distribution within the single crystal particle. Reaction heterogeneity and high irreversibility are ascribed to the characteristics of surface chemicals rock-salt phase on pristine single crystal cathodes, which may induce heterogeneous internal strain within the particle, and further results in the structural/performance degradation, as evidenced from the chemical composition analysis.

4.2. Surface side reaction

Due to the volatilization of lithium at high-temperature calcination, excessive lithium is often needed in the preparation of nickel-rich layered oxide cathode materials ($LiNi_{1-x}M_xO_2$; $x \le 0.5$; M = Co, Mn, Al, Mg, Ti etc). The remaining active lithium oxides (Li_2O, Li_2O_2) adhere to the surface of the materials, react with H_2O and CO_2 in the air, and form LiOH and Li_2CO_3 layers (Fig. 8) [100]. The Ni content increases by over 70 % and have a dynamic high affinity towards moisture and CO_2 in ambient air. They primarily react to form LiOH, Li_2CO_3 on the surface, which is commonly termed as "residual lithium". When Ni-rich layered oxide cathode materials ($LiNi_{1-x}M_xO_2$; $x \le 0.5$; M = Co, Mn, Al, Mg, Ti etc.) are exposed in air, they are more likely to absorb CO_2 and H_2O in the air to generate CO_3^{2-} and OH^-, and further react with residual lithium to generate Li_2CO_3 and LiOH. In addition, NiO was found to form on the surface of Ni-rich cathodes because of the exhaustion of Li and evolution of lattice oxygen (Fig. 8**a**). The reactions are stated as follows [101-105]:

$$Li_2O + H_2O \rightarrow 2LiOH \quad (6)$$

$$Li_2O + CO_2 \rightarrow Li_2CO_3 \quad (7)$$

$$2Li_2O_2 + 2CO_2 \rightarrow 2Li_2CO_3 + O_2\uparrow \quad (8)$$

$$Li_2O_2 + H_2O \rightarrow 2LiOH + O_2\uparrow \quad (9)$$

$$3LiMO_2 + 2xH_2O + xCO_2 \rightarrow 3Li_{1-x}H_xMO_2 + xLiOH + xLi_2CO_3 \quad (10)$$

The existence of Li_2CO_3 and LiOH will cause several complications. (1) Li_2CO_3 and LiOH not only consume Li^+ in the material, but also have no electrochemical activity. This further instigates capacity attenuation. Moreover, dense Li_2CO_3 layer on the materials surface will hinder the Li^+ diffusion, and cause irreversible capacity loss in the process of cyclic charging and discharging. Further decomposition of Li_2CO_3 during high-voltage charging generates CO_2 inside the cell, thus threatening the safe operation of the battery (Fig. 8**b-c**). (2) LiOH reacts with PVDF and $LiPF_6$, which has a negative effect on battery process and performance. In the preparation of Ni-rich cathodes slurry, PVDF dissolves in NMP and the basic groups on the surface of the material attack the adjacent C-F and C-H bonds. PVDF is also prone to bimolecular elimination reaction, forming a part of C = C bond with the molecular chain. It transforms the slurry into a gel state and restrains from adequate coating. (3) LiOH reacts with Al foil as shown below:

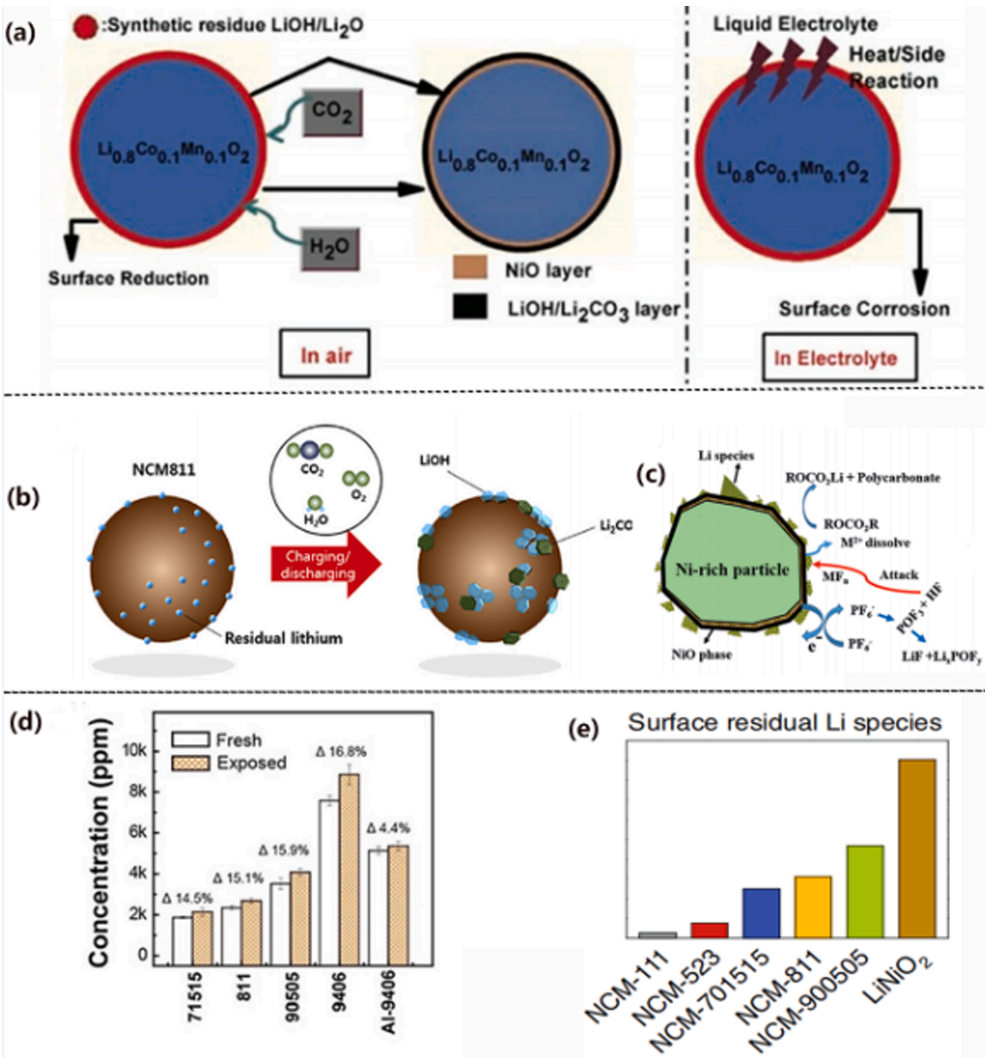

Fig. 8. (a) Scheme of $Li(Ni_{0.8}Mn_{0.1}Co_{0.1})O_2$ and its impact on suppressing unfavorable side reactions at the cathode–electrolyte interface. (b). Residual lithium change of NCM811 during charging/discharging. Reproduced with permission.[107] Copyright 2019, Elsevier. (c) The microstructure and composition of the solid-electrolyte interface at the surface of Ni-rich cathode materials. Reproduced with permission.[12] Copyright 2015, Wiley-VCH. (d) Concentration of residual Li species on high-Ni layered oxides with various nickel contents before and after being exposed to ambient air for 30 days. (e) accumulation of surface residual Li compounds. Reproduced with permission. [106] Copyright 2018, Wiley-VCH.

$$OH^{-}+2\,Al + 6\,H_2O \rightarrow 6\,OH^{-}+2\,Al(OH)_3 + 3\,H_2 \quad 6\ (11)$$

After the corrosion of Al, the electrochemical performance and safety of the battery is utterly affected. (4) LiOH also reacts with $LiPF_6$, which consumes Li^+ in electrolyte and generates HF gas. It can corrode the metal parts inside the battery and cause battery leakage. Moreover, HF can destroy SEI and react with SEI continuously.

$$4LiOH + LiPF_6 \rightarrow Li_3PO_4 + 2LiF + 4HF\uparrow \quad (12)$$

$$RCO_3Li + HF \rightarrow RCO_3H + LiF \quad (13)$$

$$2RCO3Li + LiPF_6 \rightarrow 2LiF + 2RF + LiPO_2F_2 + 2CO_2\uparrow \quad (14)$$

$$RCO3Li + LiPF_6 \rightarrow 2LiF + 2RF + POF_3 + CO_2\uparrow \quad (15)$$

In summary, degradation caused in the process of material synthesis, storage and charge discharge of lithium-ion batteries initiates from the modification of the surface structure. It is also found that different materials have different reactivity to carbon dioxide and water in the air. You et al. [106] showed that the residual lithium content on the surface of the same composite material increases with the increase in nickel content (71715, 811 and 9055) (Fig. 8**d-e**).

4.3. Irreversible phase transition

The irreversible phase transformation of Ni-rich layered oxide cathode materials occurs easily in the state of deep lithium intercalation, leading to the degradation of the particle surface structure. In the process of charging and discharging, phase transformation occurs four times along with the intercalation and deintercalation of lithium ions. When the voltage is less than 4.2 V, the transformation takes place from hexagonal phase H1 → monoclinic phase M → hexagonal phase H2; when the voltage is greater than 4.2 V, the transformation takes place from hexagonal phase H1 → monoclinic phase M → hexagonal phase H2 → H3; when the voltage is greater than 4.2 V, H2 → H3 is an irreversible phase transition, which seriously affects the cyclic stability of nickel-rich layered oxide cathode materials.

Zhang et al. [108] introduced the H2-H3 phase transition of $LiNi_{0.80}Co_{0.10}Mn_{0.10}O_2$ near 4.1 V, accompanied by the release of lattice oxygen. The precipitated lattice oxygen oxidizes the electrolyte, and transforms the material from layered structure to spinel structure and rock salt structure, resulting in the continuous decline of discharge capacity and voltage platform of $LiNi_{0.80}Co_{0.10}Mn_{0.10}O_2$ under high voltage (Fig. 9**a-b**). In the process of charge and discharge of nickel rich cathode materials, the existence of H3 phase can be used as a performance index to reflect the state of high capacity transmission and high degree of lithium removal. In fact, a large number of Li vacancies in the state of highly deintercalation will weaken the structural stability and induce structural transition. In order to improve the reversibility of H2-H3 phase transformation in nickel-rich layered oxide cathode materials, element of doping radius similar to Li^+ (0.076 nm) can improve the stability. Wu et al.[56] synthesized Ti^{4+} doped $LiNi_{0.9}Co_{0.1}O_2$ cathode material which not only improved the stability of the structure, but also

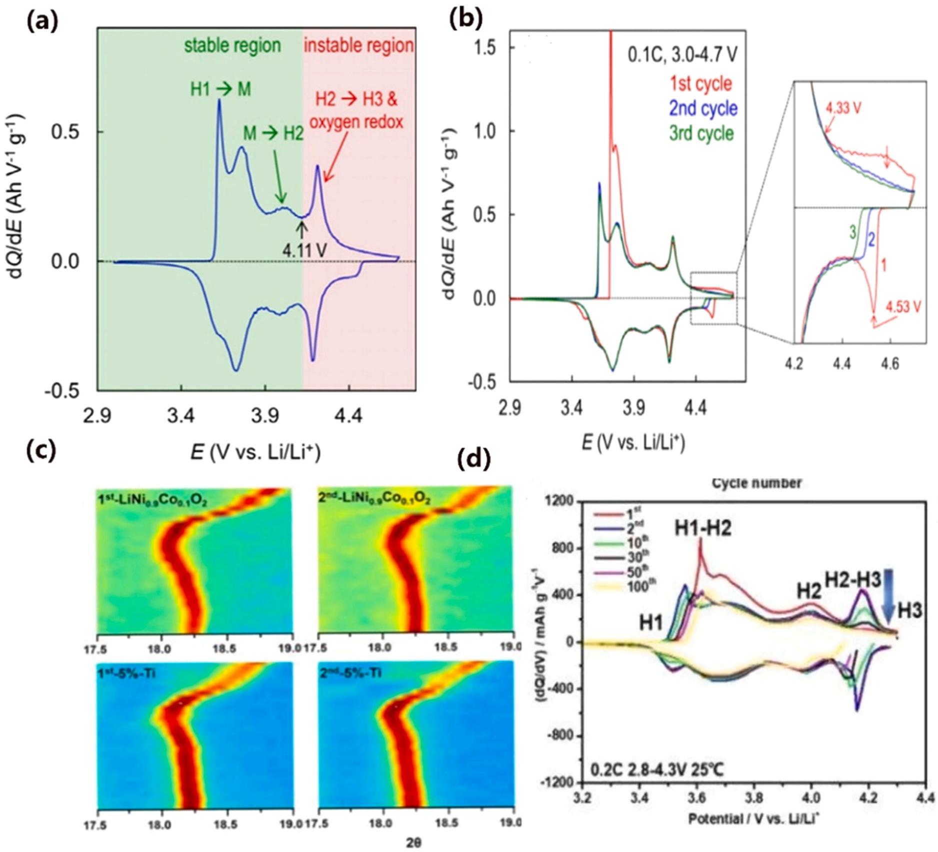

Fig. 9. (a) Typical pattern of the differential capacity vs. cell's voltage for Li/NCM811 cells. (b) plot of differential capacity vs. cell voltage. Reproduced with permission.[108] Copyright 2020, Elsevier. (c) In situ XRD (d) plot of differential capacity vs. cell voltage. Reproduced with permission.[56] Copyright 2019, Elsevier.

restrained the irreversible phase transition in the process of charging and discharging. A repeated appearance of the H3 phase during the charge discharge cycle was induced by the improvement in the reversibility of H2-H3 phase transformation. It also maintained a high capacity output. At the same time, H3 phase ensured excellent cycling stability of the material. After 100 weeks at 38 mA g^{-1} cycles, the retention rate of modified $LiNi_{0.9}Co_{0.1}O_2$ material was significantly increased from 69.7 to 97.9%. In order to observe the phase transition process directly, the undoped and Ti^{4+} doped samples were characterized by in-situ XRD. During the second cycle of charging, when charged to 3.9 V, the (0 0 3) peak of the sample shifted to a lower angle, and shifted to a higher angle when charged to 4.2 V, corresponding to the formation of H2 and H3 phases respectively (Fig. 9**c-d**). After 30 cycles, the shift angle of (0 0 3) peak of undoped samples decreased, while that of Ti^{4+}doped sample did not change significantly. Therefore, it can be concluded that the ion mixing layer in the Ti^{4+} doped sample maintained the integrity of H3 phase during the cycle. The hidden hazard of H3 phase formation is that micro cracks may be induced during the cycle. Titanium doped particles showed no micro cracks. After cycling, the layer structure of the undoped samples were destroyed, and Fm-3 m phase, mixed phase and R-3 m phase appeared successively from the surface to the interior. For Ti^{4+} doped sample, no obvious structural change was noted. Bak et al. [109] used in-situ XRD, synchrotron radiation and mass spectrometry to test the phase transformation and oxygen production of different components of nickel-rich layered oxide cathode materials during charging and discharging. During heating, mixed discharge of cations resulted in the transformation of R$\bar{3}$m to Fm-$\bar{3}$m structure, and the subsequent release of oxygen. When heated to a higher temperature, it changed to Fd-3 m structure.

4.4. Generation of micro cracks

At present, nickel rich layered cathode materials are synthesized by co-precipitation method, and the characteristic of co-precipitation is to grow into secondary particles by agglomeration of nano primary particles. In the process of co-precipitation, the primary particles are disorderly distributed and agglomerated due to violent stirring, so there are different degrees of stress and distortion in the secondary particles.

The nickel-rich layered oxide cathodes are composed of two-micron spheres formed by agglomeration of particles. In the process of lithium intercalation, the variation of lattice size results in the formation of micro cracks in the primary particles, which hinders the diffusion of lithium ions. What's more, the change of cell parameters in the process of charge and discharge leads to the repeated expansion and reduction of the crystal, which further leads to the crack between primary particles and destroys the continuity between them. It again obstructs the electronic transmission, penetration of electrolyte and the continuous growth of interface impedance. The generation of micro cracks is also closely related to the change of phase structure. In the range of high cut-off voltage, the micro cracks are generated at the boundary of the lattice due to the change of stress. When the charging voltage of the nickel layered anode material is higher than 4.2 V, the irreversible phase transition from H2 to H3 will occur, causing a large volume change. NiO phase will be produced, which will not only induce the further phase transition of the material, but also lead to the crack in the material. Increase in impedance and decrease of active materials are triggered by the generation of micro cracks. At the same time, the electrolyte permeates into the cracks, and degrades the electrochemical performance. Park et al. [55] explicitly illustrated the degree of mechanical damage sustained by each cathode during cycling. In a severe case, a crack traverses across the entire particle and nearly fractures the secondary particle, even in its first charged state before cycling (Fig. 10**a**). Nam et al. [110] summarized the relationship between specific capacity, the capacity retention rate, micro crack degree and thermal stability of NCA and $LiNiO_2$ with high nickel content. Though the specific capacity of the cathode increased with the increase in Ni content, the capacity retention and thermal stability decreased. With the increase of Ni content, the propagation degree of micro cracks also got enhanced. Fig. 10**b-c** shows the SEM of the positive cross section under different SOC and DOD. Micro cracks began to appear at 3.9 V for all three kinds of positive electrodes. At the same voltage, the percentage of micro cracks area in the discharge was higher than that of the charge, which indicated that micro cracks were not completely reversible. The electrolyte entered the secondary particles from micro cracks, accelerated the surface degradation of particles of micro cracks and formed NiO rock salt phase.

4.5. Other newly proposed failure factors

With the continuous development of research and characterization technology, some newer and deeper failure mechanisms have been proposed. Generally, the increase of nickel content in ternary materials will make it easier to react with water and carbon dioxide in the environment. CATL evaluated the NCM811/graphite soft package battery for full charge storage at high temperature, and analyzed the cell disassembly before and after storage to study the mechanism of storage performance degradation. The results show that the thickness of non-electrochemically active rock salt phase on the cathode material surface increases after storage, and spinel phase appears in the local range of grains, which can lead to the attenuation of reversible capacity of Ni-rich materials. At the same time, the deposition of by-products produced by electrolyte side reaction on the surface of cathode materials after high temperature storage can lead to poor interface conductivity and increase the battery polarization.

For a comprehensive understanding of the chemical and physical changes of NCM, and an intense study of the actual changes occurring in electrode materials in the long cycle process, Arumugram et al. [111] used an electron microscope based analysis technique to obtain microstructure images of crystals and electronic structural changes. The results of electron probe microanalysis (EPMA), X-ray energy dispersive spectroscopy (XEDS) and electron energy loss spectroscopy (EELS) combined with TEM reveal the modifications of Ni content, crystal structure and oxidation state on the surface and bulk cathode. The relationship between the change of high Ni NCM positive electrode and its electrical properties was studied by comparing the original positive electrode and the positive electrode after 500 cycles. The results show that the structure, chemical composition and oxidation state of TMS propagate from the surface to the whole bulk phase in a long cycle time. The continuous formation of Ni^{2+} and the loss of O^{2-} are the main problems leading to the degradation of high nickel NCM cathode. Yang et al. [112] and Su [43] et al. found that intrinsic crystal defects cause cycle induced degradation of cathode materials. Furthermore, the studies made by Lin et al. [41] also established that the non-radial crystal orientation of the NMC positive electrode is not conducive to the formation of continuous Li^+ conduction channel, which reduced the inhomogeneity of charge distribution in the secondary particles, and improved the cycling charge discharge stability of NMC. Recently, it has been observed that DOD has an obvious effect on the stability of ternary high nickel cathode materials. Yoon et al. [44] revealed that NCT95 cathode material had a discharge depth of 60% in the high range (3.76–4.3 V), 60% in the low range (2.7–4.0 V), and 100% in the range of 2.7–4.3 V. At the discharge depth of 60% in the high range, NCT95 cathode material had the most of the cracks, the most obvious change of cell volume, and the deterioration of cycle stability was more significant.

5. Approaches to suppress capacity failure

Although the primary nanoparticles of Ni-rich layered materials with high Ni content can enlarge the reaction interface and shorten the diffusion path of Li^+, thereby improving the cycle and rate performance of materials, there are also side reactions such as the formation of rock salt phase (NiO). Ni-rich layered materials react with the electrolyte to form solid electrolyte interface (SEI), which increases boundary impedance and leads to rapid capacity decay. [113-116] In addition, when materials are deeply charged at extreme voltage, Li/O vacancies will cause oxidized Ni^{3+}/Ni^{4+} ions to become unstable. It will result in the migration of cations and thereby forming a surface reconstruction layer consisting of NiO phase and spinel phase on the surface of the electrode. [117,118] Appearance of surface reconstruction layer will

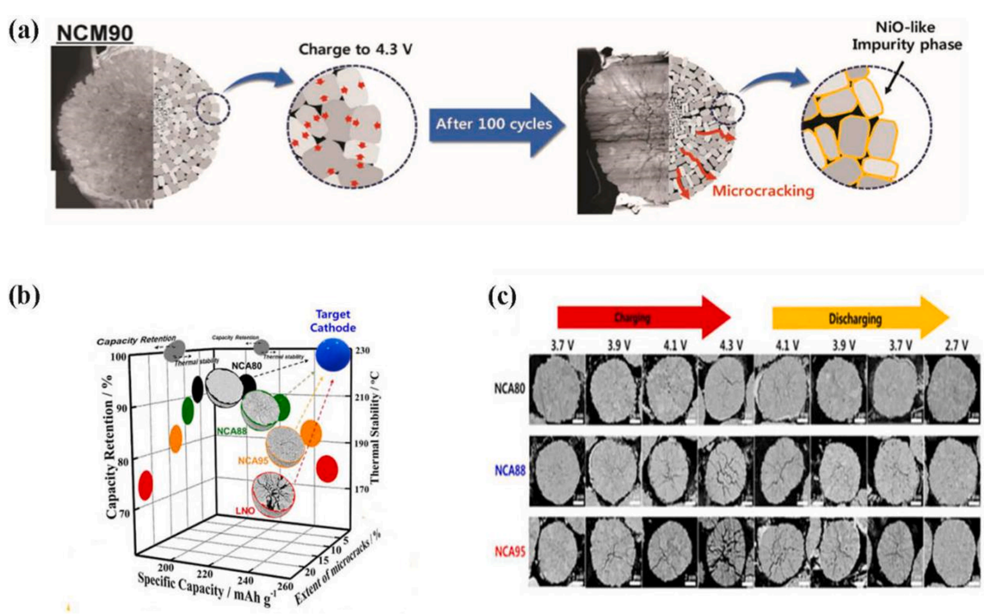

Fig. 10. (a) Schematic illustration of the effect of NCM90 cathode's mechanical stability during charge and discharge cycling. Reproduced with permission.[55] Copyright 2018, Wiley-VCH. (b) Diagram of specific capacity, capacity retention rate, micro crack degree and thermal stability of NCA and $LiNiO_2$ with high nickel content. (c) SEM comparison of NCA80, NCA88 and NCA95 under different SOC. Reproduced with permission.[110] Copyright 2019, American Chemical Society.

increase the diffusion dynamic resistance of Li^+ and will lead to capacity degradation. The commercial application of nickel rich layered material is restricted by its poor high temperature performance and low compacting density. Doping, surface coating, crystal and morphology structure regulation, DOD setting, electrolyte, binder, separator modification and assembly technology are deemed to be the main methods for effectively reducing the side reactions and improving the electrochemical properties and thermal stability of the materials (Fig. 11). Table 1 summarizes the various promising approaches in enhancing the electrochemical performances of Ni-rich cathodes.

5.1. Elemental doping

Multiple phase transitions occur in Ni rich layered oxide cathodes during the lithiation/delithiation process, especially under deep charge, which will lead to a series of unstable conditions. In order to alleviate these complications, researchers have modified the cathodes by using various doped elements to increase their energy density without sacrificing the cyclic stability. Structural modification via atomic substitution of foreign elements such as cationic doping and anionic doping, as well as co-doping of anion and anion element have been adopted. The commonly used doping elements are Zr^{4+}, Ti^{4+}, Al^{3+}, Mg^{2+}, Mo^{6+}, B^{3+} and F^-. The successful doping helps in restraining the Li/Ni mixture and stabilizes the crystal structure of the materials, further improving their comprehensive performance. Zr has become the most commonly used doping element because of its stabilizing effect on layered cathode materials. Lastly, Choi et al. [119] detected through experiments that Zr doping in $Li[Ni_{0.6}Co_{0.2}Mn_{0.2}]O_2$ can be an effective approach to enhance the cycle as well as rate performance by stabilizing the structure and increasing Li^+ diffusion rate. The doping of Zr decreased the mixing degree of ions, reduced the structure transition and promoted the diffusion of Li^+, further improving the cycle and rate performance (Fig. 12**a-c**). Gao et al. [120] synthesized NCM811 cathode material by substituting the transition metals with Zr to mitigate its structural instability and capacity degradation. It exhibited superior electrochemical performance in comparison to the undoped-NCM811 material (Fig. 12**d-e**).

Ti^{4+} and Al^{3+} are frequently used as promising dopants in stabilizing the material layered structure. Song et al. [121] synthesized Ti-doped $LiNi_{0.7}Co_{0.15}Mn_{0.15}O_2$ cathode materials via the following methods; a solution of 0.1 wt% titanium sulfate was dissolved in deionized water. $Ni_{0.7}Co_{0.15}Mn_{0.15}(OH)_2$ precursor powders were then added to the solution and continuously stirred at 100 °C until the complete evaporation of the solvent. The resulting powder was mixed with Li_2CO_3 (Li/M = 1.03) and sintered at 800 °C for 10 h under an O_2 atmosphere to produce Ti-$Ni_{0.7}Co_{0.15}Mn_{0.15}O_2$. For comparison, the $Ni_{0.7}Co_{0.15}Mn_{0.15}O_2$ was prepared with the same approach without Ti addition. Subsequently, after Ti-doping, the external morphology remains similar, but the lattice parameters of the layered structure were slightly shifted toward larger values. Ti-$Ni_{0.7}Co_{0.15}Mn_{0.15}O_2$ cathode material exhibited long cycle life and delivered better retention rate of 95% after 50 cycles at 60 °C. Titanium doping enhanced the structural strength of a high-Ni layered cathode material in lithium ion batteries during high temperature cycling which attributed to the better retention of the compressive strength of the particles. Besides, it also retarded crack formation within the particles (Fig. 13**a-f**). Zhang et al. [143] found that Ti^{4+} doping in Ni-rich cathodes can improve the robustness of the oxygen framework, which further contributes to improve the structural stability and electrochemical performance (Fig. 13**g-h**).

Among the various dopants, Al^{3+} doping can effectively improve the storage stability and prevent the reaction between H_2O and CO_2 during storage. Al^{3+} has been proven to be one of the most potential elements in mitigating the structural degradation. Successful commercialization of $LiNi_{0.8}Co_{0.15}Al_{0.05}O_2$cathodes has revived the interest in Ni rich layered materials comprising Al. Yan et al. [144] synthesized $LiNi_{0.8}Co_{0.1}Mn_{0.1}O_2$ and $LiNi_{0.78}Co_{0.1}Mn_{0.1}Al_{0.02}O_2$, prepared via co-

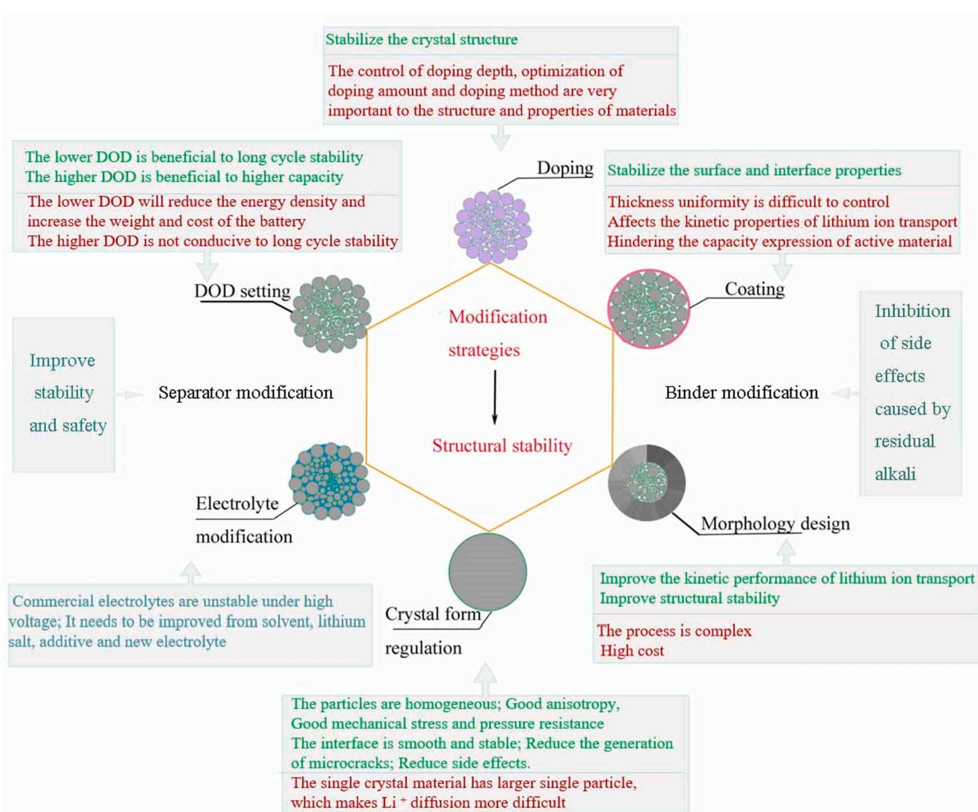

Fig. 11. Schematic diagram of the modification strategies.

Table 1
Summaries on the promising strategies in improving the electrochemical performance of Ni-rich cathodes.

Ni content	Strategies	Voltage (V)	Capacity (mAh g^{-1})	Current	Retention		Rate	Capacities		Ref
					Modified	Pristine		Modified	Pristine	
0.6	Zr-doping	4.3	185.2	0.1C	98.4@100th	83.7@100th	2C	152.9	130	2019[119]
0.8	Zr-doping	4.3	183.8	0.2C	84.2@60th	80@60th	2C	163	159	2019[120]
0.7	Ti-doping	4.3	181.05	0.1C	98.82@50th	92.84@50th	5C	150	148	2018[121]
0.82	Ti-doping	4.3	190	0.2C	97.7@200th	75.9@200th	20C	146	120	2019[122]
0.8	Mo-doping	4.6	208.9	0.2C	75@101th	65@101th	2C	180	160	2019[123]
0.94	B-doping	4.4	223(0.1C)	1/3C	85@200th	68@200th	10C	170	170	2019[124]
0.8	Zr-F-doping	4.3	179	1C	90.5@200th	75.8@200th	2C	186.9	192.8	2019[125]
0.9	B-doping	4.3	234(0.1C)	0.5C	90.4@100th	78.8@100th	0.5C	220	212	2020[30]
0.8	Mn-PO_4^{3-}-doping	4.3	210	0.1C	85.5@100th	75@100th	5C	160	140	2019[126]
0.89	Ta-doping	4.3	229(0.1C)	0.5C	94@100th	81@100th	–	–	–	2020[45]
0.9	W-doping	4.3	180.4	0.5C	89@400th	82.4@400th	–	–	–	2020[11]
0.8	In_2O_3 /$LiInO_2$ coating	4.3	207(0.1C)	1C	91.3@100th	74@100th	5C	177.1	149.9	2019[127]
0.8	GN-LPO coating	4.3	184(0.2C)	0.5C	94.3@150th	88.1@150th	10C	122.4	108.5	2019[128]
0.8	LPO coating	4.4	193	1C	92.6@100th	86.1@100th	8C	159.4	144.4	2019[129]
0.8	$LiYO_2$ coating and inner gradient Y doping	4.5	207.4	0.5C	98.4@100th	83.5@100th	10C	118.4	101.2	2019[130]
0.7	CeO_2 coating	4.3	187	0.5C	86.4@100th	70.6@100th	5C	137.1	95.5	2019[131]
0.8	La-Al doping and coating	4.3	–	1C	86.5@100th	71.3@100th	10C	136	116	2019[132]
0.8	C coating	4.3	182	0.1C	93@40th	86@40th	3C	83	46	2010[133]
0.8	Graphene coating	4.3	185	0.2C	97@80th	91@8th	10C	152	130	2012[134]
0.6	C-Al_2O_3 caoting	4.5	186.6	1C	93.5@100th		–	–	–	2019[135]
0.8	LMO coating	4.3	201	0.1C	93@100th	74@100th	2C	150	140	2019[136]
0.8	Core–shell concentration gradient	4.3	192.5	0.2C	95.9@100th	84.9@100th	10C	161.2	100	2019[137]
0.8	radially aligned	4.3	180.9	1C	95.5@300th	84.5@300th	5C	152.7	128.6	2019[48]
0.83	single-crystalline	4.4	200	1C	84.5@150th	63.8@150th	5C	175	177	2020[138]
0.5	p-toluenesulfonyl isocyanate additive	4.5	180	1C	86.2@100th	71.4@100th	10C	–	–	2017[139]
0.8	Silyl-group functionalized organic additive	4.5	200	1C	60.8@100th	41.9@100th	–	–	–	2018[140]
0.7	multi-functionalized additive	4.3	200	0.1C	91.9@100th	71.7@100th	–	–	–	2016[141]
1	flfluorinated electrolyte with LiDFOB additive	4.3	216	0.5C	80@400th	65@200th	3C	160	–	2019[142]

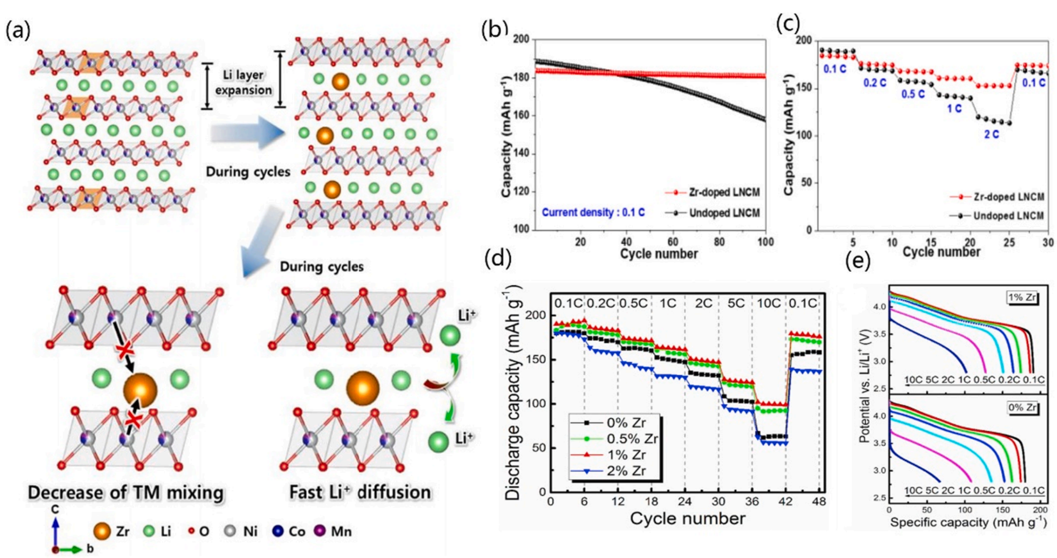

Fig. 12. (a) Schematic illustration of Zr doping effects in NCM811cathode. (b) cycling test of undoped and Zr-doped LNCM electrodes at 0.1C. (c) rate capability of undoped and Zr-doped NCM811 electrodes. Reproduced with permission.[119] Copyright 2019, Wiley-VCH. (d) Rate performance of NCM811s with different Zr concentrations. (e) Discharging curves at different C-rates of the raw NCM811 and the 1% Zr-NCM811. Reproduced with permission.[120] Copyright 2018, Elsevier.

precipitation method and followed by sintering. The $LiNi_{0.78}Co_{0.1}Mn_{0.1}Al_{0.02}O_2$cathode material showed high capacity retention of 96.15% after 50 cycles at 20 °C and of 94.38% after 50 cycles at 60 °C. In addition, Mo doping reduced the Li/Ni mixing and broadened the Li^+ migration channel. Stronger Mo-O bond might suppress precipitation of lattice oxygen and stabilized the material surface. Liu et al. [123] synthesized Mo-doped $LiNi_{0.6}Co_{0.2}Mn_{0.2}O_2$cathode material by co-precipitation method. Electrochemical impedance spectroscopy (EIS) clearly demonstrated that Mo-doped cathode reduced the charge transfer impedance and enhanced the electrochemical reaction activity of Li^+. When the doping amount of Mo is 0.01 mol, it exhibited an excellent reversible capacity of 208 mA h g^{-1} at 0.2C, corresponding to the capacity retention up to 75% even after 101 cycles. Cobalt in NMC and NCA, an expensive and scarce metal is generally considered as the

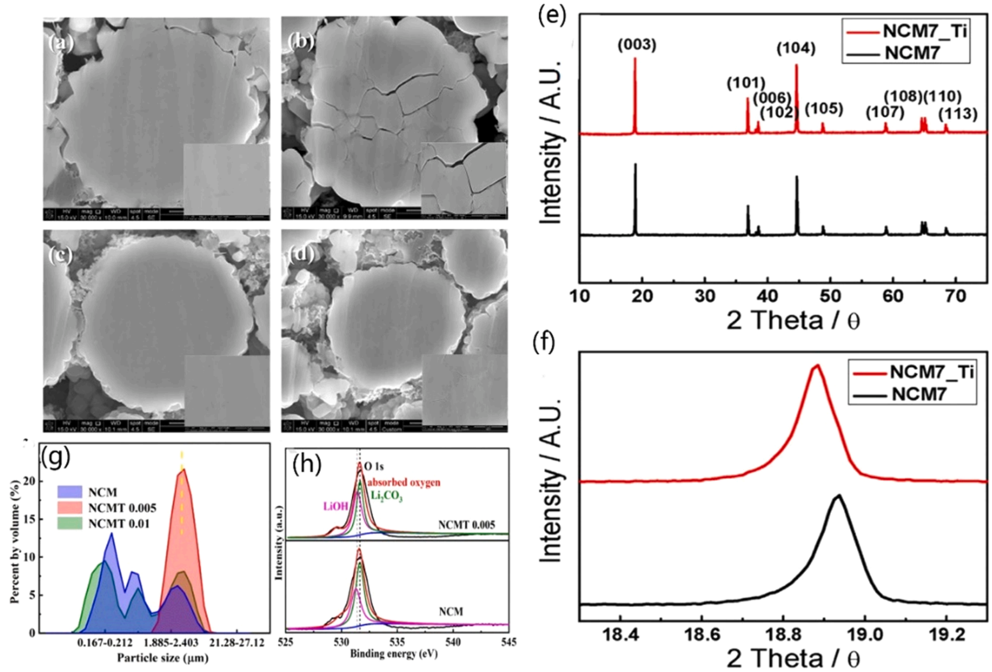

Fig. 13. FE-SEM images of polished cross-sections of (a) fresh NCM electrode (b) NCM electrode after 50 cycles. (c) fresh Ti-NCM electrode and (d) Ti-NCM electrode after 50 cycles. XRD patterns for NCM (e) and Ti-NCM (f) powders. Reproduced with permission.[121]Copyright 2018, Elsevier. (g) secondary particle size distribution of the three samples. (h) XPS spectra of the O 1 s state for the NCM and NCMT 0.005 samples. Reproduced with permission.[143] Copyright 2019, Elsevier.

key element to inhibit Li/Ni mixing, can further improve the electrochemical performance. Li et al. [33] systematically studied the influence of different cation doping including Al, Mn, Mg and Co doping in Ni-rich layered oxide cathode materials. In-situ X-ray diffraction (XRD) and differential capacity versus voltage exhibited that through the doping of Al, Mn, Mg or Co, multiple phase transition in $Li_xNi_{0.95}M_{0.05}O_2$ was restrained during lithiation/delithiation process. This phase transition was attributed to the poor capacity retention of $LiNiO_2$. The addition of 5% Al, Mn and Mg in $LiNiO_2$ reduced the Li/Ni mixing and inhibited the irreversible phase transition.

The inherent anisotropic lattice volume variations of randomly oriented primary particles lead to stress concentrations, followed by microcracks of secondary particles, The generation of microcracks causes the electrolyte to penetrate the interior of the particles and attack primary particles, which result in structural degradation and further aggravated capacity attenuation. Recently, Kim et al. [45] introduced Ta dopants into the Ni-rich cathode material $LiNi_{0.91}Co_{0.09}O_2$ (NC90) by co-precipitation-solid phase method. Ta was introduced into hydroxide precursor and LiOH was used to obtain the material of the ideal radial structure by changing surface energy. As a result, the addition of Ta hindered the coarsening of the particles. The unique microstructure of NCTa90 material led to the dissipation of anisotropic mechanical strain and inhibited the formation and propagation of micro cracks. At the same time, the cyclic stability was achieved by the radial arrangement of primary particles and the crystal structure of [0 0 3], which effectively dissipated the internal strain in the deep charge state. It exhibited excellent capacity retention of 95% even after 1000 cycles and exhibited high energy density of 850 Wh Kg^{-1} (Fig. 14).

Kim et al. [145] also found that the Nb-doped $Li(Ni_{0.855}Co_{0.13}Al_{0.015})O_2$ (NCA85) cathodes alter the morphology of primary particle to accurately adjust microstructure. With the increase of Nb-dopant content of NCA85 cathodes, the primary particles are elongated and arranged radially. which partially relieve the caused by H2-H3 phase transition during deep charging. The elimination of internal strain significantly improves the cycling stability of NCA85 cathodes even at an elevated temperature. Furthermore, Nb-doping enhances the mechanical stability and further improves the fast charging performance of

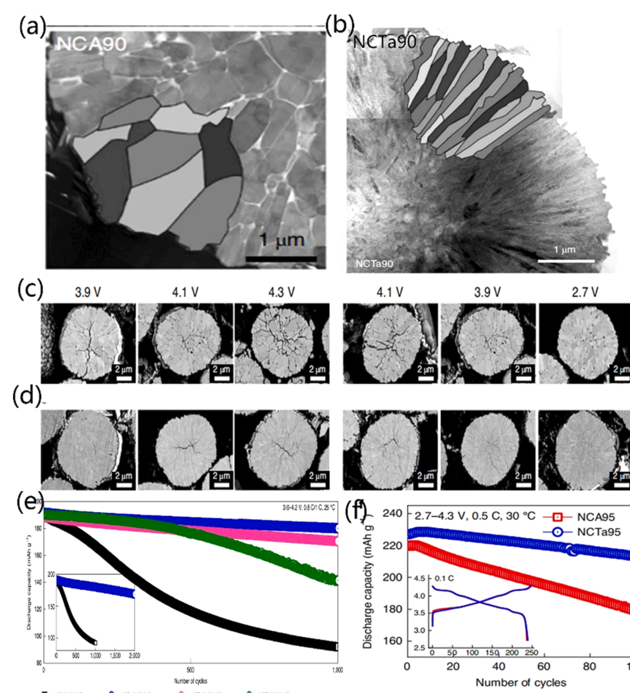

Fig. 14. STEM image of a cross-sectional cathode and the corresponding schematic of the primary particles $LiNi_{0.90}Co_{0.09}Al_{0.01}O_2$ (a) and $LiNi_{0.90}Co_{0.09}Ta_{0.01}O_2$ (b). Cross-sectional SEM images of NCA90 (c) and NCTa90 (d) cathodes at different charge/discharge state during the first cycle. (e) Long-term cycling stability in full cells for NCA90 and NCTa90 cathodes lithiated at different temperatures. (f) Cycling performance (at 0.5C) with the initial charge and discharge curves in the inset for NCA95 and NCTa95 cathodes . Reproduced with permission.[45]Copyright 2020, Nature.

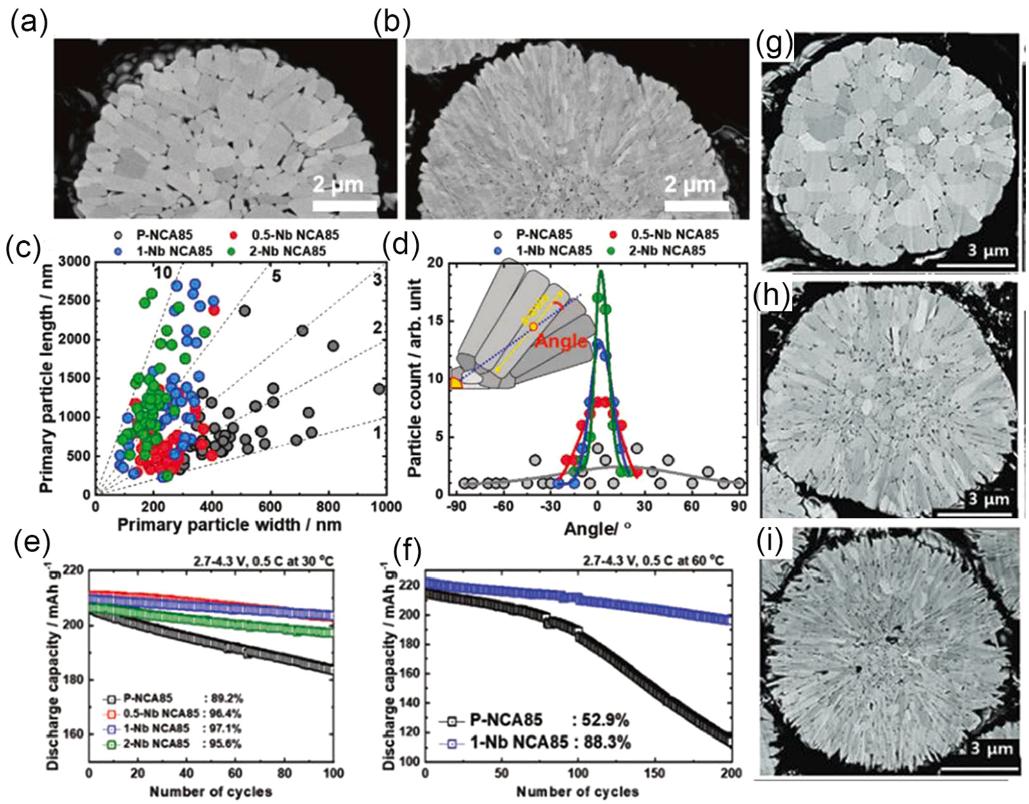

Fig. 15. (a) Cross-sectional SEM image of the primary particles of NCA85 cathode. (b) Cross-sectional SEM image of the primary particles of Nb-NCA85 cathode. (c) Aspect ratio of the primary particles. (d) orientation of the primary particles. (e) Cycling performance in half cells at 30 °C.(f) Cycling performance in half cells at 60 °C. Reproduced with permission.[145] Copyright 2021, Wiley-VCH. (g) Cross-sectional SEM image of NC90 cathode. (h) Cross-sectional SEM images of 0.5-NCB90 cathode. (i) Cross-sectional SEM images of 1-NCB90 cathode. Reproduced with permission. [30] Copyright 2021, Wiley-VCH.

batteries. Moreover, The Nb-dopant of NCA85 cathode also shows strong chemical and structural stability under aging and under thermal load (Fig. 15**a-f**). Furthermore, Ryu et al. [30] proposed B-doped Li $(Ni_{0.9}Co_{0.1})O_2$ cathodes by introducing B_2O_3. The synthesized cathodes with B doping show a highly oriented microstructure, and the with of primary particle can be changed by adjusting the boron proportion. Compared with the NC90 cathode without B, NCB cathode effectively inhibits the formation of microcracks and significantly improves the cycling stability. The cathode with wide primary particles delievers a poor stability, which indicates a strong correlation between microcrack formation and microstructure. By changing the primary particles morphology, Ni-rich cathodes with high energy density and long-term life were reasonably designed, which is suitable for the next generation of electric vehicles **(**Fig. 15**g-i)**. Park et al. [55] used B doping to change the microstructure of $Li[Ni_{0.90}Co_{0.05}Mn_{0.05}]O_2$ particles and improved the inherent poor cycling performance. Density function theory (DFT) calculations testified that 1 mol % of $Li[Ni_{0.90}Co_{0.05}Mn_{0.05}]O_2$ with B doping (B-NCM90) altered the surface energy and achieved a well textured microstructure, which further alleviated the intrinsic internal strain generated during the deep charging of NC. 1 mol % B-NCM90 showed extremely high coulombic efficiency of 91% after 100 cycles at 55 °C, however, NCM90 delivered a coulombic efficiency of 76%. By utilizing the differential capacity curve, structural changes of Ni-rich cathode materials were demonstrated during lithiation/delithiation process. It was found that NCM90 underwent a series of phase transitions. The phase transition of H2-H3 caused a sudden contraction in the c axis, further resulting in the mechanical stress and deteriorating cycle performance. Oxidation peak value of H2-H3 significantly decreased during 100 cycles, which indicated poor reversibility, and was related to the serious collapse of material structure caused by mechanical strain. Conversely, 1 mol% B-NCM90 kept good peak strength of H2-H3, which was consistent with the improvement of the cycle stability by B^{3+} doping. When compared with NCM90 material, it was noticed that the 1.0 mol% B-NCM90 material had no obvious micro crack, and B^{3+} doping significantly reduced the internal strain caused by H2-H3 phase transformation.

Xie et al. [124] stabilized the Ni- rich cathodes effectively by introducing boron-based polyanions into the $LiNi_{0.94}Co_{0.06}O_2$ materials. It delivered long cycling life, retaining a capacity of 223 mAh g^{-1} after 400 cycles and the coulombic efficiency was close to 80%. However, the $LiNi_{0.94}Co_{0.06}O_2$ (NC) without element doping exhibited a poor coulombic efficiency of 61% after 400 cycles. In addition, further study on the interface showed that a well-passivized boron/phosphorus-rich cathode electrolyte interface was formed, which exhibited excellent cycle stability. Moreover, B-NC had highly enhanced thermal stability and air-exposure as well. After being exposed in air for 30 days, it displayed a superior rate performance of 125 mAh g^{-1} at 10C. However, NC showed a rate performance of 80 mAh g^{-1} at 10C **(**Fig. 16**)**.

Zhang et al. [146] also synthesized $LiNi_{0.6}Co_{0.2}Mn_{0.2}O_2$ cathode materials with B doping via co-precipitation method. As a result, B-$LiNi_{0.6}Co_{0.2}Mn_{0.2}O_2$ cathode (B-NCM622) delivered a superior reversible capacity of 188.2 mAh g^{-1} at 1C and excellent coulombic efficiency of 86% after 200 cycles. High-resolution transmission electron microscopy (HR-TEM) and X-ray photoelectron spectroscopy (XPS) exhibited that the interaction of B^{3+} and excess Li^{+} led to the reduction of cation mixing, further resulting in rapid kinetics, stable oxygen dense packing structure, which in turn improved the cycling stability. This study has a deep understanding of the effect of B^{3+} doping and provides a feasible strategy for the development of practical high energy density ultra-high nickel rich cathodes.

In addition to the cation doping, anion doping has also become a significant approach in improving the structure and electrochemical performance of Ni-rich materials. Woo et al. [147] synthesized $LiNi_{0.8}Co_{0.1}Mn_{0.1}O_{2-z}F_z$ via co-precipitation method. X-ray diffraction (XRD) spectra showed that all peaks were indexed with hexagonal -$NaFeO_2$ structure with a space group of R3̄m. The lattice constants of a and c were increased by F^- doping. This can be accredited to the repulsive forces in the oxide matrix formed by the strong bond between Li and F, causing the lattice to expand simultaneously on both a and c axes.

The increase in the initial charging voltage of $LiNi_{0.8}Co_{0.1}Mn_{0.1}O_{2-z}F_z$

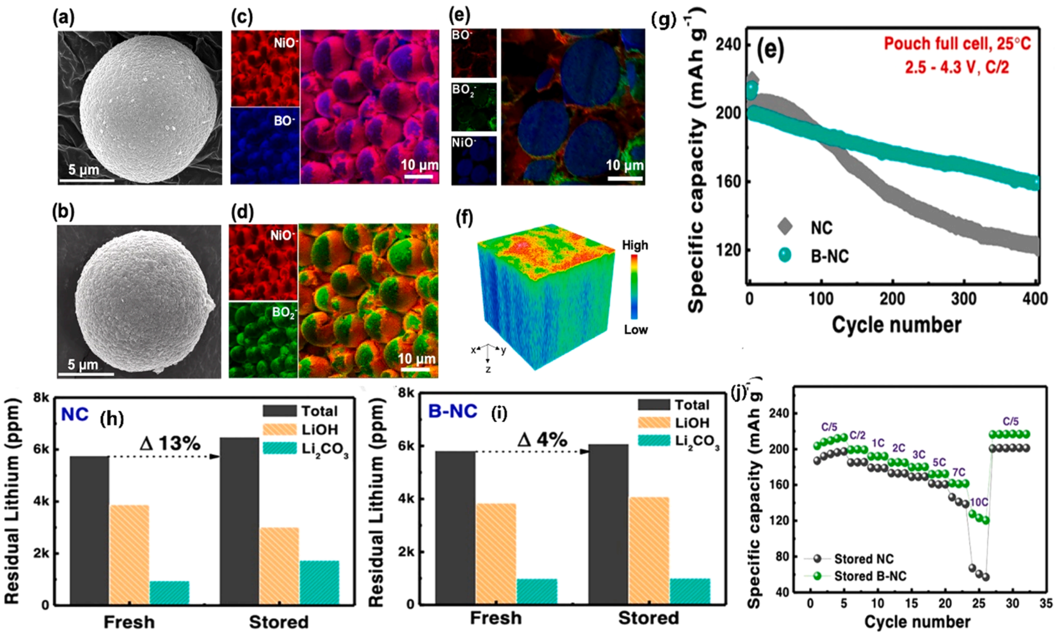

Fig. 16. SEM images of (a) fresh NC and (b) fresh B − NC. TOF-SIMS surface mapping of (c) BO^{-} and NiO^{-} species and (d) BO^{2-} and NiO^{-} species in fresh B − NC particles. (e) TOF-SIMS cross-section mapping of BO^{-}, BO^{2-}, and NiO − species in fresh B − NC. (f) TOF-SIMS three dimension depth profiling of BO_x^{-} (x = 1 or 2) species in the fresh B-NC. (g) Cycle performance of NC and B-NC cathodes in pouch full cell at 25 °C. Residual lithium content changes (h) NC and (i) B − NC. (j) Rate performance of the 30-day stored NC and B − NC over the course of C/5 to 10C rate. Reproduced with permission. [124] Copyright 2019, American Chemical Society.

material may be related to the interaction caused by the substitution of F for O. The bond energy of Li-F (577 KJ mol^{-1}) is much stronger than that of Li-O (341 KJ mol^{-1}). Therefore, $LiNi_{0.8}Co_{0.1}Mn_{0.1}O_{2-z}F_z$ delivered excellent electrochemical properties such as cycle and rate performance. Generally speaking, single ion doping can only improve one aspect of the performance of Ni-rich materials. In order to improve the comprehensive performance of Ni-rich materials, multi-ion co-doping has become the research direction of many researchers. Qiu et al. [125] synthesized $LiNi_{0.8}Co_{0.15}Al_{0.05}O_2$ cathode material by co-doping Zr^{4+} and F^{-}. X-ray diffraction (XRD), scanning electron microscope (SEM), constant current charge discharge test and cyclic voltammetry (CV) proved that F^{-} doping can stabilize the crystal structure but reduces the reversibility of the material. The doping of Zr^{4+} effectively stabilized the crystal structure and reduced the strong bond dissociation energy of ZreO. Co-

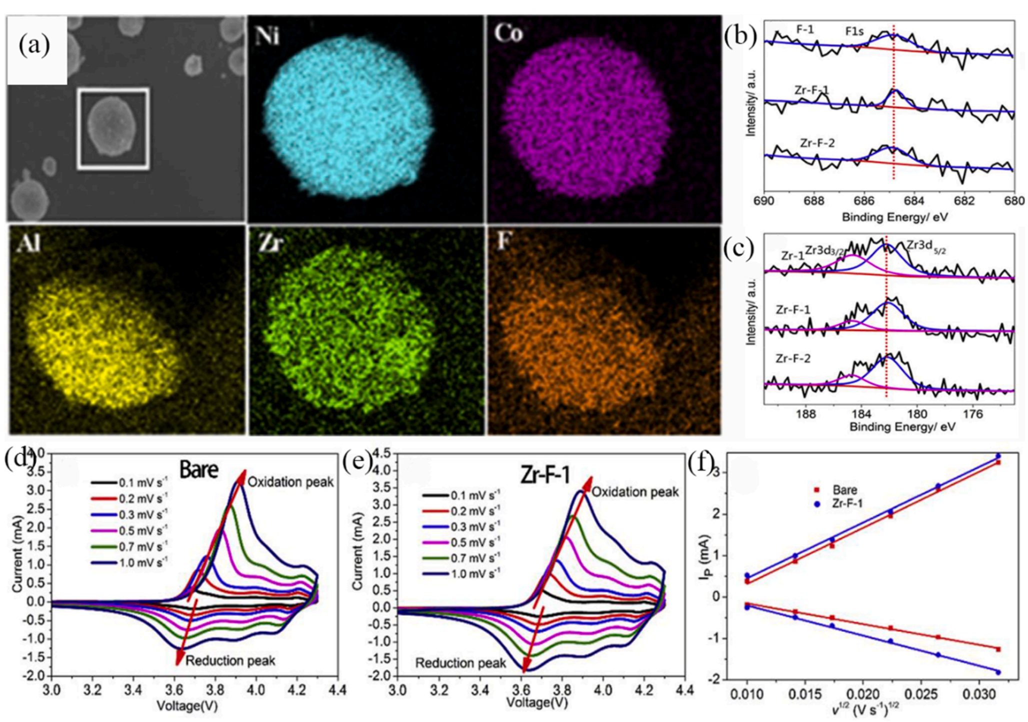

Fig. 17. (a) EDS mapping of Zr-F-1 sample. (b) XPS results of F (c) XPS results of Zr. (d) CV curves of bare samples at various scan rates. (e) CV curves of Zr-F-1 samples at various scan rates. (f) the relationship of the peak current (i_p) and the square root of scan rate ($v^{1/2}$). Reproduced with permission.[125] Copyright 2019, Elsevier.

doping of Zr^{4+} and F^- stimulated the migration of lithium ions, slowed down the electrochemical polarization and improved the electrochemical performance (Fig. 17). In addition, Qiu et al. [126] studied the effects of the coexistence of PO_4^{3-} and Mn^{4+} on the crystal structure, phase transition and electrochemical performance during lithiation/delithiation process. Appropriate co-doping of PO_4^{3-} content and Mn^{4+} increased lithiation/delithiation channel of Li^+, reduced the cation mixing and inhibited the structure deterioration during cycle process. When compared with the Ni-rich materials (un-doped), it was noted that the electrochemical performance of the Ni-rich materials with PO_4^{3-} and Mn^{4+} co-doping got improved. It exhibited an excellent reversible discharge capacity of 204 mAh g^{-1} at 0.1C for 2.7–4.3 V and stabilized at 174 mAh g^{-1} at 1C after 100 cycles, as well as a coulombic efficiency of 85.5% was achieved.

5.2. Coating modification

During the charge–discharge process, especially at higher voltage and higher temperature, Ni^{4+} easily reacts with the electrolyte, leading to the destruction of material structure. Surface coating is an effective approach in improving the performance of Ni-rich layered oxides, while coated materials are required to have good Li^+ and electronic transmission performance. On one hand, it can improve the electronic conductivity [148-151], while on the other hand, the coating materials can reduce the direct contact area between Ni-rich layered oxide cathode materials and electrolyte, hinder the formation probability of HF in the electrolyte and the side reaction and further prevent the collapse of the crystal structure due to corrosion of the cathode materials. All these aspects significantly improve their electrochemical performance.

Previous reports have almost confirmed that Ni-rich layered oxide materials through coating metal oxides can significantly improve the electrochemical stability. Oxides such as Al_2O_3, TiO_2, MgO are often used as coating materials due to their structure stability and electrochemical inertia between coating materials and electrolyte at high voltage, which shows good effects in improving the electrochemical performance. Recently, Fan et al. [152] constructed a highly effective TiO_2 nano-coating on the surface of $LiNi_{0.8}Co_{0.1}Mn_{0.1}O_2$ (NCM811) by accurately controlling the hydrolytic dynamics of Ti^{4+} in order to improve the comprehensive performance of Ni-rich cathodes for LIBs at a higher upper cut-off voltage. A systematic study on the effect of coating layer with TiO_2 was also executed. As a result, the continuous and uniform coating layer with TiO_2 offered an exhaustive protection for NCM811 and increased the reversibility of phase transition between H2 → H3 during lithiation/delithiation process. This further ensured a superior cycling stability and rate performance under the cut-off voltage of 3.0–4.5 V. High-resolution transmission electron microscopy (HR-TEM) further demonstrated the slight structural decay of the NCM811 material with TiO_2 coating when compared with the NCM811 material. Electrochemical impedance spectroscopy (EIS) established a stable interface between cathode and electrolyte, as well as fast kinetics at the surface of NCM811 material with TiO_2 coating. Comparing with NCM811cathode material, NCM811 material with TiO_2 coating delivered a superior coulombic efficiency of 72.2% at 1C after 500 cycles with 3.0–4.5 V and 63.4% at 1C after 1000 cycles with 3.0–4.3 V. This work offers a general approach for the preparation of uniform TiO_2 coatings and provides direction for the precise evaluation of the comprehensive performance of coatings (Fig. 18).

Becker et al. [153] synthesized tungsten oxide (WO_3) coating layer on the surface of $LiNi_{0.8}Co_{0.1}Mn_{0.1}O_2$ (NCM-811) via sol–gel method followed by heat treatment. As a result, tungsten oxide (WO_3) coating layer on the surface of $LiNi_{0.8}Co_{0.1}Mn_{0.1}O_2$ (NCM-811) delivered a superior capacity retention for the long-term cycling process of $LiNi_{0.8}Co_{0.1}Mn_{0.1}O_2$ (NCM-811) based LIBs full cells. Coated electrodes showed superior discharge capacity of 184 mAh g^{-1} at 0.1C and excellent capacity retention of 80% after 865cycles. Furthermore, it was confirmed that tungsten oxide (WO_3) coating composite provides thermal and structure stability. Unlike the uncoated electrode, the particle cracking of the surface modified electrode had improved after cycles. Rare earth oxides can also be used as a promising coating layer for Ni rich cathode materials. Dong et al. [131] synthesized $LiNi_{0.7}Co_{0.2}Mn_{0.1}O_2$ (NCM712) cathode materials with CeO_2 coating by a wet chemical method. X-ray powder diffraction (XRD) analysis and transmission electron microscope (TEM) results demonstrated the structural characteristics, morphology and elemental composition of bare and surface coated NCM712 materials. The CeO_2-coated NCM721 exhibited reversible discharge specific capacity of 202 mAh g^{-1} at 0.1C and showed excellent capacity

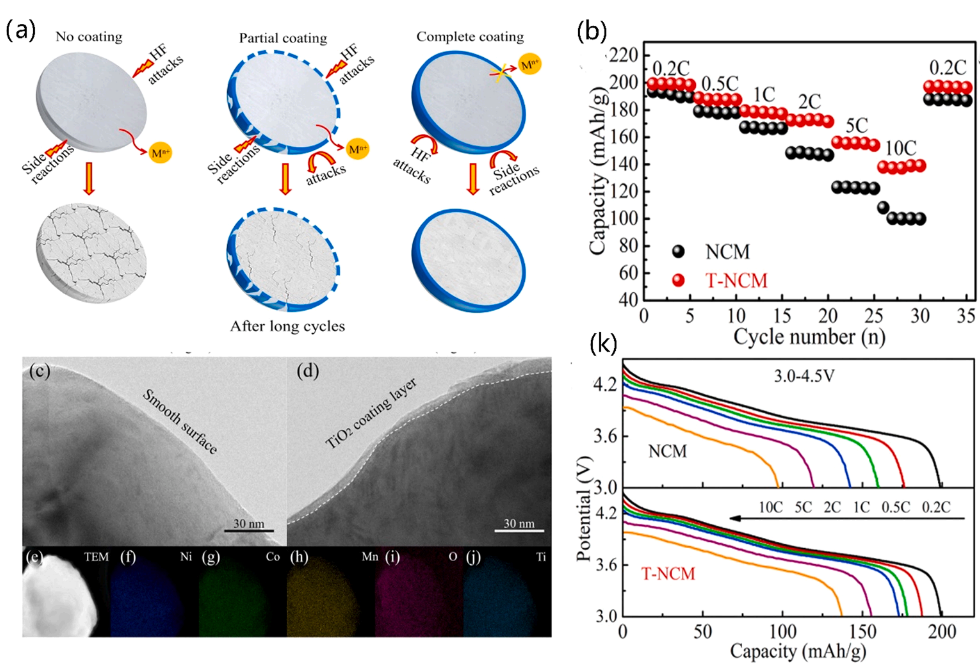

Fig. 18. (a) The protection mechanism of the TiO_2 nano-coating for Ni-rich cathode materials. (b) The rate performance of NCM and T-NCM. TEM images for NCM (c) and T-NCM. (d) TEM image of a primary T-NCM particle. (e) and corresponding elements mapping including Ni (f), Co (g), Mn (h), O (i) and Ti (j). (k) The selected discharge profiles for NCM and T-NCM at different current densities. Reproduced with permission.[152]Copyright 2020, Elsevier.

retention of 86.42% at 0.5C after 100 cycles between 3.0 and 4.3 V as well as decent rate performance of 137.1 mAh g^{-1} at 5C. For comparison, NCM721 without coating delivered a reversible discharge specific capacity of 205.7 mAh g^{-1} at 0.1C and a coulombic efficiency of 70.64% at 0.5C after 100 cycles between 3.0 and 4.3 V was noted. Again, the rate performance obtained was of 95.5 mAh g^{-1} at 5C.

Li et al. [132] constructed La-Al coating and doped co-modified $LiNi_{0.8}Co_{0.1}Mn_{0.1}O_2$ by wet coating method followed by calcination. La-Al was uniformly doped in the inner layer and the coated layer of La_2O_3 was distributed in the bulk phase. As a result, the doping and coating of La-Al promoted the migration of Li^+, decelerated the electrochemical polarization and amplified the reversibility of phase transition between H2 → H3 during lithiation/delithiation process. The La_2O_3 coating layer offered an exhaustive protection and suppressed the side reactions between materials and electrolyte, further improving the storage stability. During cycling, excellent structural stability of 86.4% at 1C was demonstrated after 100 cycles in the cell within a potential range of 2.7–4.3 V (Fig. 19).

Recently, Yoon et al. [154] prepared Co_xB-NCM811 by a room-temperature synthesis route to construct high-guality coatings. Under the strong driving force of interfacial chemical reaction, Co_xB is not only completely wrapped on the surface of secondary particles, but also injected into the grain boundary of primary particles. As a result, Co_xB-NCM811cathode dramatically improved the cycling stability and the rate capability, and delivered a superior capacity rentention of 95% at 1C after 500 cycles in practical pouch-type full-cells. Mechanically, DFT calculation also identified a strong interfacial binding between NCM and Co_xB, which offers a reasonable explanation for the reactive wetting and inhibited oxygen activity observed in the experiment. Therefore, other transition metal boride coatings may also be suitable for Ni-rich cathodes, which puts forward a simple and feasible method to improve the properties of Ni-rich cathodes (Fig. 20).

Although, coating layers of oxides can reduce the direct contact between the Ni-rich materials and the electrolyte and hinder the occurrence of side effects, most oxides exhibit electrical and electrochemical inactivity. Many researchers have also studied the role of the electronic conductive and Li^+ conductive matrix as alternative coatings. Materials with electronic conductivity include carbon, graphene oxide and polymer, and materials with Li^+ conductivity include Li_2ZrO_3, Li_2SiO_3, $LiAlO_2$ et al. Chung et al. [133] synthesized $LiNi_{0.8}Co_{0.15}Al_{0.05}O_2$ (LNCAO/C) material with conductive carbon-coating by addition of surfactant (SDS) and chemical adsorption SAM synthesis techniques. X-ray diffraction (XRD) peaks depicted that LNCAO/C cathode was also in form of a rhombohedral$R\overline{3}m$ structure, which can be derived from the ordered rock-salt structure of α-$NaFeO_2$ compared with LNCAO. The field emission transmission electron microscopy (FE-TEM) clearly showed that a distinguishable carbon coating of about 2–3 nm thickness was seen on the surface of LNCAO. The electrochemical performance

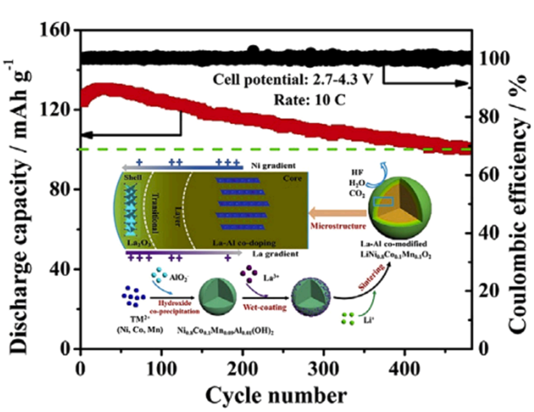

Fig. 19. Illustration for the synthesis and structure of La and Al co-modified Ni rich cathode. Reproduced with permission.[132] Copyright 2019, Elsevier.

such cyclic voltammetry (CV), discharge capacity and cyclic performance demonstrated that the carbon coating with SDS on the surface of LNCAO can effectively prevent the direct contact between electrolyte and cathodes and can avoid being attacked by HF. Further inhibition of the release of oxygen from the lattice as well as exhibition of an excellent initial discharge capacity of 183 mAh g^{-1} along with capacity retention of 93% at 1C in 2.8–4.3 V were also the outcomes of the investigation. Yoon et al. [134] obtained $LiNi_{0.8}Co_{0.15}Al_{0.05}O_2$/graphene cathode using a high energy mechanical ball milling process at 200 rpm min^{-1} for 30 min under argon atmosphere. It was found to deliver a superior discharge capacity of 180 mAh g^{-1} at constant current of 55.6 mA g^{-1} and had excellent capacity retention of 97% even after 80 cycles at 25 °C. However, $LiNi_{0.8}Co_{0.15}Al_{0.05}O_2$ without coating exhibited first discharge capacity of 172 mAh g^{-1} at a constant current of 55.6 mA g^{-1} and capacity retention of 91% after 80 cycles. The graphene coating on the $LiNi_{0.8}Co_{0.15}Al_{0.05}O_2$ enhanced the conductivity of the cathode material and reduced the polarization of the battery. Unlike other carbon coating experimental approach, this method used graphene for coating which can be directly derived from carbon source without high-temperature sintering. Although this method can save energy and protect the environment, cost-effectiveness and improvement of the homogeneity of graphene coating should be considered. Kong et al.[135] synthesized $LiNi_{0.6}Co_{0.2}Mn_{0.2}O_2$ materials with a homogeneous thickness of C-Al_2O_3 composite. Whilst comparing with $LiNi_{0.6}Co_{0.2}Mn_{0.2}O_2$ using the coating of Al_2O_3, it was seen that the dual-functional C-Al_2O_3 coating on the surface of $LiNi_{0.6}Co_{0.2}Mn_{0.2}O_2$ showed a superior reversible discharge capacity of 186.6 mAh g^{-1} and excellent capacity retention of 93.5% at 0.1C. The synergistic effect between the amorphous Al_2O_3 and conductive carbon improved the structural stability and electrochemical kinetics of $LiNi_{0.6}Co_{0.2}Mn_{0.2}O_2$ cathode material. The carbon network in dual-functional C-Al_2O_3 coating on the surface of $LiNi_{0.6}Co_{0.2}Mn_{0.2}O_2$ composite provided high electrical conductivity and reduced the charge transfer resistance on the electrode surface (Fig. 21).

Gan et al. [155] synthesized NCM811@PANI-PVP by polyvinylpyrrolidone (PVP) surfactant-induced homogeneous coating of polyaniline (PANI) on the surface of the NCM811. The coating layer of PANI not only provided a fast channel for electron conduction, but also inhibited direct contact between the electrode materials and the electrolyte. It further hindered side reactions and improved the electrochemical performance. Excellent capacity retention of 88.7% at a constant current of 200 mA g^{-1} after 100 cycles and a superior rate performance of 152 mAh g^{-1} at 1000 mA g^{-1} were achieved. In-situ X-ray diffraction and in-situ Raman spectra investigated the charge–discharge mechanism and the cyclability of NCM811@PANI-PVP upon electrochemical reaction. This surfactant-modulated surface homogeneous coating approach provided a new strategy to stabilize Ni-rich cathodes and improved the electrochemical performance for lithium ion batteries.

Du et al. [156] obtained $LiNi_{0.8}Co_{0.15}Al_{0.05}O_2$ with $LiAlO_2$ coating by spray-drying coating technique. The study revealed a capacity retention of 90.40% after 150cycles at 1.0C in 2.8–4.4 V, which was significantly higher than that of the pristine material. This effective coating technology can significantly improve the structural stability, and can be extended to other cathodes, to further obtain a higher safety and better cycle stability for Ni-rich materials. Surface coating on the surface of Ni-rich cathodes is an effective approach to solve the serious problems such as fast energy loss and structure stability in LIBs. Nevertheless, the coating of single and double layers has many serious defects. Herein, Guo et al. [157] synthesized Li_xTiO_2 nano-particles embedded in amorphous silica (LTSO) using the strategy of a dual-component in one coating layer by facile approach. The results obtained showed excellent electrochemical performance and improved the ion diffusion kinetics (Fig. 22).

Huang et al. [136] developed an in-situ coating technology, which realized the controllable construction of the material surface coating

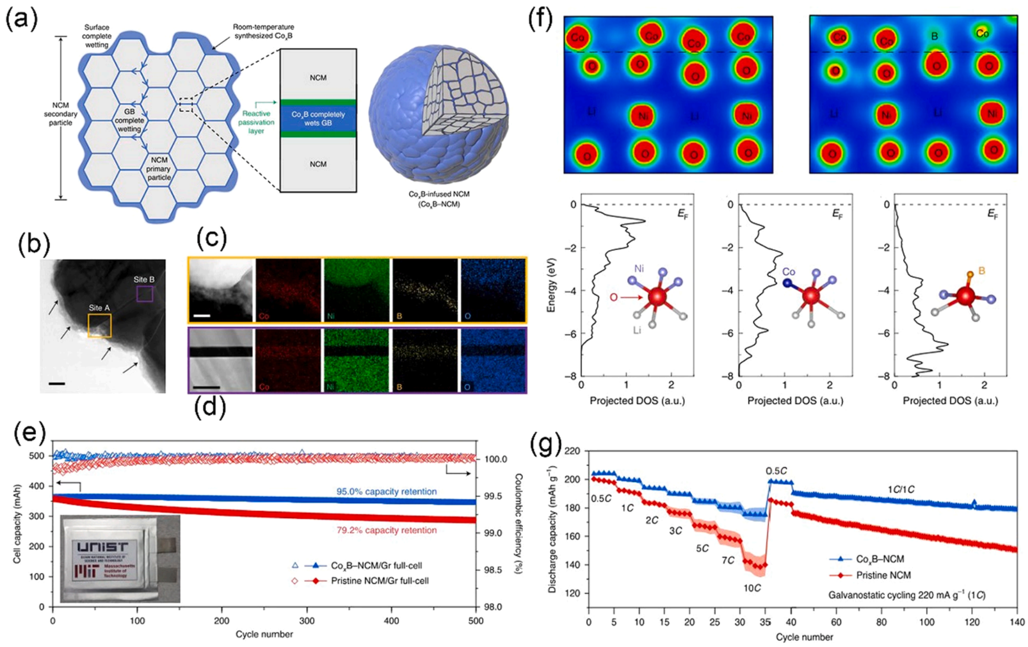

Fig. 20. (a) Schematic coating-plus-infusion microstructure. (b) TEM images of cross-sectioned Co$_x$B-NCM cathode. (c) EDS mapping of site A in b. (d) EDS mapping of site B in b. (e) Cycling performance in full-cells at 1C in the range of 2.8–4.3 V. (f) Strong interfacial bonding suppresses oxygen activity. (g) Rate performance of Co$_x$B-NCM811 and NCM811cathodes. Reproduced with permission.[154] Copyright 2021, nature.

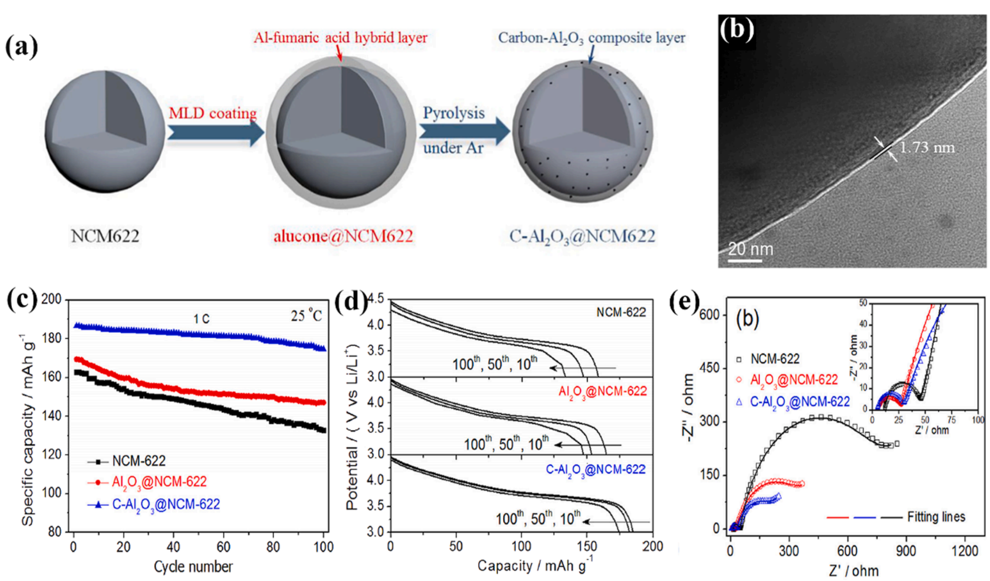

Fig. 21. (a) Schematic illustration for the synthetic procedure of MLD-derived C-Al$_2$O$_3$ coating on the surfa ce of NCM-622. (b) TEM images of C-Al$_2$O$_3$@NCM-622. (c) cyclic performanceof the pristine and coated NCM-622 electrodes at 25 °C, and the corresponding discharge profiles. (d) at the 10th, 50th, and 100th cycles. (e) Nyquist plots of pristine NCM-622, Al$_2$O$_3$@NCM-622 and C-Al$_2$O$_3$@NCM-622 electrodes at a charge state of 4.4 V for 50th cycle. Reproduced with permission.[135] Copyright 2019, Elsevier.

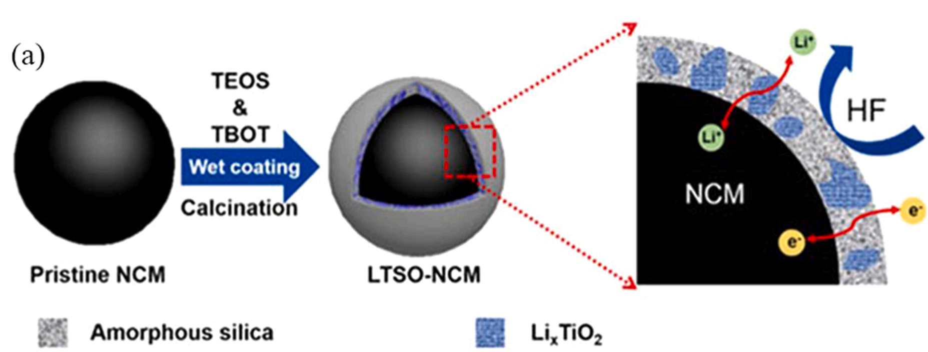

Fig. 22. Preparation of dual-component coating NCM by one-pot method. Reproduced with permission.[157] Copyright 2019, Elsevier.

and the regulation of the order degree of the layered structure. At the same time, in situ XRD and electrochemical performance test were performed which revealed the inherent mechanism of the coating layer of Li_2MnO_3 which helped to improve the cyclic stability of Ni-rich cathode materials. The results showed that the Li_2MnO_3 coating can effectively inhibit the irreversible phase transitions as well as the occurrence of interfacial side reactions during the cycling process, which effectively enhanced the long-cycling stability, rate performance and high-temperature working performance of the Ni-rich cathode materials. This work is expected to be the reference for the preparation of high energy density and Ni-rich cathode materials.

Residue lithium is considered to be one of the most critical factors affecting the electrochemical performances of Ni-rich layered oxide cathode materials. This is because residual lithium (Li_2O and Li_2O_2) on the surface of Ni-rich layered oxide cathode materials reacts with CO_2 and H_2O in the air to form Li_2CO_3 and LiOH. Li_2CO_3 and LiOH not only consume Li^+ in materials, but also have no electrochemical activity, which causes capacity degradation. The dense layer of Li_2CO_3 on the surface of particles hinders the diffusion of Li^+, and further causes irreversible capacity loss during charging and discharging. In addition, the surface LiOH reacts with $LiPF_6$ to generate HF, which results in the deterioration of lithium ion battery performance. In recent years, many researchers have testified that some coating materials can consume Li_2CO_3 and LiOH on the surface of Ni-rich layered oxide cathode materials and reduce the residual alkalinity as well as improve the electrochemical performance.

Liu et al. [127], for the first time, synthesized Ni-rich $LiNi_{0.8}Co_{0.1}Mn_{0.1}O_2$ cathode material with In_2O_3 and $LiInO_2$ co-coating layer on the surface. During sintering, the surface of $LiNi_{0.8}Co_{0.1}Mn_{0.1}O_2$ cathode material formed an In_2O_3 coating layer, and then In_2O_3 reacted with the residual lithium (LiOH and Li_2CO_3) of $LiNi_{0.8}Co_{0.1}Mn_{0.1}O_2$ to form an In_2O_3 &$LiInO_2$ coating layer. The specific reactions are as follows:

$$In_2O_3 + 2LiOH \rightarrow [2LiInO]_2 + H_2O\uparrow \quad (16)$$

$$In_2O_3 + Li_2CO_3 \rightarrow [2LiInO]_2 + CO_2\uparrow \quad (17)$$

High-resolution transmission electron microscopy (HR-TEM) proved that the surface on the NCM811 formed a homogeneous coating layer of about 12 nm thickness, and two different lattice spacing in the coating layer corresponds to In_2O_3 and $LiInO_2$, respectively. Electrochemical performance demonstrated that the NCM811 with the In_2O_3&$LiInO_2$ co-coating not only exhibited a superior capacity retention of 90% at 1C, but also delivered superb discharge capacity of 177.1 mAh g^{-1} at 5C and a capacity retention of 86.4% after 300 cycles (Fig. 23).

In addition, part of Li_2O remains behind in high temperature calcinations. H_3PO_4 also reacts with Li_2O material's surface. It is generally believed that it is impossible to completely remove water molecules from commercial electrolytes. The presence of traces of water in the electrolyte results in the decomposition of $LiPF_6$, which is further associated with the formation of HF. What's worse, the HF, generated from the hydrolysis of $LiFP_6$, accelerates the gradual disintegration of the active materials by dissolving transition metal ions. The reaction equations are as follows [129]:

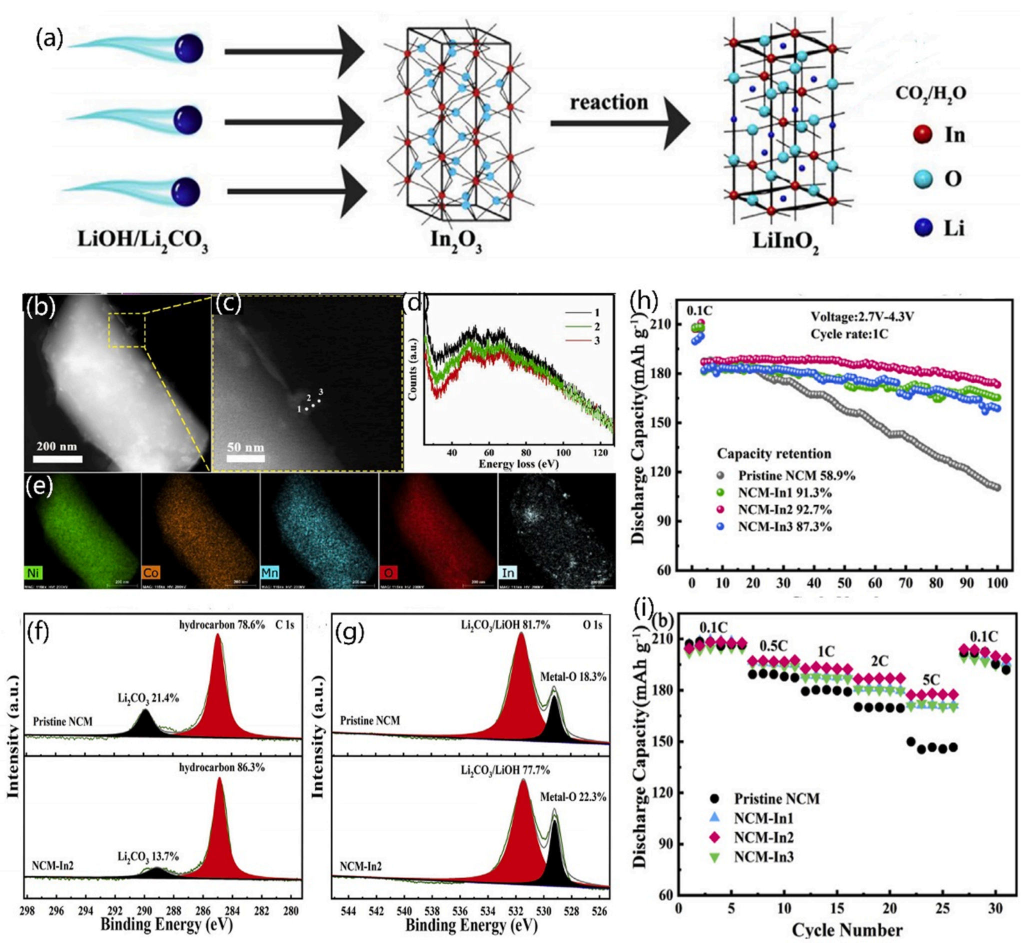

Fig. 23. (a) Schematic illustration of the formation of $LiInO_2$. (b-c) HAADF images of NCM-In2. (d) EELS spectra ranging from 25 to 130 eV for NCM-In2 at different points. (e) STEM elemental mapping of NCM-In2. (f) C 1 s and (g) O 1 s taken from the surface of pristine and NCM-In2 samples. (h) cycling performance of pristine and co-coated samples at 1C. (i) rate performance of pristine and co-coated samples. Reproduced with permission.[127] Copyright 2019, Elsevier.

$$LiPF_6 \rightarrow PF_5 + LiF \quad (18)$$

$$PF_5 + H_2O \rightarrow 2HF + POF_3 \quad (19)$$

$$POF_3 + Li_2O \rightarrow Li_xPOF_y + LiF \quad (20)$$

$$NiO + 2HF \rightarrow NiF_2 + H_2O \quad (21)$$

$$CoO + 2HF \rightarrow CoF_2 + H_2O \quad (22)$$

$$MnO + 2HF \rightarrow MnF_2 + H_2O \quad (23)$$

Fan et al. [128] used wet chemical method to convert H_3PO_4, LiOH and Li_2CO_3 on the surface of Ni- rich $LiNi_{0.8}Co_{0.1}Mn_{0.1}O_2$ (NCM811) into uniform Li_3PO_4 coating layer, and then used high conductivity graphene (GN) to connect the secondary particles of Ni-rich $LiNi_{0.8}Co_{0.1}Mn_{0.1}O_2$ (NCM811) together to obtain multi-functional coated materials (GN-LPO-NCM811) with high ionic and electronic conductivities. As a result, the electrochemical performance, safety performance and storage performance of the material have been significantly improved (Fig. 24**a-c**). Zhu et al. [129] successfully synthesized Li_3PO_4-coated $LiNi_{0.8}Co_{0.1}Mn_{0.1}O_2$(NCM811) cathode material by lithium-reactive coating. The test results showed that the Li_3PO_4-coated NCM811 achieved improved cycling performance at room temperature as well as at elevated temperatures. In addition, there are other functions like (1) removal of residual lithium (LiOH and Li_2CO_3) which impedes Li^+ migration; (2) protection of the core NCM811 materials from HF attack in the electrolyte; (3)HF scavenger to reduce the level of HF in the electrolyte **(**Fig. 24**d-f)**. The reaction equations are as follows:

$$(NH_4)_2HPO_4 + 3LiOH \rightarrow Li_3PO_4 + 2NH_3 + 3H_2O \quad (24)$$

$$2(NH_4)_2HPO_4 + 3Li_2CO_3 \rightarrow 2Li_3PO_4 + 4NH_3 + 3CO_2 + 3H_2O \quad (25)$$

$$Li_3PO_4 + HF \rightarrow LiF + Li_xH_yPO_4 \text{ (or } PO_xH_y) \quad (26)$$

$$Li_3PO_4 + HF \rightarrow Li_2O + Li_xH_yPO_4 \text{ (or } PO_xH_y) \quad (27)$$

5.3. Morphology design

Ni-rich cathodes are generally composed of mixed and disordered arrangements of initial particle reunion of secondary particles. Its structure and characteristics lead to internal stress and complex lithium ion transport path in the charging/discharging process which further lead to poor cycle stability and rate performance as well as greatly limit the application process. Due to the anisotropic properties of crystal, modification in the morphology in order to improve the stability and rate performance cycles can be realized as an effective strategy. But from the two aspects of structure and morphology, controllable synthesis with excellent cycle stability and rate performance are still a significant challenge, especially in the field of large-scale commercialization. Core-shell and concentration gradient structured materials not only inhibit the reactions between Ni^{4+} and electrolyte on the surface, but also reduce the influence of coating on discharge specific capacity and energy density, and further improve the structure stability of Ni-rich cathode materials.

Sun et al. [137] synthesized a $Li[(Ni_{0.8}Co_{0.1}Mn_{0.1})_{0.8}(Ni_{0.5}Mn_{0.5})_{0.2}]O_2$ material of spherical core shell structure, namely the high specific capacity $Li[Ni_{0.8}Co_{0.1}Mn_{0.1}]O_2$ (NCM811) cathode, and a good thermally stable $Li[Ni_{0.5}Mn_{0.5}]O_2$ regarded as the core and shell, respectively. The $[(Ni_{0.8}Co_{0.1}Mn_{0.1})_{0.8}(Ni_{0.5}Mn_{0.5})_{0.2}](OH)_2$ precursor with spherical core shell structure was initially obtained by a modified hydroxide co-precipitation method, and then uniformly mixed with the stoichiometric amount of LiOH. Next, the mixture of $[(Ni_{0.8}Co_{0.1}Mn_{0.1})_{0.8}(Ni_{0.5}Mn_{0.5})_{0.2}](OH)_2$ precursor and LiOH were sintered to obtain the $Li[(Ni_{0.8}Co_{0.1}Mn_{0.1})_{0.8}(Ni_{0.5}Mn_{0.5})_{0.2}]O_2$ with spherical core–shell structure. Scanning electron microscope (SEM) showed that the inner core was tightly wrapped by the outer shell layer. It delivered a superior long-term cycling performance and capacity retention was relative to the NCM811 at 1C after 500 cycles. A new type of Ni-rich positive cathodes with core shell structured is a major breakthrough in the development of high capacity density LIBs (Fig. 25**a-c**). Kim et al. [158] designed a new hybrid cathode material, $LiNi_{0.886}Co_{0.049}Mn_{0.05}Al_{0.015}O_2$, which was synthesized using $LiNi_{0.934}Co_{0.043}Al_{0.015}O_2$ encapsulated by $Li[Ni_{0.844}Co_{0.061}Mn_{0.080}Al_{0.015}]O_2$. Its core part was Ni-rich $LiNi_{0.934}Co_{0.043}Al_{0.015}O_2$ (NCA) and the outer layer shell part was $Li[Ni_{0.886}Co_{0.049}Mn_{0.05}Al_{0.015}]O_2$. It exhibited excellent reversibility discharge capacity of 225 mAh g^{-1} at 0.1C and a superior capacity retention of 91% at 1C after 1000 cycles. (Fig. 25**d-f**). In order to achieve high pressure density and excellent velocity performance at the same time, Su et al. [137] synthesized structural gradient $LiNi_{0.8}Co_{0.1}Mn_{0.1}O_2$ cathode materials. The gradient Ni-rich cathode material demonstrated excellent electrochemical performance, especially a rate performance of 160 mAh g^{-1} at 10C.

Porous electrodes with multi-shell structure have attracted much

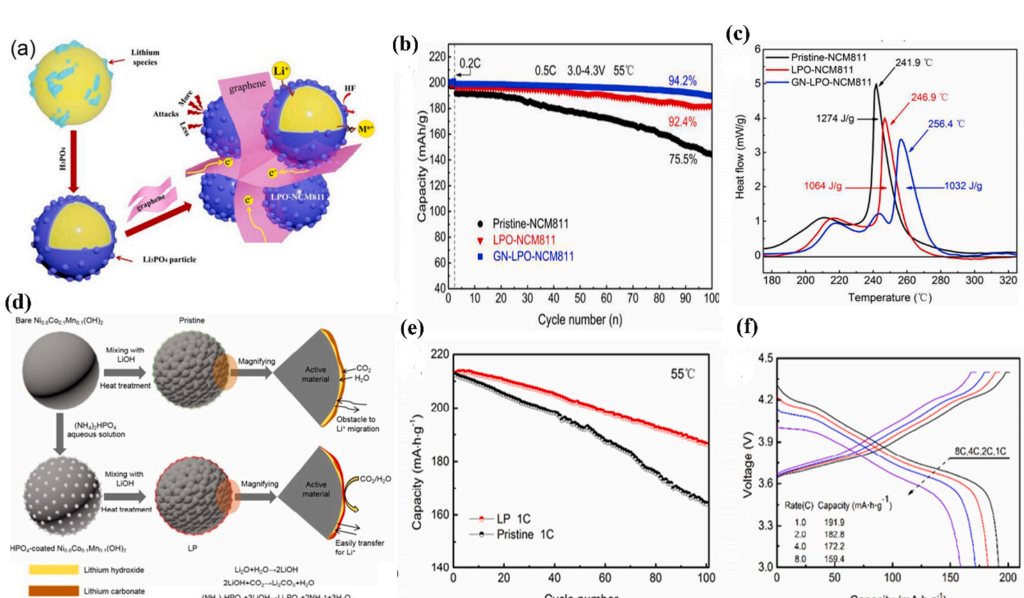

Fig. 24. (a) The synthesis schematic and working mechanism of GN-LPO-NCM811. (b) The cycling performance for pristine and modified samples in the voltage range 3.0–4.3 V at 0.5C at 55 °C. (c) The differential scanning calorimetry traces showing heat flow from the reaction of the electrolyte with pristine NCM811, LPO-NCM811, and GN-LPONCM811 charged to 4.3 V. Reproduced with permission.[128] Copyright 2019, Elsevier. (d) Schematic illustration of chemistry on the surface. (e) Cycling performance of the as-prepared samples over the voltage range of 3.0 ~ 4.4 V at 55 °C at 1C. (f) rate capability for the LP. Reproduced with permission. [129] Copyright 2019, Elsevier.

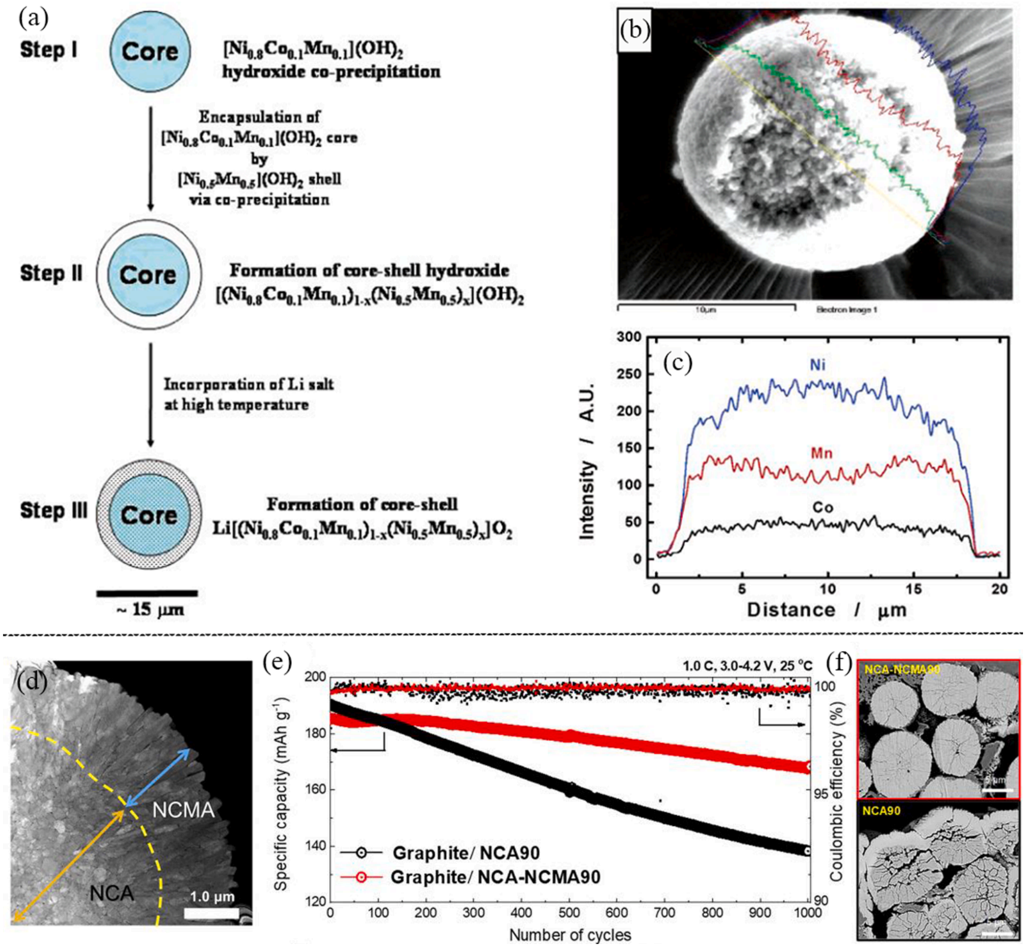

Fig. 25. (a). Schematic diagram of the structure of concentration gradient cathode materials and electrochemical performance. (b-c) The energy dispersive spectroscopic (EDS) image of the Li $[(Ni_{0.8}Co_{0.1}Mn_{0.1})_{0.8}(Ni_{0.5}Mn_{0.5})_{0.2}]O_2$ particle. Reproduced with permission. [137] Copyright 2005, American Chemical Society. (d) TEM image of an NCA-NCMA90 primary particles. (e) Long-term cycling performance of the NCA90 and NCA-NCMA90 cathodes in full cells. (f) Cross-sectional SEM images of the NCA90 and NCA-NCMA90 cathodes from the full cells after 1000 cycles. Reproduced with permission.[158] Copyright 2019, Elsevier.

interest in recent years. First, the porous multi-shell structure provides more lithium ion channels to enhance specific capacity. Second, the multi-shell structure has a lithium ion diffusion path that is very short, leading to good rate performance. As a cathode material for lithium ion batteries, exhibition of high performance is mandatory. Zou et al. [49] synthesized a nickel rich multilayer hollow fiber material with low cation mixing using green algae fiber as template. Compared with the traditional nickel rich materials, the multi-layer hollow fiber materials had lower cationic mixed defects and multi-layer hollow fiber conductive network. Thereby, the materials showed excellent electrochemical performance (Fig. 26**a-f**). In addition, Xu et al. [48] synthesized secondary spherical Ni-rich cathodes NCM811, which was formed by the primary agglomeration of radially oriented single crystal particles. The surface of the spherical secondary particles were Li^+ active (010) crystal, which formed three-dimensional Li^+ transport channels, thus improving the Li^+ transport rate and rate performance. In addition, the radial primary particles have the same orientation, which significantly reduced the grain boundary stress caused by the anisotropic volume change, further inhibiting the particle breakage and improved the cycle stability (Fig. 26**g-i**).

5.4. Crystal form regulating

In recent years, many studies have reported that oxide positive electrode can improve specific capacity when charged at high voltage, but the increase in voltage will aggravate the material decomposition and seriously affect the safety performance of the battery. It is generally believed that the transition of nickel rich cathode materials from layered to spinel or completely disordered rock salt structure, as well as the dissolution, migration and segregation of transition metals (TMs), can cause structural reconstruction, resulting in capacity attenuation. It is observed that the inhomogeneous stress can cause intra-grain cracks during the cycle, which can aggravate the collapse and capacity loss of the nickel rich cathode materials structure. Some traditional modification methods including doping and coating have been reported to inhibit the cation mixing and interface side reactions. But excessive coating and unregulated doping might hinder the migration of Li^+, thus affecting the electrochemical performance of the battery. In order to solve these defects, creative strategies must be adopted to improve the structural stability of cathodes. The ideal method is to adjust the structural and morphological characteristics simultaneously in order to impede the structural failure and inter-granular fracture. Compared with traditional polycrystalline particles, single-crystal cathode materials have attracted a solemn attention due to its excellent capacity retention rate in the long cycle. Firstly, the cracking of nickel rich oxides can be inhibited due to the inherent structural integrity and continuous conductive network of single crystal particles. Second, compared with the polycrystalline materials, single crystal electrodes have no grain boundaries in theory, which can improve the antioxidant capacity and structural stability in the process of interacting with electrolytes.

In order to further understand the correlation between surface structure, internal strain, and capacity deterioration, Qian et al. [47] directly observed the correlation between surface chemistry and phase distribution from homogeneity to heterogeneity by using X-ray spectroscopy and nano tomography, which induced heterogeneous internal strain within the particle and structural/performance degradation during cycling. The improved strategy effectively adjusted the performance degradation of single crystal cathode and provided a new idea for

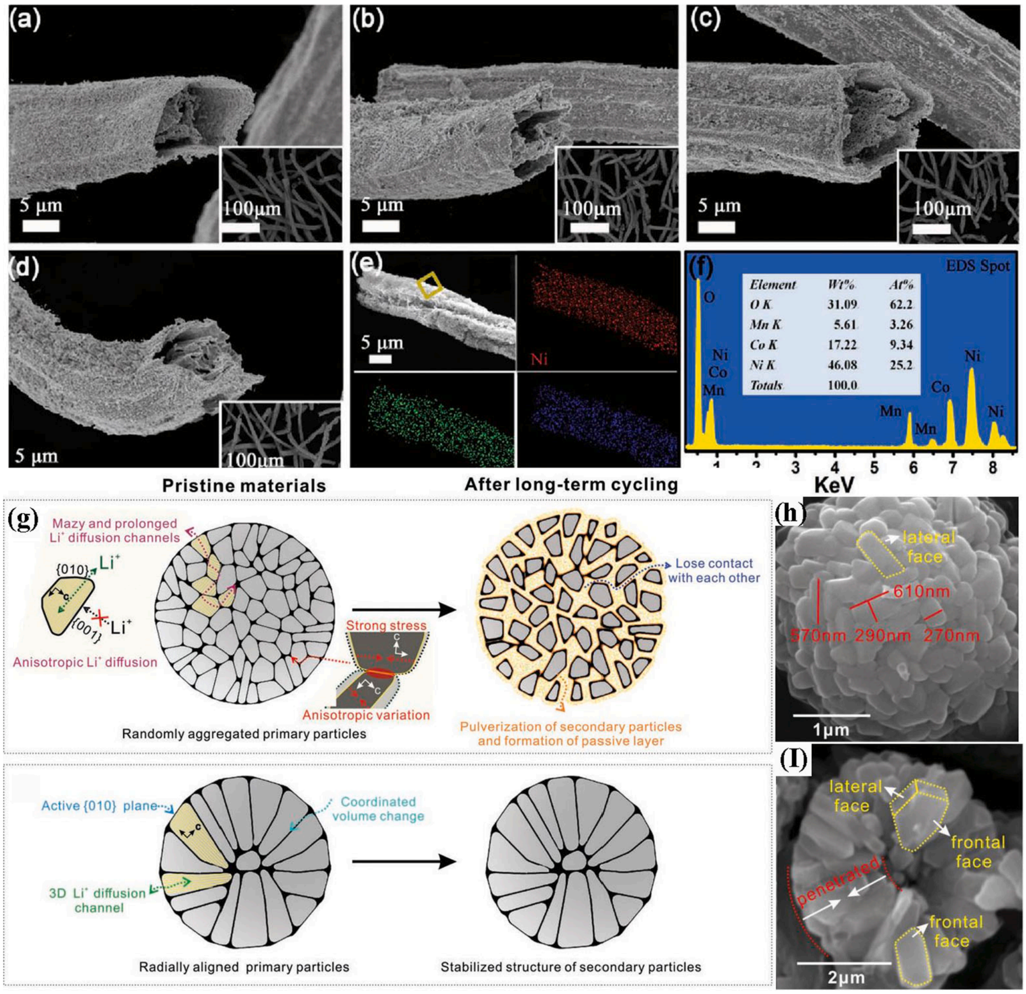

Fig. 26. Cross-section SEM images of the multi shelled $LiNi_xCo_yMn_zO_2$ hollow fibers (a) x = 0.8, (b) x = 0.7, (c) x = 0.65, (d) x = 0.5. (e) SEM image of $Li(Ni_{0.65}Co_{0.25}Mn_{0.1})O_2$ and the corresponding EDS mapping for Ni, Co, Mn elements. (f) EDS spectrum collected from the area in panel (e) of $Li(Ni_{0.65}Co_{0.25}Mn_{0.1})O_2$. Reproduced with permission.[49] Copyright 2017, Wiley-VCH. (g) Schematic illustration of the structure and characteristics of C-NCM (commercial NCM) and RASC-NCM materials. (h) SEM images of RASC-NCM. (i) cross-sectional SEM images of RASC-NCM. Reproduced with permission.[48] Copyright 2019, WILEY-VCH.

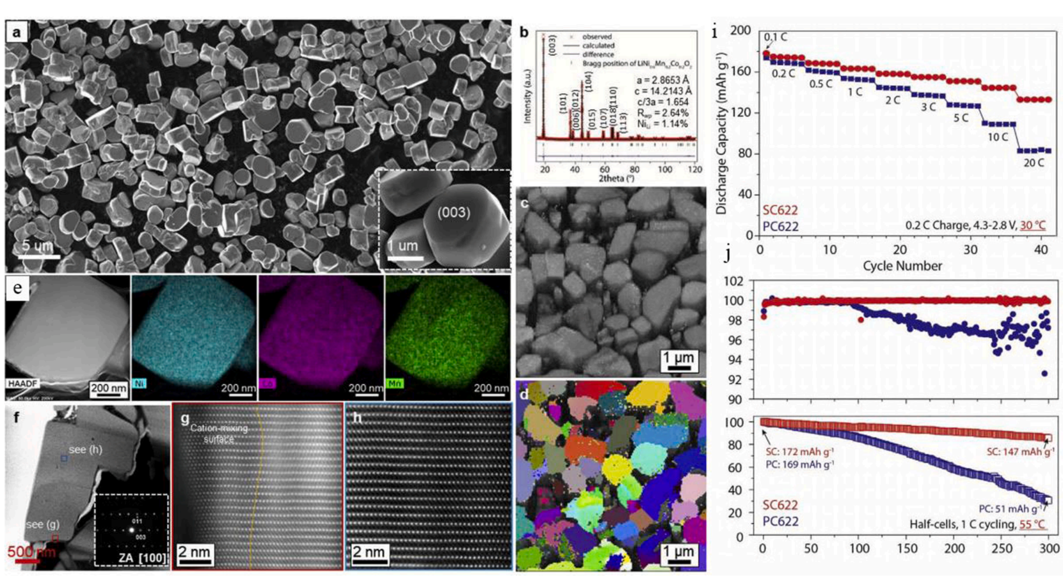

Fig. 27. (a) SEM image of the as-synthesized particles. (b) PXRD pattern and the Rietveld refinement results. (c) and (d) are band-contrast EBSD map and the EBSD orientation (Euler angles) map of the particles. Each color in (d) indicates a specific crystal orientation of the grains compared to a chosen reference. (e) STEM-EDS mapping of the particle showing homogeneous distribution of Ni, Co, and Mn elements. (f) STEM image of a particle oriented along the [99] zone axis of $LiNi_{0.6}Mn_{0.2}Co_{0.2}O_2$. (g) and (h) are HAADF-STEM images showing the particle has well-formed layered structure and a surface cation mixing layer of 3–5 nm in thickness. (i) Half-cell rate capability tests of the SC622 cathode and PC622 cathode. (j) half-cell cycling performance of the SC622 and PC622 cathodes at a current density of 1C in 2.8–4.3 V at 55 °C. Reproduced with permission.[47] Copyright 2020, Elsevier.

improving the performance of cathode (Fig. 27). Fan et al. [138] synthesized a single crystal and the secondary particle sample. It has been proved by testing that the sample of secondary particles in the process of charge–discharge cycle process still maintained the R3m-layered structure in the central bulk far away from the nano crack. However, the approached parts gradually deteriorated into disordered layered phase and defect rock-salt phase, which eventually transferred into the disordered rock-salt phase at the nano-crack surface. Compared with the materials with secondary particle morphology, nano/micro cracks were not observed in the synthesized single crystal materials, and the integrity of micron particles was well maintained both inside and outside.

5.5. DOD setting

The mechanism of capacity attenuation of high nickel positive electrodes (NCM and NCA) involves the accumulation of mechanical strain caused by the sudden collapse of layered structure during phase transformation, and the formation and development of inter granular micro cracks. A lot of research has been carried out to improve the cycle stability of high nickel positive electrode by coating and doping, but minor results have been perceived. Yoon et al. [44] found that the cycle stability of the cylindrical battery based on NCA positive electrode and graphite negative electrode was poor, and the capacity retention rate was of only 50% after 2000 cycles at 100% discharge depth. However, when the discharge depth was 60%, the cycle performance was found to be better, which indicated that the discharge depth should be limited to 60% in order to achieve long-term cycle stability. However, this reduced the energy density and increased the weight and cost of the battery.

5.6. Electrolyte modification

Electrolyte is known as the “blood” of lithium-ion batteries. It plays an important role in the performance of lithium-ion batteries (LIBs), especially in the structure and properties of the interface between electrodes and electrolyte. However, the structural changes and interface side reactions of cathode materials under high voltage and high temperature bring great challenges to the practical applications in the traditional electrolyte system. It is one of the effective methods to improve the electrochemical performance of lithium-ion battery by developing suitable electrolytes to improve the interface structure between electrode and electrolyte, which has attracted extensive attention in recent times. Since $LiFP_6$ decomposes and produces HF at high pressure and high temperature, a series of safety problems are a matter of concern. In $LiPF_6$ based electrolytes, the use of additives to establish a uniform cathode electrolyte interface (CEI) and removal of reactive HF and PF_5, is considered as a method to maintain the stable electrochemical performance of Ni rich cathodes. Before the decomposition of electrolyte solvents such as ethylene carbonate (EC), dimethyl carbonate (DMC) and lithium salt, the film-forming additives are oxidized on the surface of nickel rich cathode to form uniform CEI. The existence of uniform CEI can inhibit the side reaction of electrolyte at the cathode. Dong et al. [139] introduced p-toluenesulfonyl isocyanate (PTSI) as electrolyte additive. The test showed that the $Li/LiNi_{0.5}Co_{0.2}Mn_{0.3}O_2$ half-cell with PTSI exhibits superior rate capability when compared to that of the baseline electrolyte. The discharge capacity retention is elevated from 71.4% to 86.2% after 100 cycles at room temperature. This can be also attributed to the –S = O group in PTSI which serves as the weak base site to restrain the reactivity of PF_5, resulting in the suppression the formation of LIF and HF (Fig. 28).

Phosphite derivatives as additives are an efficient method to make a protective film on high-voltage nickel rich cathodes, to mitigate the hydrolysis reactions of $LiPF_6$, and to eliminate HF. Researchers have aroused their interest to test the effect of phosphate based additives on nickel rich cathode materials. Song et al. [159] carried out a comparative study by using organophosphorus compounds including triphenyl phosphite (TPP), trimethyl phosphite (TMP), tris(2,2,2-triflfluoroethyl) phosphite (TFEP), and tris(trimethylsilyl) phosphite(TMSP) in Li/LNMO half cells. It was found that the cycle performance and rate performance of the half-cell were significantly improved under the action of TMP. Moreover, phosphite based additives inhibited the hydrolysis of

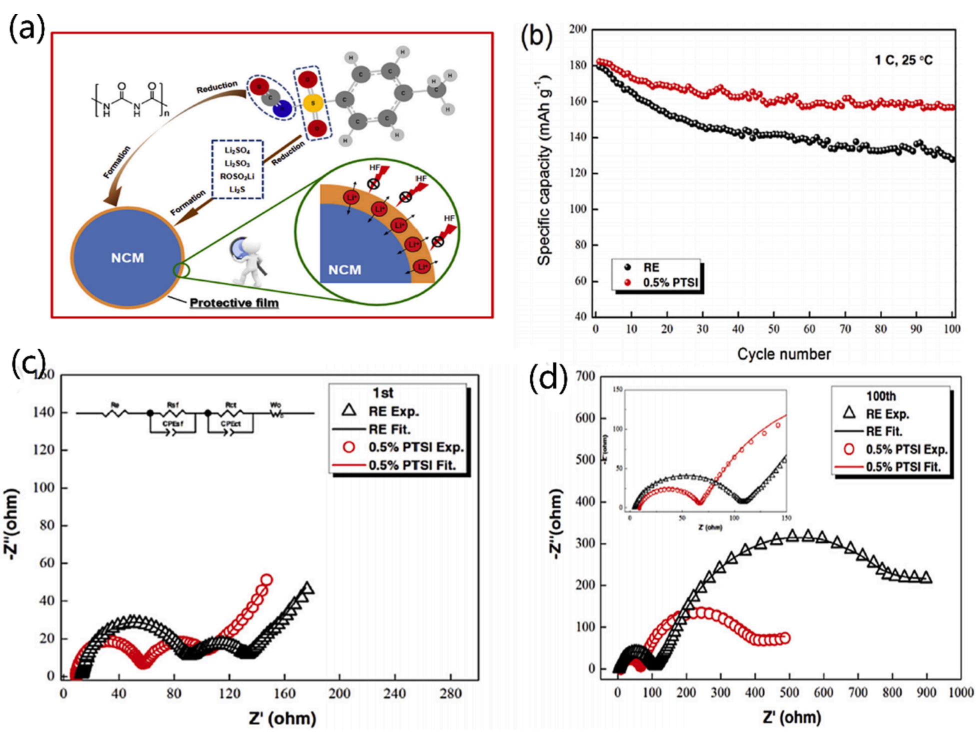

Fig. 28. (a) Schematic mechanism on the roles of PTSI to the high voltage electrochemical properties improvement of $LiNi_{0.5}Co_{0.2}Mn_{0.3}O_2$ electrode. (b) The cyclic performance at 25 °C. (c) Nyquist curves of $Li/LiNi_{0.5}Co_{0.2}Mn_{0.3}O_2$ half cells in RE and PTSI-containing electrolyte after first cycle and (d) 100 cycles under 55 °C and 1C rate. Reproduced with permission.[139] Copyright 2017, Elsevier.

$LiPF_6$ and removed HF. Jang et al. [140] proposed silyl-functionalized dimethoxydimethylsilane (DODSi) as a multi-functional additive. In contrast to the typically attempted cathode additive, silyl-functionalized dimethoxydimethylsilane had a wide electrochemical window up to 5.0 V, which indicated that DODSi will not damage the electrochemical stability of traditional carbonate based electrolytes. In terms of cycle performance, the use of DODSi effectively improved the cycle performance and rate performance at higher potential. DODSi removed F from the battery and inhibited the additional side reactions on the surface of NCM811. Presently, Yim et al. [141] showed that DVS oxidized and decomposed on the surface of NCM721 electrode material, forming an inert layer on the surface of positive electrode material and thereby reducing the decomposition of electrolyte on the surface of positive electrode. This resulted in the significant improvement of the cycle stability of NCM721 electrode material. In order to analyze the composition of the inert layer formed on the surface of NCM721 by DVS, the surface composition of NCM721 was characterized by means of FT-IR. Polycarbonate (RCO_2R) and carbonate (Li_2CO_3) were observed on the surface after one cycle, from the test results, which mainly come from the decomposition of the solvent. At the same time, the absorption signals (1275 cm^{-1} and 1371 cm^{-1}) of polyalkyl sulfone and polyolefin functional groups on the surface of NCM721 particles using DVS additive electrolyte were observed, which indicated that DVS did decompose on the surface of NCM721 particles (Fig. 29 **a-b**). Deng et al. [142] used fluoridated lithium electrolyte (FEC: FEMC: HFE, 2:6:2) and 2% LiDFOB to produce F and B rich cathode/electrolyte interface which was able to withstand the volume expansion of $LiNiO_2$. The $LiNiO_2$ with this electrolyte provided discharge capacity of 210 mAh g^{-1} at 0.5C, and the capacity retention was still maintained at 80% even after 400 cycles (Fig. 29**c-d**).

5.7. Binder

Usually, PVDF is a commonly used binder in cathode materials (used with NMP solvent) with good bond strength, electrochemical stability and insoluble in electrolyte, but its alkali resistance is poor. [160] When high nickel system is selected as the cathode material, the residual alkali content in the material becomes higher and higher with the increase of capacity. Under the strong alkali environment, PVDF will produce decomposition reaction, resulting in the separation of hydrogen fluoride and making the slurry gel (Fig. 30). At the same time, some side reactions will occur on the surface of the high nickel positive electrode,

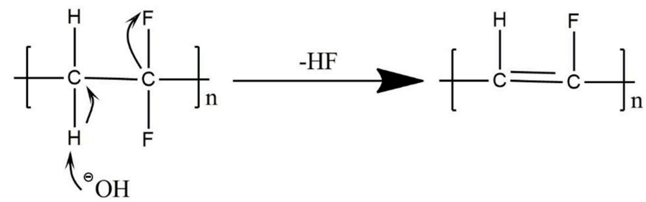

Fig. 30. Reaction formula of PVDF elimination reaction.

which will cause the secondary particles to collapse, resulting in a decrease in the conductivity of the battery. [161] At present, we have summarized the following three points to solve this problem: 1. Reduce alkaline substances. 2. The alkali resistance was improved by PVDF modification. 3. Replace PVDF with new binder. For the treatment of the Ni-rich cathode itself, the optimization of sintering process can reduce the residual alkaline impurities on its surface, but compared with water washing process, this method is not complete. At the same time, water washing will lead to the attenuation of material properties, so these two methods are not applicable. Therefore, coating a layer of stable oxide is a better choice. In addition, the addition of Lewis acid (such as $LiPF_6$) [162] which can neutralize with free alkali in the Ni-rich cathode has been reported as a feasible method. The application performance of PVDF in high nickel NCM can also be improved by modifying PVDF. For example, Maurizio Biso et al. Found that the chemical modification of PVDF by Solef was effective in preventing gelatinization of slurry compared with emulsion polymerization PVDF.[163] Meanwhile, Ki Jae Kim of Korea's Jianguo University and Jang wook Choi of Seoul University reported a high elastic binder spandex (spdx), which can overcome the problems of nickel rich layered cathode materials and significantly improve their electrochemical properties. The high elasticity of spdx enables it to uniformly coat $LiNi_{0.8}Co_{0.1}Mn_{0.1}O_2$ particles through shear force during slurry mixing, so as to prevent side reactions in the circulation process of particles, which will greatly promote the wide application of nickel rich cathode materials in the future. [164] Japan's ZEON group also said that it has developed a new fluorine-free binder, which can replace the traditional PVDF too."

5.8. Separator

Separator is a kind of functional membrane material with microporous structure, and its thickness is generally 8 ~ 40 μm. In the battery

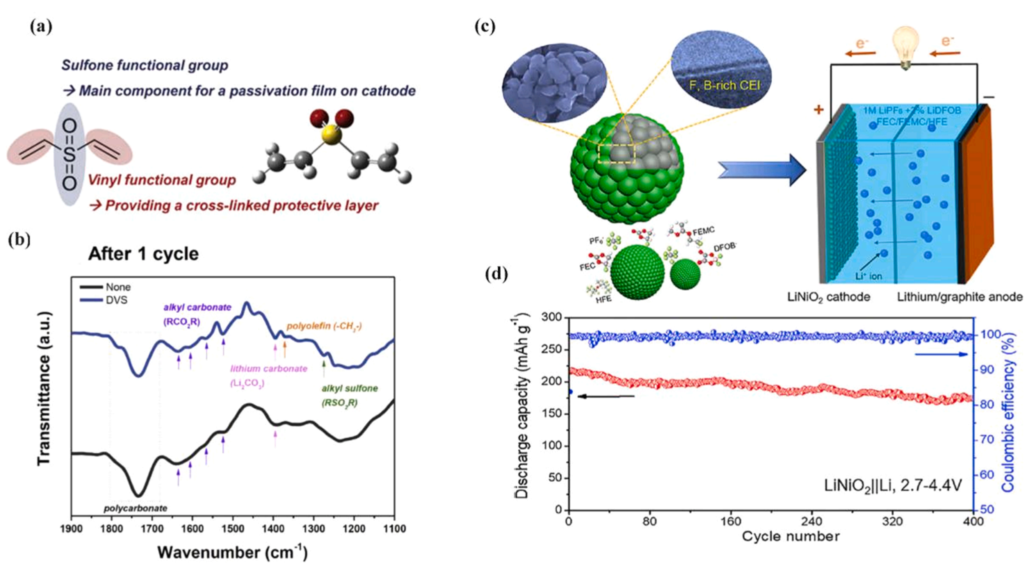

Fig. 29. (a) 2D and 3D molecular structures of DVS. (b) FT-IR analysis results of cycled NCM721 cathode after 1 cycle. Reproduced with permission.[141] Copyright 2015, Elsevier. (c) Synthesis illustrative diagram of $LiNiO_2$. (d) Cycle performance curve of $LiNiO_2$. Reproduced with permission.[142] Copyright 2019, Elsevier.

system, The separator membrane can prevent the short circuit of positive and negative electrodes and provide lithium ion diffusion channel. It can regulate the lithium ion diffusion rate, the retention of electrolyte, the internal resistance of the system and the composition of battery interface structure, so as to affect the electrochemical performance of the battery. However, polypropylene and polyethylene separator currently used commercially will shrink and melt at high temperatures, resulting in short circuit and thermal runaway. The above traditional separator can not meet the current needs of lithium-ion batteries. High porosity, high thermal resistance, high melting point, high strength and good wettability to electrolyte are the development direction of lithium-ion batteries in the future.

According to the development needs of lithium-ion battery technology, researchers have developed a variety of new separators based on the traditional polyolefin membrane. According to the development needs of lithium-ion battery technology, some polymers with better comprehensive performance, such as PVDF、PET and PI et al, have been gradually applied. [165] At the same time, coating inorganic ceramic particle layer or composite polymer layer on the substrate will further improve its comprehensive properties.

For example, Zhao et al. designed a heat-resistant and fireproof double function diaphragm by coating ammonium polyphosphate (APP) particles on a ceramic-coated separator modified with phenol–formaldehyde resin (CCS@PFR). When applied to $LiNi_{0.8}Co_{0.1}Mn_{0.1}O_2$||SiOx-Gr full battery, it has excellent safety performance, does not catch fire in 30 s combustion test and does not fail in 10 min of high temperature test above 300 °C. [166] So in the long run, the traditional separator of single component may be gradually replaced by composite separator with better comprehensive properties. With the rapid development of solid- state batteries, gel electrolytes or solid electrolytes may completely replace the diaphragm in the future

5.9. *Assembly technology*

Safety performance is the largest luxury of electric vehicles. As one of the core components of electric vehicles, the safety of batteries largely determines the safety performance basis of electric vehicles. The optimization of assembly process has a great impact on the safety of lithium-ion battery. The assembly process of the battery is cumbersome. Before assembly, the diaphragm needs 120 °C heat treatment to increase its barrier performance and safety. The battery shall be vacuum dried for 24 h before cell liquid injection to remove the moisture and moisture in the battery components, so as to prevent $LiPF_6$ from reacting with water to form HF and shorten the service life. After the whole battery assembly is completed, the battery shall use X-ray to identify whether the internal structure of the battery is normal, and check the cell misalignment, steel shell crack, solder joint, short circuit, etc. to eliminate the battery with the above defects and ensure the quality of the battery. At the same time, compared with the wound structure core, the laminated structure has more uniform current density, excellent internal heat dissipation performance, and is more suitable for high-power discharge. For example, BYD blade battery with laminated cell structure shows better cycle characteristics, safety characteristics and energy density. Although the Ni-rich cathode is thermodynamically unstable, it is believed that it will be well solved with the continuous development of assembly technology.

6. Prospect

When compared with the traditional layered $LiCoO_2$, nickel-rich layered oxide cathode materials ($LiNi_{1\text{-}x\text{-}y}M_xN_yO_2$; $x + y \leq 0.5$; M、N = Co, Mn, Al, Mg, Ti etc.) have the advantages of high reversible specific capacity (greater than200 mAh g^{-1}), comparably high operating voltage and low cost. These beneficial features are responsible in making them a research hotspot in the arena of materials, energy and other disciplines. Nickel rich layered oxide cathodes have gradually entered the stage of commercial application and have been considered as promising cathode materials for lithium-ion power batteries. In the future, Ni-rich cathodes will have further applications and development in the following aspects (Fig. 31):

6.1. *Co-free*

Due to its scarcity and strategic value, the price of cobalt has remained high for a long time. Reducing cobalt content has become the primary measure to reduce the cost of NCA or NCM cathode materials. At the same time, the redox potential of nickel is relatively high, and the increase of its content can increase the capacity. The development of high nickel and cobalt free materials has become an inevitable trend. Cobalt free high nickel materials have obvious advantages (Fig. 32**a**) [167]. There are two R & D lines for cobalt free high nickel materials: (1) Reduce the content of CO in NCM/NCA and increase the content of Ni. (2) reduce the content of nickel in $LiNiO_2$. At present, NCM/NCA with 80% Ni content has been reported commercially, and those with more than 80% (90%, 95% et al.) content have also been reported by relevant laboratories, which has been mentioned in the previous part , it will continue to develop towards ultra-high nickel content in the future. For $LiNiO_2$, because Ni^{2+} and Li^+ have the same ion radius, Ni^{2+} can easily migrate to the lattice position of Li, thus blocking the migration channel of Li^+, greatly reducing the reversible capacity of the material. Ni site doping is a main means to improve the properties of modified materials, including mg, Fe, Al, Mn and other transition metal elements. For

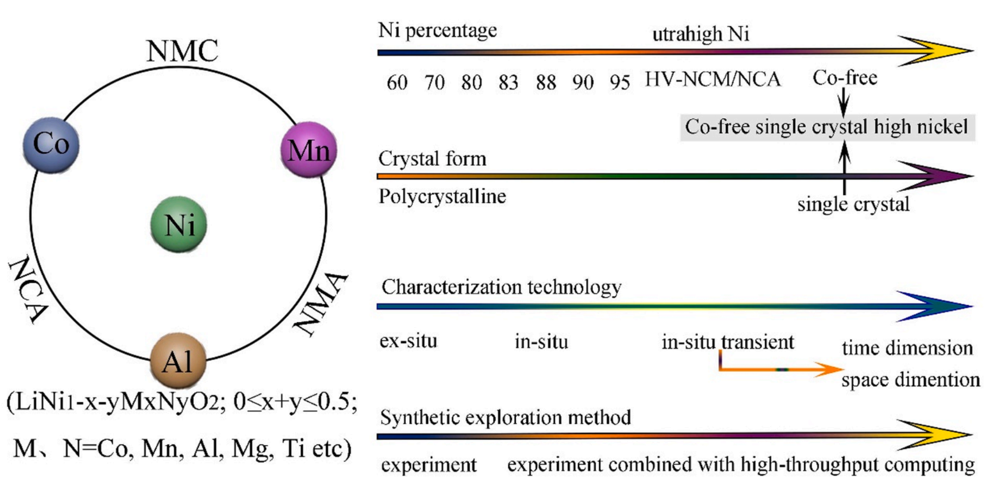

Fig. 31. Further applications and development trends of nickel rich cathodes in the future.

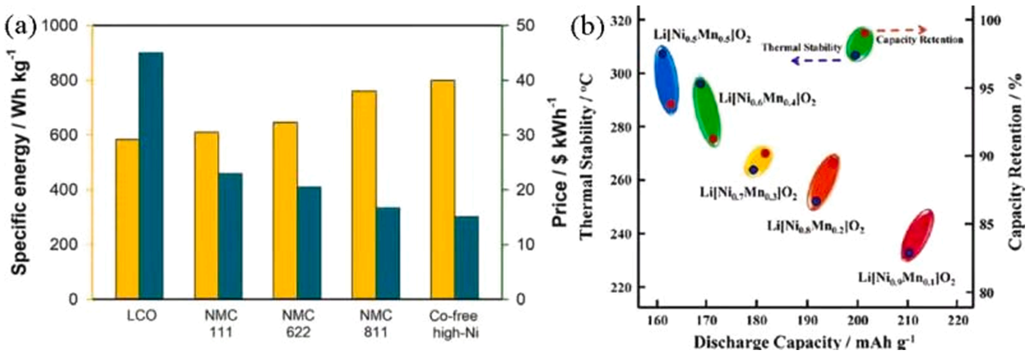

Fig. 32. (a) A comparison of specific energy and cost per energy of LCO, NMC111, NMC622, NMC811, and Co-free high-Ni layered oxides. Reproduced with permission.[167] Copyright 2020, Elsevier. (b) Effect of Mn concentration on electrochemical properties and thermal stability of high nickel materials. Reproduced with permission.[168] Copyright 2013, American Chemical Society.

example, Yang kook sun and others found that Mn content is inversely proportional to the capacity of the material, but directly proportional to the capacity retention and thermal stability of the material (Fig. 32**b**) [168].

6.2. Single crystal

Compared with the secondary spherical polycrystalline material of about 10 μm formed by the agglomeration of hundreds of nano-sized primary particles, the single crystal material is directly composed of independent crystals with a diameter of 2–5 μm. Due to the higher crystallinity, more stable layered structure and anisotropy, the single crystal material has both cyclic performance and thermal stability, And gas production are better than the traditional secondary particle NCM materials [169]. At present, high nickel single crystal cathode materials have been studied mainly for single crystal nickel cobalt lithium manganate (NCM) [170] nickel cobalt lithium aluminate (NCA) [171] ternary cathode materials with nickel content of more than 80% and single crystal nickel cobalt lithium manganate (NCMA) [172] quaternary cathode materials. Although single crystal materials contribute to cyclic stability, the low diffusion kinetics of lithium ion limits the multiplier performance and reversible capacity. Therefore, the optimization of single crystal microstructure, particle size and test environment will play a decisive role in achieving rapid charge–discharge. Recently, J. R. Dahn of dalhouse University studied the synthesis of Mg doped cobalt free single crystal LNO by one-step lithium method. Compared with polycrystalline cells cycled at 30 °C, cycling single crystal materials at 55 °C can restore the discharge capacity of about 20 mAh g^{-1} and produce similar irreversible capacity. [173] With the development of lithium-ion battery technology, people began to demand a cathode material with large capacity, high voltage and good stability to break through the existing energy density. Cobalt free nickel rich single crystal cathode material is expected to achieve this goal. However, it is still a long way from industrialization, which still needs a lot of efforts and attempts.

6.3. Characterization technology

The development of characterization technology is very important to analyze the microstructure morphology and chemical characteristics of electrode materials. Especially in the process of electrochemical charge and discharge, in-situ characterization technology must be introduced to observe the structural transformation of electrode materials, redox process, solid–liquid interface formation, side reactions and lithium ion transport characteristics in real time [174]. In addition, the process of lithium diffusion and decay reaction in high nickel ternary materials depends on the transient properties of material particle size. The performance degradation of subsequent cycles can be attributed to several causes like complex chemical and mechanical interactions among lithium diffusion, anisotropic lattice strain, surface oxygen consumption and cathode particle deterioration. Amongst them, the transient performance of particle size of material remains the key factor of diffusion and deterioration process. Once the electrochemical process is interrupted for diffraction measurement, the charge rebalancing will occur, the movement of lithium ions will be along the radial direction of the particles and the anisotropy of the lattice parameters will be masked. Therefore, it is indispensable to use high-resolution experimental technology in time (subsecond) and space dimensions (submicro) in order to explore the undisturbed charge discharge process for better understanding of the potential decomposition degradation mechanism. [42]

6.4. High-throughput calculations

In the era of big data, high throughput computing method based on material genome and AI technology can quickly determine and select appropriate electrode materials and components and configurations of the whole battery system. Therefore, we also describe the screening and modification of electrode materials by high-throughput calculations. The traditional research and development of battery materials is based on the development mode characterized by "trial and error method". The cycle from discovery to application is very long, which generally takes 20 years or more. In the process of lithium battery material design and development, the theoretical method of high-throughput computing began with ceder research group. They have carried out research called "genetic engineering of lithium ion battery materials" since 2010. In this method, new compounds are produced by replacing the elements in compounds containing polyanion xO_4 (x = P, s, as, SI). The parameters such as energy density, voltage and volume change after Li removal are calculated, and the new materials are selected. Starting from the mineral sidorenkite structure existing in nature, they replaced its elements, constructed more than 270 components and structures, calculated its properties, and screened out several materials: $Li_3Mn(CO_3)(PO_4)$, $Li_2V(CO_3)(PO_4)$, $Li_3V(CO_3)(SiO_4)$, etc. [175] Based on theoretical calculations, gerbrand ceder of the University of California, Berkeley and others carried out a comprehensive high-throughput search in five aspects: phase stability, electrochemical stability, chemical stability, ionic conductivity and electronic conductivity, and quickly found suitable coating materials for cathode materials (Fig. 33**a**). From the results of the author's study, it is obvious that the selection of coating materials needs to be careful to the specific solid-state electrolyte (SSE)/cathode electrode combination (Fig. 33**b**). The author believes that lithium borate is recommended regardless of the interface, because lithium borate has good chemical stability and high oxidation limit. Although the results show that $LiBa(B_3O_5)_3$ has a high migration barrier for lithium ion conduction, other borates with high lithium content may still show high ionic conductivity [176]. Meanwhile, Professor Mo Yifei's

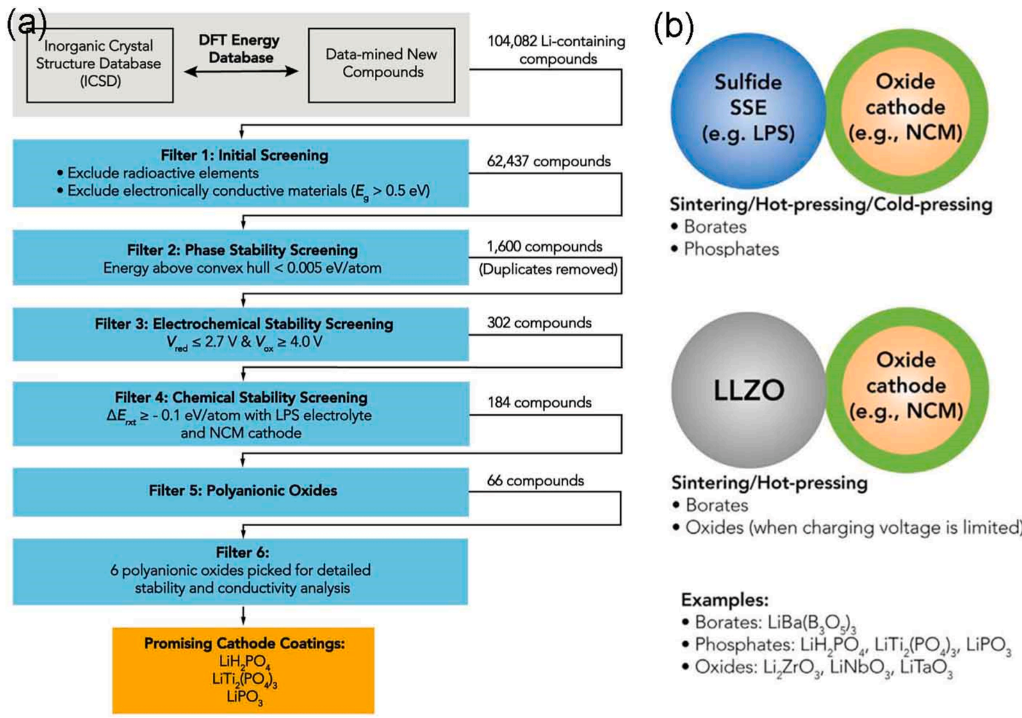

Fig. 33. (a) Flowchart describing the computational screening of cathode-coating materials (Following the initial screening, phase stability, electrochemical stability, and chemical stability were used as sequential filters for the high-throughput screening. Eg is the density functional theory (DFT)-calculated Kohn-Sham band gap; Vred and Vox are the reduction and oxidation limits of the electrochemical stability window in V versus Li metal, respectively; DErxt is the reaction energy of the material with the cathode or electrolyte in eV/atom; LPS denotes the SSE material Li_3PS_4;and NCM denotes the fully lithiated cathode material $LiNi_{1/3}Co_{1/3}Mn_{1/3}O_2$). (b) Coating Recommendations for Various Cathode/SSE Interfaces under Different Processing Conditions (Oxide cathode/sulfide SSE and Oxide cathode/LLZO). Reproduced with permission. [176] Copyright 2019, American Chemical Society.

team from the University of Maryland studied, analyzed and screened the interaction and interfacial thermodynamic stability of a series of solid compounds for cathode materials of high specific energy lithium-ion batteries through high-throughput thermodynamic calculation. By studying and analyzing the chemical reactions of a large number of compounds on cathode materials, the effects of different material chemistry and components on the interface stability of cathode materials are explained, and the strategy of selecting solid electrolyte and coating materials for different cathode materials is put forward [177].

With the continuous development of material genome and artificial intelligence technology, we believe that it will provide strong guidance for the specific design strategy and material selection of lithium cathode materials such as ternary high nickel. However, at present, the research work on high-throughput screening of lithium battery materials is in its infancy, and there are still the following problems. [178,179] 1) It focuses on the calculation of thermodynamic properties of materials, such as formation energy and thermal stability, and lacks the consideration of lithium ion transport, an important dynamic property; 2) The constraints used in screening are lack of pertinence and hierarchy, resulting in a large number of repeated and unnecessary calculations; 3) The first principle method based on density functional theory is mostly used in the calculation, but it has not been combined with other calculation methods or software; ④ A large number of calculated data have not been effectively mined. However, it can be predicted that in the next few years, the application of high-throughput computing methods, combined with experimental research, will greatly accelerate our R & D of lithium battery materials, deepen our understanding of various problems in lithium batteries, reveal the structure performance relationship and internal physical laws of materials, so as to shorten the whole process from R & D to application. The application of high-throughput computing method to explore and design new lithium battery materials is an important way for future material scientific research and development. It can shorten the whole process from R & D to application, and provide strong support for the development of new battery materials and even battery systems.

7. Summary

In summary, the structure, surface properties and electrochemical performance of nickel rich layered oxide cathodes have been preferably awarded and have shown substantial improvements these years. Of course, nickel rich layered oxide cathodes still have numerous challenges related to structural instability, surface side reactions, and safety concerns. Nevertheless, it is believed that unceasing and thorough investigations and honest efforts of the scientific researchers can undeniably inaugurate the application of nickel rich layered oxide cathodes as the next generation of lithium ion batteries high-energy cathode materials in the impending future.

Declaration of Competing Interest

The authors declare that they have no known competing financial interests or personal relationships that could have appeared to influence the work reported in this paper.

Acknowledgement

We thank the financial supports from the National Natural Science Foundation of China (51774251), Hebei Natural Science Foundation for Distinguished Young Scholars (B2017203313), Hundred Excellent Innovative Talents Support Program in Hebei Province (SLRC2017057), Talent Engineering Training Funds of Hebei Province (A201802001), and the opening project of the state key laboratory of Advanced Chemical Power Sources (SKL-ACPS-C-11).

References

[1] Liu Y, He X, Hanlon D, Harvey A, Khan U, Li Y, et al. Electrical, mechanical, and capacity percolation leads to high-performance MoS_2/nanotube composite lithium ion battery electrodes. ACS Nano 2016;10(6):5980–90.
[2] Luo K, Roberts MR, Hao R, Guerrini N, Pickup DM, Liu Y-S, et al. Charge-compensation in 3d-transition-metal-oxide intercalation cathodes through the generation of localized electron holes on oxygen. Nat Chem 2016;8(7):684–91.
[3] Wu T, Fan J, Li Q, Shi P, Xu Q, Min Y. Palladium nanoparticles anchored on anatase titanium dioxide-black phosphorus hybrids with heterointerfaces: highly

electroactive and durable catalysts for ethanol electrooxidation. Adv Energy Mater 2018;8(1):1701799.
[4] Xin F, Zhou H, Chen X, Zuba M, Chernova N, Zhou G, et al. Li-Nb-O coating/ substitution enhances the electrochemical performance of $LiNi_{0.8}Mn_{0.1}Co_{0.1}O_2$ (NMC811) cathode. ACS Appl Mater Interfaces 2019;11(38):34889–94.
[5] Huang SF, Lv Y, Tie D, Yu Y, Zhao YF. Realizing simultaneously enhanced energy and power density full-cell construction using mixed hard carbon/$Li_4Ti_5O_{12}$ electrode. Rare Met 2021;40(1):65–71.
[6] Yu Y, Huang S, Wang B, Tie D, Wang Q, Hou Y, et al. Achieving high energy full-cell lithium storage performance by coupling high capacity V_2O_3 with low potential Ni_2P anode. ACS Appl Mater Interfaces 2018;11(1):19–25.
[7] Chang G, Zhao Y, Dong L, Wilkinson DP, Zhang L, Shao Q, et al. A review of phosphorus and phosphides as anode materials for advanced sodium-ion batteries. J Mater Chem A 2020;8(10):4996–5048.
[8] Yin X, Sarkar S, Shi S, Huang QA, Zhao H, Yan L, et al. Recent progress in advanced organic electrode materials for sodium-ion batteries: synthesis, mechanisms, challenges and perspectives. Adv Funct Mater 2020;30(11): 1908445.
[9] Ryu HH, Park NY, Seo JH, Yu YS, Sharma M, Mücke R, et al. A highly stabilized Ni-rich NCA cathode for high-energy lithium-ion batteries. Mater Today 2020;36: 73–82.
[10] Yang Y, Xu R, Zhang K, Lee SJ, Mu L, Liu P, et al. Quantification of heterogeneous degradation in Li-ion batteries. Adv Energy Mater 2019;9(25):1900674.
[11] Kim S, Cho W, Zhang X, Oshima Y, Choi JW. A stable lithium-rich surface structure for lithium-rich layered cathode materials. Nat Commun 2016;7(1):1–8.
[12] Liu W, Oh P, Liu X, Lee MJ, Cho W, Chae S, et al. Nickel-rich layered lithium transition-metal oxide for high-energy lithium-ion batteries. Angew Chem Int Ed 2015;54(15):4440–57.
[13] Reddy MV, Subbarao GV, Chowdari BVR. Preparation and characterization of $LiNi_{0.5}Co_{0.5}O_2$ and $LiNi_{0.5}Co_{0.4}Al_{0.1}O_2$ by molten salt synthesis for Li ion batteries. J Phys Chem C 2007;111(31):11712–20.
[14] Xu S, Du C, Xu X, Han G, Zuo P, Cheng X, et al. A mild surface washing method using protonated polyaniline for Ni-rich $LiNi_{0.8}Co_{0.1}Mn_{0.1}O_2$ material of lithium ion batteries. Electrochim Acta 2017;248:534–40.
[15] Dwibedi D, Gond R, Dayamani A, Araujo RB, Chakraborty S, Ahuja R, et al. $Na_{2.32}Co_{1.84}(SO_4)_3$ as a new member of the alluaudite family of high-voltage sodium battery cathodes. Dalton Trans 2017;46(1):55–63.
[16] Fei LF, Sun TY, Lu W, An XQ, Hu ZF, Jimmy CY, et al. Direct observation of carbon nanostructure growth at liquid-solid interfaces. Chem Commun 2014;50 (7):826–8.
[17] Li W, Liu T, Zhang J, Peng N, Zheng R, Yu H, et al. Commercially available InSb as a high-performance anode for secondary batteries towards superior lithium storage. Sustainable Energy Fuels 2019;3(10):2668–74.
[18] Zhou G, Li F, Cheng HM. Progress in flexible lithium batteries and future prospects. Energy Environ Sci 2014;7(4):1307–38.
[19] Shi S, Li Z, Sun Y, Wang B, Liu Q, Hou Y, et al. A covalent heterostructure of monodisperse Ni_2P immobilized on N, P-co-doped carbon nanosheets for high performance sodium/lithium storage. Nano Energy 2018;48:510–7.
[20] Huang S, Li Z, Wang B, Zhang J, Peng Z, Qi R, et al. N-doping and defective nanographitic domain coupled hard carbon nanoshells for high performance lithium/ sodium Storage. Adv Funct Mater 2018;28(10):1706294.
[21] Huang S, Wang M, Jia P, Wang B, Zhang J, Zhao Y. N-graphene motivated SnO_2@ SnS_2 heterostructure quantum dots for high performance lithium/sodium storage. Energy Storage Mater 2019;20:225–33.
[22] Whittingham MS. Lithium batteries and cathode materials. Chem Rev 2004;104 (10):4271–302.
[23] Park OK, Cho Y, Lee S, Yoo HC, Song HK, Cho J. Who will drive electric vehicles, olivine or spinel? Energy Environ Sci 2011;4(5):1621–33.
[24] Yan B, Lin S, Kang L, Song X, Tian Z, Jia K. Spinel structured $LiMn_2O_4$ prepared by laser annealing. Mater Technol 2020;35:606–11.
[25] Ding Y, Mu D, Wu B, Wang R, Zhao Z, Wu F. Recent progresses on nickel-rich layered oxide positive electrode materials used in lithium-ion batteries for electric vehicles. Appl Energy 2017;195:586–99.
[26] Hassoun J, Kim J, Lee DJ, Jung HG, Lee SM, Sun YK, et al. A contribution to the progress of high energy batteries: A metal-free, lithium-ion, silicon–sulfur battery. J Power Sources 2012;202:308–13.
[27] Wang Y, He P, Zhou H. Olivine $LiFePO_4$: development and future. Energy Environ Sci 2011;4(3):805–17.
[28] Yamada A, Takei Y, Koizumi H, Sonoyama N, Kanno R, Itoh K, et al. Electrochemical, magnetic, and structural investigation of the $Li_x(Mn_yFe_{1-y})PO_4$ olivine phases. Chem Mater 2006;18(3):804–13.
[29] Tarascon JM, Armand M. Issues and challenges facing rechargeable lithium batteries. Materials for sustainable energy: a collection of peer-reviewed research and review articles from Nature Publishing Group 2011:171–9.
[30] Ryu HH, Park NY, Yoon DR, Kim UH, Yoon CS, Sun YK. New class of Ni-rich cathode materials $Li(Ni_xCo_yB_{1-x-y})O_2$ for next lithium batteries. Adv Energy Mater 2020;10(25):2000495.
[31] Ryu HH, Park KJ, Yoon DR, Aishova A, Yoon CS, Sun YK. $Li[Ni_{0.9}Co_{0.09}W_{0.01}]O_2$: A new type of layered oxide cathode with high cycling stability. Adv Energy Mater 2019;9 (44):1902698.
[32] Aishova A, Park GT, Yoon CS, Sun Y-K. Cobalt-free high-capacity Ni-rich layered $Li[Ni_{0.9}Mn_{0.1}]O_2$ cathode. Adv Energy Mater 2020;10(4):1903179.
[33] Li H, Cormier M, Zhang N, Inglis J, Li J, Dahn JR. Is cobalt needed in Ni-rich positive electrode materials for lithium ion batteries? J Electrochem Soc 2019; 166(4):A429.
[34] Liu A, Zhang N, Li H, Inglis J, Wang Y, Yin S, et al. Investigating the effects of magnesium doping in various Ni-rich positive electrode materials for lithium ion batteries. J Electrochem Soc 2019;166(16):A4025–33.
[35] Mu L, Zhang R, Kan WH, Zhang Y, Li L, Kuai C, et al. Dopant distribution in Co-free high-energy layered cathode materials. Chem Mater 2019;31(23):9769–76.
[36] Li W, Lee S, Manthiram A. High-nickel NMA: A cobalt-free alternative to NMC and NCA cathodes for lithium-ion batteries. Adv Mater 2020;32(33):2002718.
[37] Zhao S, Yan K, Zhang J, Sun B, Wang G. Reaction mechanisms of layered lithium-rich cathode materials for high-energy lithium-ion batteries. Angew Chem Int Ed 2021;60(5):2208–20.
[38] Sun G, Yu FD, Que LF, Deng L, Wang ZB. Local electronic structure modulation enhances operating voltage in Li-rich cathodes. Nano Energy 2019;66:104102.
[39] Lee J, Gong Y, Gu L, Kang B. Long-term cycle stability enabled by the incorporation of Ni into Li_2MnO_3 Phase in the Mn-based Li-rich layered materials. ACS Energy Lett 2021;6(2):789–98.
[40] Sicklinger J, Metzger M, Beyer H, Pritzl D, Gasteiger HA. Ambient storage derived surface contamination of NCM811 and NCM111: Performance implications and mitigation strategies. J Electrochem Soc 2019;166(12):A2322–35.
[41] Xu Z, Jiang Z, Zhao K, Xu R, Qin C, Zhang Y, et al. Charge distribution guided by grain crystallographic orientations in polycrystalline battery materials. Nat Commun 2020;11(1):1–9.
[42] Brandt LR, Marie JJ, Moxham T, Förstermann DP, Salvati E, Besnard C, et al. Synchrotron X-ray quantitative evaluation of transient deformation and damage phenomena in a single nickel-rich cathode particle. Energy Environ Sci 2020;13 (10):3556–66.
[43] Li S, Yao Z, Zheng J, Fu M, Cen J, Hwang S, et al. Direct observation of defect-aided structural evolution in a nickel-rich layered cathode. Angew Chem Int Ed 2020;132(49):22276–83.
[44] Park KJ, Hwang JY, Ryu HH, Maglia F, Kim SJ, Lamp P, et al. Degradation mechanism of Ni-enriched NCA cathode for lithium batteries: Are Microcracks Really Critical? ACS Energy Lett 2019;4(6):1394–400.
[45] Kim UH, Park GT, Son BK, Nam GW, Liu J, Kuo LY, et al. Heuristic solution for achieving long-term cycle stability for Ni-rich layered cathodes at full depth of discharge. Nat Energy 2020;5(11):860–9.
[46] Xiaoxuan C, Sheng LI, Yonggang HU, Shiyao Z, Yunxuan C, Dongjiang LI, et al. Failure mechanism of $Li_{(1+x)}(NCM)_{(1-x)}O_2$ layered oxide cathode material during capacity degradation. Energy Storage Science and Technology 2019;8(6):1003.
[47] Qian G, Zhang Y, Li L, Zhang R, Xu J, Cheng Z, et al. Single-crystal nickel-rich layered-oxide battery cathode materials: synthesis, electrochemistry, and intra-granular fracture. Energy Storage Mater 2020;27:140–9.
[48] Xu X, Huo H, Jian J, Wang L, Zhu H, Xu S, et al. Radially oriented single-crystal primary nanosheets enable ultrahigh rate and cycling properties of $LiNi_{0.8}Co_{0.1}Mn_{0.1}O_2$ cathode material for lithium-ion batteries. Adv Energy Mater 2019;9(15):1803963.
[49] Zou Y, Yang X, Lv C, Liu T, Xia Y, Shang L, et al. Multishelled Ni-rich Li $(Ni_xCo_yMn_z)O_2$ hollow fibers with low cation mixing as high-performance cathode materials for Li-Ion batteries. Adv Sci 2017;4(1):1600262.
[50] Caballero A, Cruz M, Hernán L, Melero M, Morales J, Castellón ER. Nanocrystalline materials obtained by using a simple, rapid method for rechargeable lithium batteries. J Power Sources 2005;150:192–201.
[51] Saavedra-Arias JJ, Karan NK, Pradhan DK, Kumar A, Nieto S, Thomas R, et al. Synthesis and electrochemical properties of Li $(Ni_{0.8}Co_{0.1}Mn_{0.1})O_2$ cathode material: Ex situ structural analysis by Raman scattering and X-ray diffraction at various stages of charge–discharge process. J Power Sources 2008;183(2):761–5.
[52] Xu C, Märker K, Lee J, Mahadevegowda A. Bulk fatigue induced by surface reconstruction in layered Ni-rich cathodes for Li-ion batteries. Nat Mater 2021;20 (1):84–92.
[53] Yang Y, Xu S, Xie M, He Y, Huang G, Yang Y. Growth mechanisms for spherical mixed hydroxide agglomerates prepared by co-precipitation method: A case of $Ni_{1/3}Co_{1/3}Mn_{1/3}(OH)_2$. J Alloy Compd 2015;619:846–53.
[54] Islam N, Li S, Ren G, Zu Y, Warzywoda J, Wang S, et al. High-frequency electrochemical capacitors based on plasma pyrolyzed bacterial cellulose aerogel for current ripple filtering and pulse energy storage. Nano Energy 2017;40: 107–14.
[55] Park KJ, Jung HG, Kuo LY, Kaghazchi P, Yoon CS, Sun Y. Improved cycling stability of Li $[Ni_{0.90}Co_{0.05}Mn_{0.05}]O_2$ through microstructure modification by boron doping for Li-ion batteries. Adv Energy Mater 2018;8(25):1801202.
[56] Wu F, Liu N, Chen L, Su Y, Tan G, Bao L, et al. Improving the reversibility of the H2–H3 phase transitions for layered Ni-rich oxide cathode towards retarded structural transition and enhanced cycle stability. Nano Energy 2019;59:50–7.
[57] Wang J, Li C, Xu B. Basic principle, advance and current application situation of sol-gel method. Chemical Industry and Engineering 2009;26(3):273–7.
[58] Subramaniyam CM, Celio H, Shiva K, Gao H, Goodneough JB, Liu HK, et al. Long stable cycling of fluorine-doped nickel-rich layered cathodes for lithium batteries. Sustainable Energy Fuels 2017;1(6):1292–8.
[59] Lu H, Zhou H, Svensson AM, Fossdal A, Sheridan E, Lu S, et al. High capacity Li $[Ni_{0.8}Co_{0.1}Mn_{0.1}]O_2$ synthesized by sol-gel and co-precipitation methods as cathode materials for lithium-ion batteries. Solid State Ionics 2013;249:105–11.
[60] Li D, Sasaki Y, Kobayakawa K, Noguchi H, Sato Y. Preparation, morphology and electrochemical characteristics of $LiNi_{1/3}Mn_{1/3}Co_{1/3}O_2$ with LiF addition. Electrochim Acta 2006;52(2):643–8.
[61] Yue P, Wang Z, Peng W, Li L, Chen W, Guo H, et al. Spray-drying synthesized $LiNi_{0.6}Co_{0.2}Mn_{0.2}O_2$ and its electrochemical performance as cathode materials for lithium ion batteries. Powder Technol 2011;214(3):279–82.

[62] Ahn W, Lim SN, Jung KN, Yeon SH, Kim KB, Song HS, et al. Combustion-synthesized $LiNi_{0.6}Mn_{0.2}Co_{0.2}O_2$ as cathode material for lithium ion batteries. J Alloy Compd 2014;609:143–9.
[63] Nitta N, Wu F, Lee JT, Yushin G. Li-ion battery materials: present and future. Mater Today 2015;18(5):252–64.
[64] Wang L, Li J, He X, Pu W, Wan C, Jiang C. Recent advances in layered $LiNi_xCo_yMn_{1-x-y}O_2$ cathode materials for lithium ion batteries. J Solid State Electrochem 2009;13(8):1157–64.
[65] Ellis BL, Lee KT, Nazar LF. Positive electrode materials for Li-ion and Li-batteries. Chem Mater 2010;22(3):691–714.
[66] Zeng D, Cabana J, Bréger J, Yoon WS, Grey C. Cation Ordering in Li $[Ni_xMn_xCo_{(1-2x)}]O_2$-Layered Cathode Materials: A Nuclear Magnetic Resonance (NMR), Pair Distribution Function, X-ray Absorption Spectroscopy, and Electrochemical Study. Chem Mater 2007;19(25):6277–89.
[67] He P, Yu H, Zhou H. Layered lithium transition metal oxide cathodes towards high energy lithium-ion batteries. J Mater Chem 2012;22(9):3680–95.
[68] Koyama Y, Tanaka I, Adachi H, Makimura Y, Ohzuku T. Crystal and electronic structures of super structural $Li_{1-x}[Co_{1/3}Ni_{1/3}Mn_{1/3}]O_2$ ($0\leq x\leq 1$). J Power Sources 2003;119:644–8.
[69] Myung ST, Lee MH, Komaba S, Kumagai N, Sun YK. Hydrothermal synthesis of layered Li $[Ni_{1/3}Co_{1/3}Mn_{1/3}]O_2$ as positive electrode material for lithium secondary battery. Electrochim Acta 2005;50(24):4800–6.
[70] Chen H, Dawson JA, Harding JH. Effects of cationic substitution on structural defects in layered cathode materials $LiNiO_2$. J Mater Chem A 2014;2(21):7988–96.
[71] Gui S, Zhang Q, Zhuo H, Liu J. Enhancing the electrochemical performance of $LiNi_{0.8}Co_{0.15}Al_{0.05}O_2$ by a facile doping method: Spray-drying doping with liquid polyacrylonitrile. J Power Sources 2019;409:102–11.
[72] Wu F, Tian J, Su Y, Wang J, Zhang C, Bao L, et al. Effect of Ni^{2+} content on lithium/nickel disorder for Ni-rich cathode materials. ACS Appl Mater Interfaces 2015;7(14):7702–8.
[73] Zhang Q, Su Y, Chen L, Lu Y, Bao L, He T, et al. Pre-oxidizing the precursors of Nickel-rich cathode materials to regulate their Li^+/Ni^{2+} cation ordering towards cyclability improvements. J Power Sources 2018;396:734–41.
[74] Fu C, Li G, Luo D, Li Q, Fan J, Li L, et al. Nickel-rich layered microspheres cathodes: lithium/nickel disordering and electrochemical performance. ACS Appl Mater Interfaces 2014;6(18):15822–31.
[75] Yue P, Wang Z, Peng W, Li L, Guo H, Li X, et al. Preparation and electrochemical properties of submicron $LiNi_{0.6}Co_{0.2}Mn_{0.2}O_2$ as cathode material for lithium ion batteries. Scr Mater 2011;65(12):1077–80.
[76] Saadoune I, Delmas C. $LiNi_{1-y}Co_yO_2$ positive electrode materials: relationships between the structure, physical properties and electrochemical behaviour. J Mater Chem 1996;6(2):193–9.
[77] Chen CY, Xiao SQ, Davis ME. Studies on ordered mesoporous materials III. Comparison of MCM-41 to mesoporous materials derived from kanemite. Microporous Mater 1995;4(1):1–20.
[78] Marom R, Amalraj SF, Leifer N, Jacob D, Aurbach D. A review of advanced and practical lithium battery materials. J Mater Chem 2011;21(27):9938–54.
[79] Mukhopadhyay A, Guo F, Tokranov A, Xiao X, Hurt RH, Sheldon B. Engineering of graphene layer orientation to attain high rate capability and anisotropic properties in Li-ion battery electrodes. Adv Funct Mater 2013;23(19):2397–404.
[80] Shaju KM, Rao GVS, Chowdari BVR. Performance of layered $Li(Ni_{1/3}Co_{1/3}Mn_{1/3})O_2$ as cathode for Li-ion batteries. Electrochim Acta 2002;48(2):145–51.
[81] Thackeray MM. Structural considerations of layered and spinel lithiated oxides for lithium ion batteries. J Electrochem Soc 1995;142(8):2558–63.
[82] Wu F, Li Q, Chen L, Lu Y, Su Y, Bao L, et al. Use of Ce to Reinforce the Interface of Ni-Rich $LiNi_{0.8}Co_{0.1}Mn_{0.1}O_2$ Cathode Materials for Lithium-Ion Batteries under High Operating Voltage. ChemSusChem 2019;12(4):935–43.
[83] Zhang C, Liu M, Pan G, Liu S, Liu D, Chen C, et al. Enhanced Electrochemical Performance of $LiNi_{0.8}Co_{0.1}Mn_{0.1}O_2$ Cathode for Lithium-Ion Batteries by Precursor Preoxidation. ACS Applied Energy Materials 2018;1(8):4374–84.
[84] Deng D. Li-ion batteries: basics, progress, and challenges. Energy Sci Eng 2015;3(5):385–418.
[85] de Biasi L, Kondrakov AO, Geßwein H, Brezesinski T, Hartmann P, Janek J. Between scylla and charybdis: Balancing among structural stability and energy density of layered NCM cathode materials for advanced lithium-ion batteries. The Journal of Physical Chemistry C 2017;121(47):26163–71.
[86] Manthiram A, Knight JC, Myung ST, Oh SM, Sun Y. Nickel-rich and lithium-rich layered oxide cathodes: progress and perspectives. Adv Energy Mater 2016;6(1):1501010.
[87] Cherkashinin G, Motzko M, Schulz N, Späth T. Jaegermann WJCoM. Electron spectroscopy study of Li[Ni Co, Mn]O_2/electrolyte interface: electronic structure, interface composition, and device implications. Chem Mater 2015;27(8):2875–87.
[88] Gauthier M, Carney TJ, Grimaud A, Giordano L, Pour N, Chang HH, et al. Electrode–electrolyte interface in Li-ion batteries: current understanding and new insights. J Phys Chem Lett 2015;6(22):4653–72.
[89] Chen Z, Zhang C, Zhang Z, Li J. Correlation of intercalation potential with d-electron configurations for cathode compounds of lithium-ion batteries. PCCP 2014;16(26):13255–61.
[90] Reed J, Ceder G. Role of electronic structure in the susceptibility of metastable transition-metal oxide structures to transformation. Chem Rev 2004;104(10):4513–34.
[91] Croguennec L, Bains J, Bréger J, Tessier C, Biensan P, Levasseur S, et al. Effect of aluminum substitution on the structure, electrochemical performance and thermal stability of $Li_{1+x}(Ni_{0.40}Mn_{0.40}Co_{0.20-z}Al_z)_{1-x}O2$. J Electrochem Soc 2011;158(6):A664–70.
[92] Jung R, Metzger M, Maglia F, Stinner C, Gasteiger H. Oxygen release and its effect on the cycling stability of $LiNi_xMn_yCo_zO_2$ (NMC) cathode materials for Li-ion batteries. J Electrochem Soc 2017;164(7):A1361.
[93] Kim JH, Park KJ, Kim SJ, Yoon CS, Sun YK. A method of increasing the energy density of layered Ni-rich Li [Ni1−2xCoxMnx]O2 cathodes (x=0.05, 0.1, 0.2). 2019, 7:2694-2701.
[94] Kim H, Kim MG, Jeong HY, Nam H, Cho J. A new coating method for alleviating surface degradation of $LiNi_{0.6}Co_{0.2}Mn_{0.2}O_2$ cathode material: nanoscale surface treatment of primary particles. Nano Lett 2015;15(3):2111–9.
[95] Han B, Xu S, Zhao S, Lin G, Feng Y, Chen L, et al. Enhancing the structural stability of Ni-rich layered oxide cathodes with a preformed Zr-concentrated defective nanolayer. ACS Appl Mater Interfaces 2018;10(46):39599–607.
[96] Zou L, Zhao W, Liu Z, Jia H, Zheng J, Wang G, et al. Revealing cycling rate-dependent structure evolution in Ni-rich layered cathode materials. ACS Energy Lett 2018;3(10):2433–40.
[97] Zhao J, Zhang W, Huq A, Misture ST, Zhang B, Guo SM, et al. In situ probing and synthetic control of cationic ordering in Ni-rich layered oxide cathodes. Adv Energy Mater 2017;7(3):1601266.
[98] Duan Y, Yang L, Zhang MJ, Chen Z, Bai J, Amine K, et al. Insights into Li/Ni ordering and surface reconstruction during synthesis of Ni-rich layered oxides. J Mater Chem A 2019;7(2):513–9.
[99] Zhang SS. Problems and their origins of Ni-rich layered oxide cathode materials. Energy Storage Mater 2020;24:247–54.
[100] Cho DH, Jo CH, Cho W, Kim YJ, Yashiro H, Sun YK, et al. Effect of residual lithium compounds on layer Ni-rich $Li[Ni_{0.7}Mn_{0.3}]O_2$. J Electrochem Soc 2014;161(6):A920–6.
[101] Chen Z, Wang J, Huang J, Fu T, Sun G, Lai S, et al. The high-temperature and high-humidity storage behaviors and electrochemical degradation mechanism of $LiNi_{0.6}Co_{0.2}O_2$ cathode material for lithium ion batteries. J Power Sources 2017;363:168–76.
[102] Li T, Yuan XZ, Zhang L, Song D, Shi K, Bock C. Degradation mechanisms and mitigation strategies of nickel-rich NMC-based lithium-ion batteries. Electrochemical Energy Reviews 2020;3(1):43–80.
[103] Hamam I, Zhang N, Liu A, Johnson MB, Dahn JR. Study of the reactions between Ni-rich positive electrode materials and aqueous solutions and their relation to the failure of Li-ion cells. J Electrochem Soc 2020;167(13):130521.
[104] Azhari L, Zhou X, Sousa B, Yang Z, Gao G, Wang Y. Effects of extended aqueous processing on structure, chemistry, and performance of polycrystalline $LiNi_xMn_yCo_zO_2$ cathode powders. ACS Appl Mater Interfaces 2020;12(52):57963–74.
[105] Hawley WB, Meyer III HM, Li J. Enabling aqueous processing for $LiNi_{0.80}Co_{0.15}Al_{0.05}O_2$ (NCA)-based lithium-ion battery cathodes using polyacrylic acid. Electrochim Acta 2021;380:138203.
[106] You Y, Celio H, Li J, Dolocan A, Manthiram A. Modified high-nickel cathodes with stable surface chemistry against ambient air for lithium-ion batteries. Angew Chem Int Ed 2018;57(22):6480–5.
[107] Lee SH, Park GJ, Sim SJ, Jin B, Kim H. Improved electrochemical performances of $LiNi_{0.8}Co_{0.1}Mn_{0.1}O_2$ cathode via SiO_2 coating. J Alloy Compd 2019;791:193–9.
[108] Zhang SS. Understanding of performance degradation of $LiNi_{0.80}Co_{0.10}Mn_{0.10}O_2$ cathode material operating at high potentials. Journal of Energy. Chemistry 2020;41:135–41.
[109] Bak SM, Hu E, Zhou Y, Yu X, Senanayake SD, Cho SJ, et al. Structural changes and thermal stability of charged $LiNi_xMn_yCo_zO_2$ cathode materials studied by combined in situ time-resolved XRD and mass spectroscopy. ACS Appl Mater Interfaces 2014;6(24):22594–601.
[110] Nam GW, Park NY, Park KJ, Yang J, Liu J, Yoon CS, et al. Capacity fading of Ni-rich NCA cathodes: Effect of microcracking extent. ACS Energy Lett 2019;4(12):2995–3001.
[111] Ko DS, Park JH, Yu BY, Ahn D, Kim K, Han HN, et al. Degradation of high nickel layered oxide cathodes from surface to bulk: A comprehensive structural, chemical, and electrical analysis. Adv Energy Mater 2020;10(36):2001035.
[112] Yang C, Shao R, Wang Q, Zhou T, Lu J, Jiang N, et al. Bulk and surface degradation in layered Ni-rich cathode for Li ions batteries: Defect proliferation via chain reaction mechanism. Energy Storage Mater 2021;35:62–9.
[113] Cho J, Kim TJ, Kim J, Noh M, Park B. Synthesis, thermal, and electrochemical properties of $AlPO_4$-coated $LiNi_{0.8}Co_{0.1}Mn_{0.1}O_2$ cathode materials for a Li-Ion cell. J Electrochem Soc 2004;151(11):A1899–904.
[114] Myung ST, Maglia F, Park KJ, Yoon CS, Lamp P, Kim SJ, et al. Nickel-rich layered cathode materials for automotive lithium-ion batteries: achievements and perspectives. ACS Energy Lett 2017;2(1):196–223.
[115] Noh HJ, Myung ST, Lee YJ, Sun YK. High-energy layered oxide cathodes with thin shells for improved surface stability. Chem Mater 2014;26(20):5973–9.
[116] Yoon SJ, Park KJ, Lim BB, Yoon CS, Sun YK. Improved performances of Li $[Ni_{0.65}Co_{0.08}Mn_{0.27}]O_2$ cathode material with full concentration gradient for Li-ion batteries. J Electrochem Soc 2014;162(2):A3059–63.
[117] Cho Y, Oh P, Cho J. A new type of protective surface layer for high-capacity Ni-based cathode materials: nanoscaled surface pillaring layer. Nano Lett 2013;13(3):1145–52.
[118] Zheng J, Gu M, Xiao J, Polzin BJ, Yan P, Chen X, et al. Functioning mechanism of AlF_3 coating on the Li-and Mn-rich cathode materials. Chem Mater 2014;26(22):6320–7.
[119] Choi J, Lee SY, Yoon S, Kim KH, Kim M, Hong SH. The role of Zr doping in stabilizing Li $[Ni_{0.6}Co_{0.2}Mn_{0.2}]O_2$ as a cathode material for lithium-ion batteries. Chem Sus Chem 2019;12(11):2439–46.

[120] Gao S, Zhan X, Cheng YT. Structural, electrochemical and Li-ion transport properties of Zr-modified $LiNi_{0.8}Co_{0.1}Mn_{0.1}O_2$ positive electrode materials for Li-ion batterie. J Power Sources 2019;410:45–52.
[121] Song JH, Bae J, Lee K, Lee I, Hwang K, Cho W, et al. Enhancement of high temperature cycling stability in high-nickel cathode materials with titanium doping. J Ind Eng Chem 2018;68:124–8.
[122] Kong D, Hu J, Chen Z, Song K, Li C, Weng M, et al. Ti-gradient doping to stabilize layered surface structure for high performance high-Ni oxide cathode of Li-ion battery. Adv Energy Mater 2019;9(41):1901756.
[123] Liu Q, Zhao Z, Wu F, Mu D, Wang L, Wu B. The effects of molybdenum doping on $LiNi_{0.6}Co_{0.2}Mn_{0.2}O_2$ cathode material. Solid State Ionics 2019;337:107–14.
[124] Xie Q, Li W, Dolocan A, Manthiram A. Insights into boron-based polyanion-tuned high-nickel cathodes for high-energy-density lithium-ion batteries. Chem Mater 2019;31(21):8886–97.
[125] Qiu Z, Liu Z, Fu X, Liu J, Zeng Q. Improving the cycling performance of $LiNi_{0.8}Co_{0.15}Al_{0.05}O_2$ cathode materials via zirconium and fluorine co-substitution. J Alloy Compd 2019;806:136–45.
[126] Qiu L, Xiang W, Tian W, Xu CL, Li YC, Wu ZG, et al. Polyanion and cation co-doping stabilized Ni-rich Ni–Co–Al material as cathode with enhanced electrochemical performance for Li-ion battery. Nano Energy 2019;63:103818.
[127] Liu Y, Tang L, Wei H, Zhang X, He Z, Li Y, et al. Enhancement on structural stability of Ni-rich cathode materials by in-situ fabricating dual-modified layer for lithium-ion batteries. Nano Energy 2019;65:104043.
[128] Fan Q, Yang S, Liu J, Liu H, Lin K, Liu R, et al. Mixed-conducting interlayer boosting the electrochemical performance of Ni-rich layered oxide cathode materials for lithium ion batteries. J Power Sources 2019;421(1):91–9.
[129] Zhu J, Li Y, Xue L, Chen Y, Lei T, Deng S, et al. Enhanced electrochemical performance of Li_3PO_4 modified $Li[Ni_{0.8}Co_{0.1}Mn_{0.1}]O_2$ cathode material via lithium-reactive coating. J Alloy Compd 2019;773:112–20.
[130] Zhang M, Zhao H, Tan M, Liu J, Hu Y, Liu S, et al. Yttrium modified Ni-rich $LiNi_{0.8}Co_{0.1}Mn_{0.}1O_2$ with enhanced electrochemical performance as high energy density cathode material at 4.5V high voltage. J Alloy Compd 2019;774:82–92.
[131] Dong S, Zhou Y, Hai C, Zeng J, Sun Y, Shen Y, et al. Ultrathin CeO_2 coating for improved cycling and rate performance of Ni-rich layered $LiNi_{0.7}Co_{0.2}Mn_{0.1}O_2$ cathode materials. Ceram Int 2019;45(1):144–52.
[132] Li YC, Xiang W, Xiao Y, Wu ZG, Xu CL, Xu W, et al. Synergy of doping and coating induced heterogeneous structure and concentration gradient in Ni-rich cathode for enhanced electrochemical performance. J Power Sources 2019;423:144–51.
[133] Chung YM, Ryu SH, Ju JH, Bak YR, Hwang MJ, Kim KW, et al. A surfactant-based method for carbon coating of $LiNi_{0.8}Co_{0.15}Al_{0.05}O_2$ Cathode in Li ion batteries. Bull Korean Chem Soc 2010;31(8):2304–8.
[134] Yoon S, Jung KN, Yeon SH, Jin CS, Shin K-H. Electrochemical properties of $LiNi_{0.8}Co_{0.15}Al_{0.05}O_2$–graphene composite as cathode materials for lithium-ion batteries. J Electroanal Chem 2012;683:88–93.
[135] Kong JZ, Chen Y, Cao YQ, Wang QZ, Li AD, Li H, et al. Enhanced electrochemical performance of Ni-rich $LiNi_{0.6}Co_{0.2}Mn_{0.2}O_2$ coated by molecular layer deposition derived dual-functional C-Al_2O_3 composite coating. J Alloy Compd 2019;799:89–98.
[136] Huang X, Zhu W, Yao J, Bu L, Li X, Tian K, et al. Suppressing structural degradation of Ni-rich cathode materials towards improved cycling stability enabled by a Li_2MnO_3 coating. J Mater Chem A 2020;8(34):17429–41.
[137] Su Y, Chen G, Chen L, Lu Y, Zhang Q, Lv Z, et al. High-rate structure-gradient Ni-rich cathode material for lithium-ion batteries. ACS Appl Mater Interfaces 2019;11(40):36697–704.
[138] Fan X, Hu G, Zhang B, Ou X, Zhang J, Zhao W, et al. Crack-free single-crystalline Ni-rich layered NCM cathode enable superior cycling performance of lithium-ion batteries. Nano Energy 2020;70:104450.
[139] Dong P, Wang D, Yao Y, Li X, Zhang Y, Ru J, et al. Stabilizing interface layer of $LiNi_{0.5}Co_{0.2}Mn_{0.3}O_2$ cathode materials under high voltage using p-toluenesulfonyl isocyanate as film forming additive. J Power Sources 2017;344:111–8.
[140] Jang SH, Jung K, Yim T. Silyl-group functionalized organic additive for high voltage Ni-rich cathode material. Curr Appl Phys 2018;18(11):1345–51.
[141] Yim T, Kang KS, Mun J, Lim SH, Woo SG, Kim KJ, et al. Understanding the effects of a multi-functionalized additive on the cathode–electrolyte interfacial stability of Ni-rich materials. J Power Sources 2016;302:431–8.
[142] Deng T, Fan X, Cao L, Chen J, Hou S, Ji X, et al. Designing In-Situ-Formed Interphases Enables Highly Reversible Cobalt-Free $LiNiO_2$ Cathode for Li-ion and Li-metal Batteries. Joule 2019;3(10):2550–64.
[143] Zhang D, Liu Y, Wu L, Feng L, Jin S, Zhang R, et al. Effect of Ti ion doping on electrochemical performance of Ni-rich $LiNi_{0.8}Co_{0.1}Mn_{0.1}O_2$ cathode material. Electrochim Acta 2019;328:135086.
[144] Yan W, Xie Y, Jiang J, Sun D, Ma X, Lan Z, et al. Enhanced rate performance of Al-doped Li-rich layered cathode material via nucleation and post-solvothermal method. ACS sustainable chemistry& engineering 2018;6(4):4625–32.
[145] Kim UH, Park JH, Aishova A, Ribas RM, Monteiro RS, Griffith KJ, et al. Microstructure engineered Ni-rich layered cathode for electric vehicle batteries [J]. Adv Energy Mater 2021;11:2100884.
[146] Zhang C, Xu S, Han B, Lin G, Huang Q, Ivey DG, et al. Towards rational design of high performance Ni-rich layered oxide cathodes: The interplay of borate-doping and excess lithium. J Power Sources 2019;431:40–7.
[147] Woo SU, Park BC, Yoon CS, Myung ST, Prakash J, Sun YK. Improvement of electrochemical performances of Li $[Ni_{0.8}Co_{0.1}Mn_{0.1}]O_2$ cathode materials by fluorine substitution. J Electrochem Soc 2007;154(7):A649.
[148] Qian Y, Niehoff P, Börner M, Grützke M, Mönnighoff X, Behrends P, et al. Influence of electrolyte additives on the cathode electrolyte interphase (CEI) formation on $LiNi_{1/3}Mn_{1/3}Co_{1/3}O_2$ in half cells with Li metal counter electrode. J Power Sources 2016;329:31–40.
[149] Sun F, Markötter H, Manke I, Hilger A, Kardjilov N, Banhart JJA, et al. Three-dimensional visualization of gas evolution and channel formation inside a lithium-ion battery. ACS Appl Mater Interfaces 2016;8(11):7156–64.
[150] Wagner MR, Raimann PR, Trifonova A, Möller KC, Besenhard J, Winter M, et al. Dilatometric and mass spectrometric investigations on lithium ion battery anode materials. Anal Bioanal Chem 2004;379(2):272–6.
[151] Zhang SS. Insight into the gassing problem of Li-ion battery. Front Energy Res 2014;2:59.
[152] Fan Q, Lin K, Yang S, Guan S, Chen J, Feng S, et al. Constructing effective TiO_2 nano-coating for high-voltage Ni-rich cathode materials for lithium ion batteries by precise kinetic control. J Power Sources 2020;477:228745.
[153] Becker D, Börner M, Nölle R, Diehl M, Klein S, Rodehorst UC, et al. Surface modification of Ni-rich $LiNi_{0.8}Co_{0.1}Mn_{0.1}O_2$ cathode material by tungsten oxide coating for improved electrochemical performance in lithium-ion batteries. ACS Appl Mater Interfaces 2019;11(20):18404–14.
[154] Yoon M, Dong Y, Hwang J, Sung J, Cha H, Ahn K, et al. Reactive boride infusion stabilizes Ni-rich cathodes for lithium-ion batteries. Nature Energy, 202, 6: 362-371.
[155] Gan Q, Qin N, Zhu Y, Huang Z, Zhang F, Gu S, et al. Polyvinylpyrrolidone-induced uniform surface-conductive polymer coating endows Ni-rich $LiNi_{0.8}Co_{0.1}Mn_{0.1}O_2$ with enhanced cyclability for lithium-ion batteries. ACS Appl Mater Interfaces 2019;11(13):12594–604.
[156] Du K, Xie H, Hu G, Peng Z, Cao Y, Yu FJA, et al. Enhancing the thermal and upper voltage performance of Ni-rich cathode material by a homogeneous and facile coating method: spray-drying coating with nano-Al_2O_3. ACS Appl Mater Interfaces 2016;8(27):17713–20.
[157] Guo S, Yuan B, Zhao H, Hua D, Shen Y, Sun C, et al. Dual-component silica functional coating in one layer for performance enhanced $LiNi_{0.6}Co_{0.2}Mn_{0.2}O_2$ cathode. Nano Energy 2019;58:673–9.
[158] Kim UH, Kim JH, Hwang JY, Ryu HH, Yoon CS, Sun YK. Compositionally and structurally redesigned high-energy Ni-rich layered cathode for next-generation lithium batteries. Mater Today 2019;23:26–36.
[159] Song YM, Kim CK, Kim KE, Hong SY, Choi NS. Exploiting chemically and electrochemically reactive phosphite derivatives for high-voltage spinel $LiNi_{0.5}Mn_{1.5}O_4$ cathodes. J Power Sources 2016;302:22–3.
[160] Suzuki H, Maruyama S, Ohe K. Polymeric solid electrolyte and lithium secondary cell using the same: U.S. Patent 6,051,343. 2000-4-18.
[161] Cho JW, Song HY. Dehydrofluorination of a copolymer of vinylidene fluoride and tetrafluoroethylene by phase transfer catalysis reaction. J Polym Sci, Part A: Polym Chem 1995;33(13):2109–12.
[162] Zhang SS, Fan X, Wang C. Enhanced electrochemical performance of Ni-rich layered cathode materials by using $LiPF_6$ as a cathode additive. ChemElectroChem 2019;6(5):1536–41.
[163] Biso M, Colombo R, Uddin MJ, Stanga M, Cho SJ. A rheological behavior of various polyvinylidene difluoride binders for high capacity $LiNi_{0.6}Mn_{0.2}Co_{0.2}O_2$. Polym Eng Sci 2016;56(7):760–4.
[164] Chang B, Kim J, Cho Y, Hwang I, Jung MS, Char K, et al. Highly elastic binder for improved cyclability of nickel-rich layered cathode materials in lithium-ion batteries. Adv Energy Mater 2020;10(29):2001069.
[165] Jang J, Oh J, Jeong H, Jang J, Oh J, Jeong H, et al. A review of functional separators for lithium metal battery applications. Materials 2020;13(20):4625.
[166] Peng L, Kong X, Li H, Wang X, Shi C, Hu T, et al. A rational design for a high-safety lithium-ion battery assembled with a heatproof–fireproof bifunctional separator. Adv Funct Mater 2021;31(10):2008537.
[167] Kim Y, Seong WM, Manthiram A. Cobalt-free, high-nickel layered oxide cathodes for lithium-ion batteries: Progress, challenges, and perspectives. Energy Storage Mater 2021;34:250–9.
[168] Sun YK, Lee DJ, Lee YJJ, Chen Z, Myung ST. Cobalt-free nickel rich layered oxide cathodes for lithium-ion batteries. ACS Appl Mater Interfaces 2013;5(21):11434–40.
[169] Jing L, Cameron AR, Li H, Glazier S, Dahn JR. Comparison of single crystal and polycrystalline $LiNi_{0.5}Mn_{0.3}Co_{0.2}O_2$ positive electrode materials for high voltage Li-ion cells. J Electrochem Soc 2017;164(7):A1534–44.
[170] Kim Y. Lithium nickel cobalt manganese oxide synthesized using alkali chloride flux: morphology and performance as a cathode material for lithium ion batteries. Acs Appl Mater Interfaces 2012;4(5):2329–33.
[171] Duan J, Wu C, Cao Y, Huang D, Du K, Peng Z, et al. Enhanced compacting density and cycling performance of Ni-riched electrode via building mono dispersed micron scaled morphology. J Alloy Compd 2017;695:91–9.
[172] Hu G, Tan C, Du K, Peng Z, Cao Y, Liang L, et al. Preparation of high voltage solid nickel rich cathode material $LiNi_{0.85}Co_{0.06}Mn_{0.06}Al_{0.03}O_2$. Journal of inorganic chemistry 2017;33(08):1450–6.
[173] Liu A, Zhang N, Stark JE, Arab P, Li H, Dahn JR. Synthesis of Co-free Ni-rich single crystal positive electrode materials for lithium ion batteries: part II. one-step lithiation method of Mg-doped $LiNiO_2$. J Electrochem Soc 2021;168(5):050506.
[174] Liu D, Shadike Z, Lin R, Qian K, Li H, Li K, et al. Review of recent development of In situ/operando characterization techniques for lithium battery research. Adv Mater 2019;31(28):1806620.
[175] Hautier G, Jain A, Chen H, Moore C, Ong SP, Ceder G. Novel mixed polyanions lithium-ion battery cathode materials predicted by high-throughput ab initio computations. J Mater Chem 2011;21(43):17147–53.
[176] Xiao Y, Miara LJ, Wang Y, Ceder G. Computational Screening of Cathode Coatings for Solid-State Batteries. Joule 2019;3(5):1252–75.

[177] Nolan AM, Liu Y, Mo Y. Solid-state chemistries stable with high-energy cathodes for lithium-ion batteries. ACS Energy Lett 2019;4(10):2444–51.
[178] Xiao RJ, Li H, Chen LQ. Development of new lithium battery materials by material genome initiative. Acta Physica Sinica 2018;67(12):128801.
[179] Ling SG. Application of high-throughput calculations for screening lithium battery materials. Materials China 2015;34(4):272–81.